THE UNIVERSITY *of* EDINBURGH

This thesis has been submitted in fulfilment of the requirements for a postgraduate degree (e.g. PhD, MPhil, DClinPsychol) at the University of Edinburgh. Please note the following terms and conditions of use:

- This work is protected by copyright and other intellectual property rights, which are retained by the thesis author, unless otherwise stated.
- A copy can be downloaded for personal non-commercial research or study, without prior permission or charge.
- This thesis cannot be reproduced or quoted extensively from without first obtaining permission in writing from the author.
- The content must not be changed in any way or sold commercially in any format or medium without the formal permission of the author.
- When referring to this work, full bibliographic details including the author, title, awarding institution and date of the thesis must be given.

Acknowledgements

A Doctor of Philosophy course can be an enlightening experience. Mostly, I found this to be true in ways irrelevant to the knowledge acquired pertinent to the subject matter, though that knowledge, too, is not to be underestimated. There are certain individuals to whom I'm indebted for making this experience richer.

First and foremost I thank my Parents, who not only enabled me to embark on such an undertaking, yet allowed me to do so in the most generous of manners. They showed remarkable support and patience throughout the duration. I thank my uncle, Professor K. Thanos, and his family. He has supported me throughout a series of events in my life like a second father. The generosity of my dear friend Professor J. B. Kennedy exceeded by far ordinary standards of expectation.

Considerable amounts of not only help and guidance, but also patience and understanding both academically and personally have been given to me by my Supervisor, Dr. Vasileios Koutsos. I shall try to take heed of his advice. I am grateful to Dr. I. Bitsanis and Dr. A. Rissanou for their hospitality during my stay in Crete, for training me on computer simulation methods, and their ongoing support. Dr. A. Rissanou's contribution towards the creation of the largest part of the MC algorithm ought to be mentioned.

I thank my colleagues Mr. I. Albaijan and Miss J. Morris for their support and company in our shared office. Also my colleague Mr. M. Kalloudis for our scientific exchanges, support, and daily companionship in King's Buildings' premises. Dr. P. Gerakios for his valuable knowledge on computer programming and his friendship and support throughout the entirety of my years as a student. Dr. C. Retsa for lending me a laptop for computer simulations. Mr. Y. Kyvellos for inspiring scientific conversations. Mr. D. Orejon for helping me print out in the last hours. All IMP students for making daily routine seem more pleasant.

I am grateful for financial assistance from the Alexander S. Onassis Public Benefit Foundation by means of a Scholarship towards the completion of this course.

"It doesn't matter how beautiful your theory is, it doesn't matter how smart you are. If it doesn't agree with experiment, it's wrong." — Richard Feynman.

Preface

Compared to the solid and gaseous phases, liquids are more closely related to biological processes and the life sciences. In fact, it is generally believed that abiogenesis occurred in the liquid environment of the primordial sea which, itself, was formed only when appropriate conditions came to prevail on the young Earth, providing a striking illustration of the marginal character of the liquid state, in contrast with the solid and gaseous phases of the same substances, which exist over much wider ranges of temperature and pressure: the liquid state arises from a delicate balance between packing of molecules and cohesive forces or, more formally, between entropy and energy. The importance of a full quantitative understanding of liquids is only obvious.

Following research in simple liquids, a new area of complex liquids emerged for the study of systems which exhibit flow, but whose liquid-like behaviour cannot be explained by the standard one-body picture used in simple liquids, as interatomic forces are significantly different from the hard-sphere type. The term complex liquid can be interchangeably used with complex fluid or soft matter —following P.G. de Gennes. Many examples of complex liquids involve the mixing of different phases, be they fluid or not in their own right, such as solid and liquid (to make up gel or sol), liquid and gas (to make up foam or liquid aerosol), and solid and gas (to make up solid foam or solid aerosol). Under appropriate conditions, these complex liquid examples, known as colloids, will exhibit fluid-like behaviour on the macroscopic scale. Further examples of complex fluids include polymers and liquid crystals.

This Thesis focuses on polymers. Specifically, it researches polymers from a theoretical and a computer simulation perspective, in particular their interaction with surfaces in such a way that they become adsorbed. Setting out with a definition, examples of polymers, and a brief discussion of the practical applications of this work, the General Introduction gives an overview of the theoretical progress in the area of polymer adsorption. This sets the context for a subsequent description

of the objectives of this Thesis. The General Introduction closes with an outline of the remainder of the chapters that follow.

Contents

List of Tables

List of Figures

Chapter 1

General Introduction

A polymer is a substance that has molecular structure built up chiefly or entirely from a large number of similar units bonded together; in other words, a large molecule (macromolecule) composed of repeating molecular units (monomers or structural units)[1]. Polymers encompass an impressively wide range of materials, from naturally occurring to manmade. Examples of natural polymers are silk, wood, DNA (deoxyribonucleic acid), proteins, shellac, amber, and natural rubber. The list of synthetic polymers is virtually endless and includes synthetic rubber, low density polyethylene (LDPE), high density polyethylene (HDPE), polystyrene (PS), polyvinyl chloride (PVC), and nylon as organic examples, and polydimethylsiloxane (PDMS), polymethylhydrosiloxane (PMHS), polyphosphazene, and polysulfides as inorganic examples. Polymers are ubiquitous and the volume of polymers produced already exceeds that of metals (although not in weight). The production and use of the aforementioned materials is a result of their demand in numerous and diverse applications.

As demonstrated in this Thesis, a polymer nanodroplet's elastic modulus (Part I) and internal chain architecture (Part II) are critically related to how and whether it will be adsorbed upon interaction with a substrate, therefore shape its mechanical response. The importance of such knowledge may be a guide for the selection of appropriate materials, depending on the application. An example is portrayed from the field of biomedical engineering: Implants are selected primarily for technological aspects such as mechanical properties, stability, permeability, non-toxicity, and hemocompatibility. Insufficient hemocompatibility impairs functionality and safety. For instance, adsorption of plasma proteins onto the surface of a blood-

[1] In some areas of science (particularly chemistry), one may encounter a differentiation between monomer and structural unit, the former referring to the molecular unit in an isolated state, while the latter in the polymerized state.

contacting implant may trigger a cascade of chemical reactions, leading to the formation of a blood clot surrounding the implant (Werner et al. [2007]). To increase hemocompatibility, polymers are adsorbed instead around the surface of implants, decreasing the probability of further adsorption of proteins or negative interactions with the blood (Werner et al. [2007]). One such polymer is the hydrophilic heparin. Heparin interacts with thrombin to prevent coagulation and suppressed platelet adhesion (Vendra et al. [2011]). Further applications relating to polymer adsorption include: adhesion (Lee [1980]), surface lubrication and friction modification (Brown [1994]), chromatography (Svec and Frechet [1992]), surface nanopatterning (Cox et al. [1999]), drug delivery (Imanishi and Yoshihiro [1995]), and biocompatibility of artificial organs (Ruckenstein and Chung [1988]).

The foundations of polymer theory were set by Flory and Kuhn, while scientists like Lifshitz, Edwards, and de Gennes, turned polymer theory into polymer physics, an independent field of research. Striking analogies between problems in polymer physics and general physics were revealed, such as the analogy between a polymer chain and a random walk. Though a discovery as old as dating back to the 1930s (Kuhn [1934]) and for a most simple system of a single flexible chain in an unconfined environment, the random walk model for polymers has continued to attract attention over half a century later (Haber et al. [2000]). When a chain is adsorbed on a surface or interface, the analogy translates into a random walk in the presence of a boundary constraint (DiMarzio [1965]). To draw further analogies, polymer adsorption is related to a wide class of order-disorder transitions, such as surface magnetism (Daoud et al. [1975], de Gennes [1976]) and the helix-coil transition in biopolymers (Roe [1965], Hoeve et al. [1965]).

One of the first significant works aiming at developing a theory for the equilibrium state of a polymer chain adsorbed on a surface was that of Simha et al. [1953]. The model treated the ideal chain, i.e. one that does not experience monomer-monomer interactions, also known as a Gaussian chain, and was based on a Gaussian-statistics description of the end-to-end distance[2]. Simha et al. [1953] established the classic picture of the adsorbed chain consisting of trains (segments attached along the surface), loops (non-attached segments between trains), and tails (free ends). They also established a relationship between the degree of adsorption and chain flexibility, concluding that higher flexibility allows for greater adsorption. Discreet (on a lattice) (Rubin [1965a], Rubin [1965b], Rubin [1966a], Rubin [1966b]) and continuum (off-lattice) (Dolan and Edwards [1974], Chan et al. [1975],

[2]Simply, the distance in space between the two ends of the chain.

Lépine and Caillé [1978]) random-walk models that followed, further contributed to the description of the conformational properties of surface-interacting Gaussian chains. Incorporation of monomer-monomer interactions added to sophistication, and the real (as opposed to ideal) chains featured the excluded volume[3] effect as modeled by the self-avoiding random walk (Whittington [1975], Hammersley et al. [1982], Hammersley and Whittington [1985], Torrie et al. [1976], Middlemiss and Whittington [1976]).

Following the Gaussian-statistics description of ideal chains, the exact or direct enumeration method is an algebraic method which enables one to count the total number of random walks on a lattice —though discretization of space is not compulsory (Lax and Windwer [1971]). The basis of this method is the transfer matrix technique (Conway et al. [1992]). Given that the computational complexity of enumerating walks of N steps is of order $3^{N/4}$ times a polynomial in N, this approach turns out much more efficient to direct counting techniques. Regarding polymer adsorption, Lax [1974a] and Lax [1974b], for example, directly enumerated self-avoiding walks on a computer to obtain data for the adsorption-energy and molecular-weight dependence of configurational properties, such as the mean-square end-to-end distance, the average and root-mean-square normal to the surface distance of the chain ends, and the average number of adsorbed segments. Other works include Douglas et al. [1986], Torrie and Whittington [1975], and Middlemiss and Whittington [1976].

A powerful theoretical tool extensively used in the context of polymers is scaling theory, which involves performing simple dimensional analysis on elementary information and arguments with the aim of extrapolating those to a different scale. In the context of an adsorbed chain, an example calculation is the following: from consideration of a given energy of attraction between a monomer and the surface and competition between that attraction and thermal motion, one can identify a relevant size scale below which a segment will spontaneously be adsorbed and above which it will spontaneously be desorbed (on smaller scales the attraction will dominate over thermal motion, and vice versa). By performing dimensional analysis on this elementary result, one may extrapolate to the scale of the whole chain, and deduce an estimate on the scaling dependence of the free energy (a macroscopic quantity) on chain size, temperature, and adsorption strength. Detailed calculations for this example can be found in Rubinstein and Colby [2003]. Eisenriegler et al. [1982] use scaling theory to study features like the polymer's linear dimensions

[3]Volume inaccessible to a monomer due to the presence of another.

parallel and perpendicular to the surface, as well as the behaviour of monomers as a function of distance from the surface. They also discuss various power laws in polymer adsorption in relation to surface magnetism. de Gennes [1976] relates power laws for the adsorbed layer with power laws of corresponding self-avoiding walks. Further examples of applying scaling theory to polymer adsorption can be found in the works of Daoud and Jannink [1976], Alexander [1977], de Gennes [1979], de Gennes [1981], de Gennes [1982], and Usatenko [2006].

Self-consistent field theory (SCFT) / mean-field theory (MFT) is an example of an analytic theory approach, where the combined effect of many-body interactions is parameterized through a mean-field approximation. An early development of this approach is the work of Jones and Richmond [1977]. In the limit where the adsorbed segment density is uniform, so that the self-consistent method is valid, Jones and Richmond [1977] obtain analytical solutions for a critical segment free energy of adsorption, adsorbed layer thickness, and number of polymers adsorbed per unit area. As another example, Levine et al. [1978] approximate the excluded volume and nearest-neighbour interactions by appropriate mean fields to derive the adsorbed-segment density profile and free energy. More recent MFT accounts are the works of Whitmore and Vavasour [1992] and Avalos et al. [2004]. Comprehensive reviews are offered by Schmid [1998], Matsen [2002], and Fredrickson et al. [2002], the latter focusing on field-theoretic methods used in computer simulations.

A further achievement in analytic theory is the renormalization group (RG) method. Freed [1983] used this method to analytically calculate such properties as the end-to-end distance and radius of gyration[4] of adsorbed chains. Nemirovsky and Freed [1985] used the RG method to study excluded volume effects of adsorbed polymers and evaluate several moments of the end-to-end vector. Further examples of use of this method are to be found in the works of Kosmas [1981], Eisenriegler [1983], Kremer [1983], and Douglas et al. [1986].

Given the increasing sophistication, versatility, processing capacity, and availability of computers, computer simulations have secured a very prominent place among all of this theoretical development. The two principal methods used are molecular dynamics (MD) and Monte Carlo (MC). MD, conceived by Alder and Wainwright [1959], involves the numerical solution of the equations of motion of all particles of a system, so that, in conjunction with a set of initial conditions, a future state can be calculated. Evidently, MD is most suitable for tracking the evolution of a system, however is limited by the memory capacity and speed of the computing

[4] A measure of size, defined later.

machine in terms of the size of the system studied and the length of time during which its evolution is to be tracked. Examples of applications of the MD method on polymers on surfaces are given in the works of Michel and Kreitmeier [2001], Michel et al. [2002], Liu et al. [1999], Liu and Chakrabarti [2009]. It appears natural to address dynamical problems via MD, however, if one is interested in equilibrating long chains, then the MC method is most suitable. This method was coined in the late 1940s by John von Neumann, Stanislaw Ulam and Nicholas Metropolis, but only appeared as a scientific publication in 1953 (Metropolis et al. [1953]), and was named after the Monte Carlo Casino[5]. Instead of trying to reproduce the dynamics of a system, the MC method generates states according to appropriate Boltzmann probabilities. The method is presented in Section 7.1. Examples of applications of the MC method on polymers on surfaces are given in the works of Clark and Lal [1978], Lai [1994], Sikorski [2001], and Metzger et al. [2002].

For completeness of this brief overview of the general literature of polymers on surfaces, examples of experimental work and techniques ought to be cited: Takahashi et al. [1984], Killmann et al. [1988], Cohen-Stuart and Tamai [1988], Barnett et al. [1982], Rennie et al. [1989], Barnett et al. [1981], Cosgrove et al. [1990], Granier et al. [1993], Granier and Sartre [1995], Sommer et al. [1995], Johnson and Lenhoff [1996], Unertl [1998], Portigliatti et al. [2000], Kirsch et al. [2005], Lau et al. [2002], Kugge et al. [2004], Yamamoto et al. [2005], Tan et al. [2005], Lafon and Trannoy [2006], Engqvist et al. [2007]. Finally, examples of articles reviewing developments in theory, simulation, or experimental work on polymer adsorption are Takahashi and Kawaguchi [1982] (theory and experiment), Kawaguchi and Takahashi [1992] (theory and experiment), Varnik and Binder [2009] (simulation), and Rychlewski and Whittington [2011] (theory).

I followed two independent approaches in my investigation of polymers on surfaces. For this reason this Thesis is divided into two Parts. Part I refers to a purely theoretical model for the adsorption of a nanoscopic polymeric droplet on a substrate. The model is a continuum theory which combines surface and elasticity theories with an aim to predict the droplet's elasticity, given (experimental) knowledge of its adsorbed height. Being a continuum (macroscopic) theory, the model is not concerned with microscopic elements such as the chemical details of its atoms, or the tertiary structure[6] of its chains, both of which are parameterized

[5]This choice of name by Metropolis was not unrelated to the fact that Ulam had an uncle who would borrow money from relatives because he "just had to go to Monte Carlo" (Metropolis [1987]).

[6]A term commonly used in biochemistry and molecular biology to denote the three-dimensional structure as defined by the atomic coordinates of a macromolecule.

through the droplet's macroscopic properties, such as its surface tension. Part II refers to a MC computer simulation for the adsorption of a polymer droplet comprising a single chain or an aggregate of chains on a substrate. The simulation uses a coarse-grained molecular model for a chain to calculate the polymer's equilibrium conformation. A separate computer code calculates its radius of gyration.

Parts I and II clearly share the connection of studying the same conceptual system. In their direction of approach, they are quite opposite: Part I involves a macroscopic, 'top-down' approach on a small-scale system, whereas Part II involves a coarse-grained molecular, 'bottom-up' approach, looking at large-scale properties of a related system. A fundamental motivation for the top-down approach is to discover the continuum theory's limits as one approaches the nanoscale, at what size-scale it ceases to be valid, and in what way it breaks down. The bottom-up approach, on the other hand, being a coarse-grained model, ignores the molecular details of the chain and finds its justification through a phenomenon that is most striking: Polymers share universal properties by virtue of general physical characteristics they have in common. That is to say, these properties are not related to a specific chemical composition of the polymer or its environment, but arise from the chain-like structure. "*The universality*[7] *has found its full recognition and usefulness when polymers have been shown to behave, in the asymptotic limit of infinite molecular weight, as scale invariant critical objects and when the renormalization group ideas have been introduced to polymer theory.*" (Singh et al. [1999]).

Parts I and II share a similar structure. Both open with introductory chapters (2 and 7, respectively) offering prerequisite theoretical background and a more subject-specific review of the literature. For Part I, then, follows a detailed development of the theoretical model (Chapter 3), while for Part II the simulation method is explained (Chapter 8). Following chapters (4-5 and 9, respectively) offer results and discussion, and brief concluding chapters (6 and 10, respectively) close each Part. Ultimately, Chapter 11 summarizes the important findings of each Part, draws general conclusions, brings continuum theory and computer simulation together by illustrating how the two studies complement each other, and brings this Thesis to a close with proposed work for the future. Lists of symbols and abbreviations can be found as Appendices B and C, respectively, for the reader's convenience.

[7]The concept of universality in statistical mechanics refers to the observation that certain systems, though seemingly unrelated, will behave similarly in a scaling limit, when a large number of interacting parts comes together.

Part I

Continuum Theory

Abstract

A theoretical model was redeveloped, which, in conjunction with atomic force microscopy (AFM), can be used as a non-invasive method for the determination of the elastic modulus of a polymer nanodroplet residing on a flat, rigid substrate. The model is a continuum theory which combines surface and elasticity theories for the prediction of the droplet's elastic modulus, given experimental measurement of its adsorbed height. Utilization of AFM-measured heights for relevant droplets reported in the literature and from our research group's experiments illustrated the following: the significance of both surface and elasticity effects in determining a polymer droplet's spreading behaviour; the extent of a continuum theory's validity as one approaches the nanoscale; a droplet size effect on the elastic modulus.

Chapter 2

Introduction

2.1 Background Theory

2.1.1 Free Energy and Thermodynamic Equilibrium

A thermodynamic potential or characteristic function, Φ, is defined with respect to pressure, P, and temperature, T (Landau and Lifshitz [1980]):

$$\Phi = I - TS_{\mathrm{E}} + PV \tag{2.1}$$

I is the internal energy of our system, S_{E} the entropy, V the volume, and Φ is widely known as the Gibbs free energy, henceforth referred to as the free energy, for simplicity. The system is defined as the polymer with its surrounding solid and gas phases, isolated from the rest of the universe.

In thermodynamic equilibrium, the bulk of a thermodynamic phase is characterized by translational invariance of its local structural properties, giving rise to a corresponding bulk free energy. Deviations from this translational invariance cause an excess in free energy which scales with the dimensionality of the defect. A surface or interface are examples of defects, and their corresponding surface or interfacial energies ought to be incorporated into Φ. With $U \equiv I - TS + PV$ associated with the bulk and dU_{DEF} with defects,

$$d\Phi = dU + dU_{\mathrm{DEF}} = 0 \tag{2.2}$$

is the requirement for equilibrium.

2.1.2 Surface Energy and Surface Tension

Bonds between molecules and their constituent atoms shape small and large-scale behaviour of matter, therefore an understanding of such interactions is valuable. They are commonly divided into two types: the strong bonds (whose rupture corresponds to a large amount of energy, $\sim 10^2$ kcal/mol), viz ionic, covalent and metallic and the weak bonds (~ 1 kcal/mol), viz the hydrogen bond and the Van der Waals forces.

Molecules in the bulk of a liquid or solid have neighbours in all three dimensions to interact with. In the surface layer, molecules may interact either towards the bulk, or laterally, within the surface plane. By implication, surface molecules find themselves in a state of higher potential energy and experiencing an anisotropy in pressure between the perpendicular and tangential to the surface directions. It is these features that give rise to surface energy and surface tension.

One of the earliest references on this topic takes us back to the seventeenth century, by Cabeo [1629]. Surface energy and surface tension are equivalent dimensionally, and often equal in value. They also share the deeper connection that both refer to the difference in state between surface and bulk atoms or molecules. For the purposes of the present work, no distinction is made between surface energy and surface tension, while the latter term is used throughout. It should, however, be born in mind that, by definition, surface energy and surface tension are distinct concepts. The reader is referred to Shuttleworth [1949] and Maugis [2000], where the two concepts are compared and contrasted.

Surface tension if defined as the work, γ, required to reversibly create an elemental area dA of new surface in equilibrium with the medium. Creation of new surface means breaking the bonds which ensure the cohesion of that condensed phase and slightly reorganizing molecules near that surface. It does not mean stretching an existing one, because the equilibrium interatomic distances must be preserved. Surface tension is an intensive quantity, commonly expressed in units of Jm^{-2}.

Experimentally, the simplest ways of estimating the surface tension of a liquid are either by direct measurement of the force acting against increasing the area of the corresponding liquid film, or by indirect measurement using a capillary, provided that the walls are completely wetted by the liquid. The capillary force that causes the liquid to rise through the capillary tube is due to surface tension balancing the weight of the liquid inside the capillary which is above the level of the liquid outside the capillary.

Striking large scale manifestations of surface tension are to be witnessed in everyday life. These give rise to an apparent tension along the surface of a liquid, causing the surface layer to behave as if it were an elastic membrane. This can be observed, for example, when an insect walks on water, when small needles and foil fragments rest on its surface, or when a drop hangs at the edge of a tube. Even though surface tension phenomena are easily observable with liquids, this concept also relates to solids. A practical way of thinking about the meaning of surface tension of a solid is the following: The solid is cut along any plane and the two surfaces are separated. The work required against the cohesive forces to take the surfaces to infinity, divided by the total area would be equal to the surface energy.[1]

Clearly, surface tension reflects the nature of the bonds between its atoms. Covalently-bonded matter and metals are consequently expected to exhibit high surface tensions ($\sim 1 \times 10^3$ mJ/m^2), ionic solids slightly lower ($\sim 1 \times 10^2$ mJ/m^2), whereas molecular crystals, having surfaces whose molecules are bonded only through van der Waals forces, are expected to have the least surface tensions ($\sim 1 \times 10$ mJ/m^2). Indicatively, the surface tension of a pure water surface (containing hydrogen bonds) in air is about 73 mJ/m^2, whereas of triglyceride oil it is about 30 mJ/m^2 (Maugis [2000]).

2.1.3 Line Tension

One of the first documented references to the concept of line tension was made by Gibbs in a brief footnote in one of his papers (Gibbs [1961]), commenting that a complete description of systems that involve a one-dimensional boundary between phases, e.g. a three-phase equilibrium where all phases neighbour each other, requires treatment of the excess energy, entropy, etc. along that line of discontinuity. This means that Gibbs introduced line tension by analogy to surface tension, only the boundary is of different dimensionality due to a difference in number of coexisting phases.[2] What is more, Gibbs heeded an important difference between surface and line tensions: while the former must be positive, the latter can have either sign.[3] The main theoretical objection towards the idea of negative line tension has

[1] This can only be thought experiment, as cleavage and fracture always involve irreversible processes, such as defect generation.

[2] One paper claims that the situation is not as trivial, discussing the presence of extra surface phases created on the boundary (Seppecher [2001]).

[3] "We may here add that linear tension there mentioned may have a negative value. This would be the case with respect to a line in which three surfaces of discontinuity are regarded as meeting. [...] We may regard two soap-bubbles adhering together as an example of this case. The reader will easily convince himself that in an exact treatment of the equilibrium of such a

been that the free energy functional, whose minima offer observable equilibria, is unbounded from below, so that any equilibrium configuration becomes unstable by appropriate perturbation (Steigmann and Li [1995] (mathematical), Alberti et al. [1998]). On the other hand, counter-arguments have been proposed justifying the existence of stable, hence observable, equilibria under negative line tension, as long as that is not too large in absolute value (Rosso and Virga [2004a], Rosso and Virga [2004b]). The same idea is supported by Guzzardi et al. [2006], only their objective is different and the criterion they work out more general —encompassing line tension, as well as inhomogeneities and arbitrary substrate shapes.

Over the past few decades, line tension has attracted the attention of numerous theoretical (Rowlinson and Widom [1982], Toshev et al. [1988], Toshev and Avramov [1993], Getta and Dietrich [1998], Dobbs [1999]) and experimental (Gaydos et al. [1990], Toshev et al. [1988], Li [1996], Wang et al. [2001], Pompe and Herminghaus [2000]) research groups, as it plays an important role in phenomena such as the dynamics of contact line spreading, the wetting and nucleation behaviour of microscopic droplets on surfaces, the rupture of thin films and the formation of Newton black films and foam films. In the present work the concept of line tension is treated as an excess thermodynamic quantity that brings into correspondence two systems: a real system, with a transition region between the phases, and an ideal system, without, i.e. where the finite-sized transition region is reduced to an infinitesimally thin 'line of contact', or, 'line of tension', a one-dimensional analog to the surface of tension mentioned previously. According to this analogy, an expression for the excess energy corresponding to the one-dimensional defect of a line of tension τ, suitable for our system of a polymer droplet on a rigid substrate surrounded by air is

$$2\pi a\tau, \tag{2.3}$$

where a is the radius of the circular interface between the droplet and the substrate.

2.1.4 Adhesion

When two materials, 1 and 2, are in contact over an area A, their total energy is $U + \gamma_{12}A$, γ_{12} being the interfacial tension. When separated to infinity, the total energy becomes $U + (\gamma_1 + \gamma_2)A$, and when the separation process is reversible and adiabatic, the corresponding work expended per unit area, the difference between

double bubble we must recognize a certain negative tension in the line of intersection of three surfaces of discontinuity." (Gibbs [1961], p. 296) That is where Gibbs's comments about line tension unfortunately ended.

the two energy states divided by A, becomes the definition of the Dupré energy of adhesion, w:

Definition.

$$w = \gamma_1 + \gamma_2 - \gamma_{12} \tag{2.4}$$

In the case of the two solids 1 and 2 being of the same kind, $\gamma_{12} = 0$ and Eq. (2.4) reduces to $w = 2\gamma$, the solid's cohesive energy.

2.1.5 The Spreading Parameter

First defined by Carlo Marangoni in his 1865 doctoral dissertation (Ross and Becher [1992]):

Definition.

$$S = \gamma_{\mathrm{SG}} - (\gamma_{\mathrm{SL}} + \gamma_{\mathrm{LG}}), \tag{2.5}$$

where S, L, and G denote the solid, liquid, and gaseous phases.

S describes the spreading behaviour of a liquid on a solid substrate in the presence of gas. For $S \geqslant 0$ the liquid wets the surface, forming a covering film, and for $S < 0$ the liquid de-wets or partially wets the surface. S essentially defines a competition between the surface energy of the solid-gas interface and the sum of the surface energies of the solid-liquid and liquid-gas interfaces. Upon wetting, the solid-gas interface area reduces while the solid-liquid and liquid-gas interface areas increase, and vice-versa for de-wetting. The principle of minimization of energy will determine which of the two processes is energetically favourable, depending on which of the two terms is smaller, γ_{SG} or $(\gamma_{SL} + \gamma_{LG})$.

2.1.6 Young's Law

In his original essay of 1805 (Young [1805]), Thomas Young wrote:

> *"But it is necessary to premise one observation, which appears to be new, and which is equally consistent with theory and experiment; that is, that for each combination of a solid and a fluid, there is an appropriate angle of contact between the surfaces of the fluid, exposed to air and the solid."*

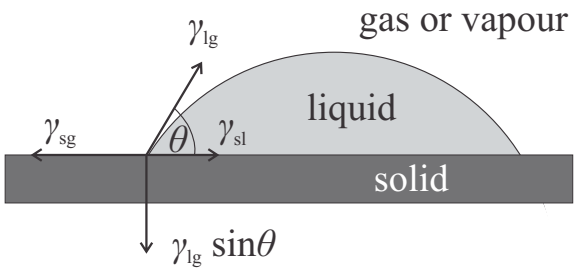

Figure 2.1: Cross section of a drop of liquid on a solid substrate and surrounded by air, depicted along with the surface tension forces, γ, acting at the three-phase contact point. Mechanical equilibrium of the surface tension forces along the horizontal implies Eq. (2.6).

Attributed to Young, is the equivalent, in words, of the following famous equation, referred to as Young's Law:[4]

$$\gamma_{\mathrm{SG}} = \gamma_{\mathrm{SL}} + \gamma_{\mathrm{LG}} cos\theta, \tag{2.6}$$

where θ denotes the angle at which the solid-liquid and liquid-gas interfaces meet, with the convention of $\theta = 0^\circ$ corresponding to complete wetting and $\theta = 180^\circ$ to complete de-wetting, all values in between referred to as partial wetting, of the solid by the liquid. The geometry is illustrated in Fig. 2.1.

There exist more than one ways of proving Eq. (2.6). The quickest, though not most rigorous, is by vectorial summation of the horizontal components of the forces in Fig. 2.1 when the drop is in mechanical equilibrium.[5] Equilibrium requires the balance of the vertical components, also, hence the existence of a downward $\sigma_{\mathrm{LG}} \sin\theta$ force to balance the vertical component of σ_{lg}. Physically, this corresponds to a reaction force of the stress field on the surface of the solid caused by the sum of the applied surface forces. It is interesting to note that, in cases of adequately soft substrates, e.g. soft polymers, on top of which drops of adequately strong interaction reside (small θ), the aforementioned stress field causes finite

[4]Intriguingly enough, Adam [1957] explains why, according to his view, it really should be the so-called Young-Dupré equation ($W = \gamma_{\mathrm{LG}}(1+\cos\theta)$) that should be called Young's Law, instead of (2.6), by locating the relevant passage in Young's *'Essay on the Cohesion of Fluids'* (Young [1805], section VII) and translating prose to equation. He further argues that the Young-Dupré equation would also do more justice to the importance of Young's work than the obvious (2.6), because it relates the contact angle to the relative adhesion of liquid to solid and of liquid to liquid.

[5]This way also happens to be the first, employed by Thomas Young, himself (Young [1805]). Due to the lack of development of thermodynamics at that time, the mechanical tensions γ_{SG} and γ_{SL} are defined only by analogy to γ_{LG}, rendering this proof less rigorous.

strain, which appears as micro-humps on the substrate surface (Shanahan [1985], Shanahan and de Gennes [1987], Shanahan and Carré [1994]). In such cases, the validity of Young's Law is compromised to an extent depending on the size of the micro-humps, since the interfacial boundary does not remain planar (Lester [1961]). By considering the excess capillary free energy consumed during spreading by the mechanical, viscoelastic hysteresis in the solid, it is possible to show how the spreading properties may be modified (Shanahan [1988]). Scanning interferometric microscopy experiments are reported in Carré et al. [1996], demonstrating that the mesoscopic surface deformation can significantly alter macroscopic phenomena, revealing important links between the two scales.

A more elegant proof of Young's law came in 1880 by Gibbs (Gibbs [1961], chapter III), who developed the thermodynamics of solid-liquid-vapour systems and establishing the study of surface-tension–related phenomena on more fundamental grounds. For the reader's satisfaction, a compact proof in the spirit of Gibbs's approach is offered:

Proof. A differential change, dU, in the excess free energy of this system with respect to a differential change, dA, in the area of the solid covered, due to displacement of the liquid drop, can be written as

$$dU = dA(\gamma_{\mathrm{sl}} - \gamma_{\mathrm{sv}}) + dA\gamma_{\mathrm{lg}} \cos(\theta - d\theta). \tag{2.7}$$

The equilibrium[6] requirement, a minimum in the excess free energy, is

$$\lim_{dA \to 0} \frac{dU}{dA} = 0.$$

In taking the limit $dA \to 0$, $d\theta/dA$ drops out, behaving like a second-order differential, hence,

$$\frac{dU}{dA} = (\gamma_{\mathrm{sl}} - \gamma_{\mathrm{sv}}) + \gamma_{\mathrm{lg}} \cos\theta = 0.$$

Q.E.D. □

In closing this Section, I would like to say that many scientists in the field of wetting and surface phenomena think of Thomas Young as the father of contact angles and wetting. But probably the earliest direct recognition of such phenomena was given by Galileo (Galilei [1612]), who might be called the grandfather of the field.

[6] Shanahan [2002] offers a short-yet-concise and thought-provoking discussion on the meaning of equilibrium for the case of a sessile drop surrounded by its vapour on a substrate.

2.2 Literature Review

Whereas adsorption and deformation of isolated polymer droplets has attracted considerable attention through experimental techniques (Granier et al. [1993], Granier and Sartre [1995], Sommer et al. [1995], Johnson and Lenhoff [1996], Unertl [1998], Portigliatti et al. [2000], Kirsch et al. [2005], Lau et al. [2002], Kugge et al. [2004], Yamamoto et al. [2005], Tan et al. [2005], Lafon and Trannoy [2006], Engqvist et al. [2007]), ranging from light scattering to scanning electron microscopy (SEM) and atomic force microscopy (AFM), continuum theoretical and computational approaches (Seemann et al. [2001], Lau et al. [2002], Engqvist et al. [2007], Araujo et al. [2008]) have fallen behind, with the exception of molecular dynamics (Kramarenko et al. [1995], Michel and Kreitmeier [2001], Liu and Chakrabarti [2009]) (MD) and Monte Carlo (Gottstein et al. [1997], Metzger et al. [2002], Livne and Meirovitch [1988], Baumgärtner and Muthukumar [1991], Hegger and Grassberger [1994], Binder and Paul [2008]) (MC) simulations, which offer treatments from a microscopic viewpoint and are usually limited to short time scales for equilibration and to length scales in the 10 nm range (Binder [1995]). Structures usually examined in experiments can be larger by one order of magnitude or more, calling for an alternative approach. The first to develop one were Lau et al. [2002], employing surface physics and elasticity theory to construct a model that describes the spreading of polymer droplets. Lau et al. [2002] also scanned profiles of latex droplets adsorbed on silica using AFM. Recently, Araujo et al. [2008] developed a simple computer model according to which a polymer droplet is conceptualized as a spherical spring matrix, with each spring representing a polymer segment between two crosslinks. Two types of forces were introduced in their algorithm, governing the droplet's wetting behaviour: elastic forces between crosslinks and attraction forces between each crosslink and the substrate. Araujo et al. [2008] tested their model with success against the experimental data of Lau et al. [2002]. Engqvist et al. [2007] performed similar experiments to those of Lau et al. [2002], investigating statics as well as dynamics of spreading. They borrowed the theoretical model of Lau et al. [2002] not for the purposes of testing it against their own experiments, rather for illustrating its mathematical consistency, unlike Lau et al. [2002], who did compare their theory against experiment. The comparison essentially comprised the following steps: Given the droplet size and AFM-measured height, the droplet's contact angle with the substrate was deduced by geometry; the contact angle was substituted into their theoretical model to produce a value for the spreading parameter as a function of the elastic modulus of the droplet; given the spreading

parameter, Young's law and the Dupré adhesion equation (Dupré [1869]) were combined to deduce the adhesion energy; the adhesion energy was used in conjunction with the Johnson-Kendall-Roberts (JKR) theory (Johnson et al. [1971]) to predict the droplet-substrate contact radius; ultimately, this prediction was compared to the AFM-measured contact radius, and the theoretical model was thus assessed.

I have the following reservations regarding this method: 1. For the stage of recovering the spreading parameter, the droplet's Young's modulus was required. That was obtained from mechanical testing of macroscopic polymer films made up of such close-packed droplets; however it is not at all obvious (also noted by Lau et al. [2002] themselves) that the modulus of a film corresponds to that of a droplet. In assemblies of small-scale–sized objects or structures that introduce a large amount of interface (such as the aforementioned array of close-packed droplets comprising the polymer film) the surface-to-volume ratio becomes significant, causing the global properties to deviate from those of the constituents. Dingreville et al. [2005] and references therein offer material in support of this argument. 2. For the stage of deducing the adhesion energy, Lau et al. [2002] employed Young's law and the Dupré equation, both of which ignore any effects of elasticity altogether. In a sense, this step defeats the original purpose of the model by treating the adhesion energy as independent of elastic effects (it should, however, be recognized that the value attributed to the spreading parameter, from which the adhesion energy followed, incorporated both surface and elastic effects). 3. A final reservation concerns the use of AFM-measured contact radii. Measurements in the lateral direction potentially bear considerable uncertainty due to AFM tip convolution effect, therefore it would have been preferable to deduce the contact radii from geometry, given the droplet sizes and measured heights.

The above was motivation to seek a way of utilizing such a theory more soundly. I redeveloped in detail the model introduced by Lau et al. [2002], to produce a free energy equation which differs somewhat from theirs due to minor algebraic discrepancies in calculations (resulting in different coefficients in the equation of the elastic contribution to the system's free energy.) For the first time in the literature has such a theory been employed to predict an effective elastic modulus for adsorbed droplets of a range of nanoscopic sizes ($5 - 100$ nm) from their AFM-measured heights (experiments of Lau et al. [2002], Engqvist et al. [2007], and Glynos (Evangelopoulos et al. [2012])). Through a continuum theory approach, as opposed to a microscopic theory, the model was not confined to a particular type of polymeric material, as is, for example, the case with the work of Araujo et al. [2008], where their computer code specifically models the cross-linked elastomeric

structure. We offer an extensive discussion of our findings. These findings carry implications for the appropriateness of such a (continuum) theory for meso- and nanoscale systems and demonstrate its strengths and limitations as we approach nanodroplets of single chains.

When it comes to nanoscale droplet spreading, line tension has been one the of the most popular correction terms to the classical Young's law. Indeed, a proper thermodynamic account involves not only bulk and surface contributions to the free energy of the system, but also a contribution related to the three-phase contact region; and the smaller the length scale concerned, the higher the relative contribution of the latter to the total free energy. One of the first documented references of line tension came with a footnote by Gibbs in one of his papers (Gibbs [1961]), where he introduced it as a lower-dimension analogue of surface tension, with the distinction that not only positive but also negative values are observable. Line tension has since attracted much theoretical (Rowlinson and Widom [1982], Toshev et al. [1988], Toshev and Avramov [1993], Getta and Dietrich [1998], Dobbs [1999]), computational (Bresme and Quirke [1998], Ingebrigtsen and Toxvaerd [2007], Werder et al. [2003], Djikaev [2005]), and experimental (Gaydos et al. [1990], Toshev et al. [1988], Li [1996], Wang et al. [2001], Pompe and Herminghaus [2000]) attention, creating at the same time a lot of controversy, not just over its sign (Rosso [2005], Amirfazli and Neumann [2004]), but also over its definition and what has been at one time or another perceived by the concept (Schimmele et al. [2007], Schimmele and Dietrich [2009]) including arguments, in the extreme case, for its redundancy (Ward and Wu [2008]), provided other effects and trends that influence spreading are properly accounted for. It seems that the consensus is currently led towards the view that line tension is more complicated than what originally thought of (Schimmele et al. [2007]) and its measurement is extremely sensitive to the details of the model employed (Schimmele et al. [2007]) and experimental procedure followed (Li [1996]), even for a simple liquid. Only a couple authors have yet attempted to study the three-phase contact line in polymeric systems (Liu et al. [1999], Vandecan and Indekeu [2008]), and they do not deal with pure polymers but chains in solution or colloidal suspension. The problems that arose with incorporating line tension into the present model are reported in the relevant discussion sections. While I am not dismissive of the possibility of line tension effects altogether, treating them goes beyond the scope of this work. It is, however, quite telling, having mentioned the above, that the model predicts reasonable results down to ~ 10 nm without taking line tension into account.

Scale invariance does not absolutely hold regarding (intrinsic) properties of ma-

terials. Specifically the elastic modulus, which concerns the present study, has been shown, not just for polymers, to become size-dependent in the vicinity of the nanoscopic scale, through both experiment (Cuenot et al. [2003, 2000], Chen et al. [2006], Shin et al. [2006], Tan et al. [2007], Villain et al. [2002], Salvadori et al. [2003], Nilsson et al. [2004], Kopycinska-Muller et al. [2005], Xiong et al. [2006]) and theory (Streitz et al. [1994], Shenoy [2005], Zhou and Huang [2004], Widom [1991], Miller and Shenoy [2000], Yang and Zhao [2007], Villain et al. [2004], Gu et al. [2007]), supporting either stiffening (Cuenot et al. [2000], Chen et al. [2006], Shin et al. [2006], Tan et al. [2007]) or softening (Villain et al. [2002], Salvadori et al. [2003], Nilsson et al. [2004], Kopycinska-Muller et al. [2005], Xiong et al. [2006]) with decrease in size. As a result, nanoscale-sized materials do not exhibit the behaviour anticipated through an analysis of their macroscopic counterparts. And polymers are a marked example (Forrest and Dalnoki-Veress [2001], Alcoutlabi and McKenna [2005]). Whereas most investigations on polymers have focused on glass transition temperature (Ellison and Torkelson [2003], Alcoutlabi and McKenna [2005]) and structural relaxation (Akabori et al. [2003], Priestley et al. [2005]), their elastic properties —especially of compliant polymers— have received less attention (Torres et al. [2009]), owing to experimental challenges, such as the measuring instrument's poor sensitivity (Pharr and Oliver [1992], Miyake et al. [2006]), imaging resolution (Du et al. [2001]), and its interaction with the sample (Briscoe and Sebastian [1996]). Polymer molecules have an associated characteristic size, the r.m.s. end-to-end distance, which scales as a rational power of the polymerization index. This inherent length scale introduces the possibility of chain confinement effects as the system size becomes smaller than the unperturbed molecular size (Forrest and Dalnoki-Veress [2001]). Confinement effects, deformation-induced structure rearrangement effects (Amitay-Sadovsky et al. [2002]), and substrate interactions (Tsui and Pharr [1999], Miyake et al. [2006]), are key mechanical interactions that cause the elastic modulus to deviate from that of the corresponding macroscopic system. The present model provides a step towards estimating the elastic modulus via a non-invasive experimental procedure, therefore avoiding a plethora of errors associated with mechanical testing and shedding light on the relation between the material's response and intrinsic effects. The benefits of non-mechanical testing are acknowledged by Torres et al. [2009]. Examination of the elastic modulus of a purely polymeric substance of spherical geometry has not been previously undertaken, except by Ishikawa et al. [2004], who used the direct peeling method with atomic force microscope tip (DPAT) to separate spherical polymer aggregates from a resist pattern and deduced the elastic modulus from the separation force, poten-

tially involving the aforementioned drawbacks of mechanical testing, however. Thin films have received the most attention and considerable work has also been done on small molecules in nanoporous structures (Alcoutlabi and McKenna [2005], Forrest and Dalnoki-Veress [2001]). Glynos et al. [2009] measured the Young's modulus of the shell of microspheres used as ultrasound contrast agents in medicine, revealing a decreasing Young's modulus with increasing size, converging to the expected value for the macroscopic material. Very few authors have investigated individual nanofibers: Tan et al. [2005] examined nanostructural and elastic properties but of a size too large for size effects to be observed; Shin et al. [2006] examined the size-dependency of elasticity and found that the elastic modulus increased exponentially with decreasing fiber diameter below 70 nm; Burman et al. [2008] set the upper limit at 500 nm for observable size dependency, however via a different mechanical testing method.

The rest of Part I is structured as follows: A detailed exposition of the theoretical model is given in Chapter 3, arriving at a free-energy equation which describes the equilibrium state of adsorption. Chapter 4 sees the application of the model on experimental work by Lau et al. [2002] and Engqvist et al. [2007], dealing with $50 - 100$ nm droplets. Chapter 5 repeats a similar process for the experiments of Glynos (Evangelopoulos et al. [2012]), dealing with $5 - 50$ nm droplets. Results and discussion sections are given separately relevant to each set of experiments in the respective chapters. A brief conclusions Chapter 6 brings Part I to a close.

Chapter 3

Theoretical Model

3.1 Geometrical considerations

The geometry of the system is illustrated in Fig. 3.1, where the undeformed spherical droplet (not to scale) is superimposed on the deformed droplet, adsorbed on the substrate. R_0 is the radius of curvature in the undeformed state (e.g. when suspended in the same medium); R, the radius of curvature in the adsorbed state (cap radius); ρ is the horizontal radius of the cap from the spherical symmetry axis; h is the height at the apex; θ is the contact angle between the solid-polymer and polymer-air interface. h and θ can be used equivalently as a measure of deformation upon adsorption, during which the droplet's volume remains constant by assumption of the polymer's incompressibility (Brown [1999]). The effect of gravity to be negligible compared to surface and elasticity effects in the given size range ($\lesssim 100$ nm), in other words, the adsorbed cap retains a spherical shape. The condition for this to be true is that h be less than the capillary length (Widom [1995]) which is fulfilled in the present case. The volume, V_{cap}, of the adsorbed cap may be found by elementary calculus:[1]

$$\begin{aligned} V_{\text{cap}} &= \int_h^0 \pi\rho^2(h)dh \\ &= \frac{\pi R^3}{3}\left[\cos^3\theta - 3\cos\theta + 2\right] \end{aligned} \tag{3.1}$$

Incompressibility means $V_{\text{cap}} = V_0$, where V_0 is the volume of the same droplet in the undeformed state, and leads to a few useful relations (for which it is required

[1] Detailed derivation in Appendix A.

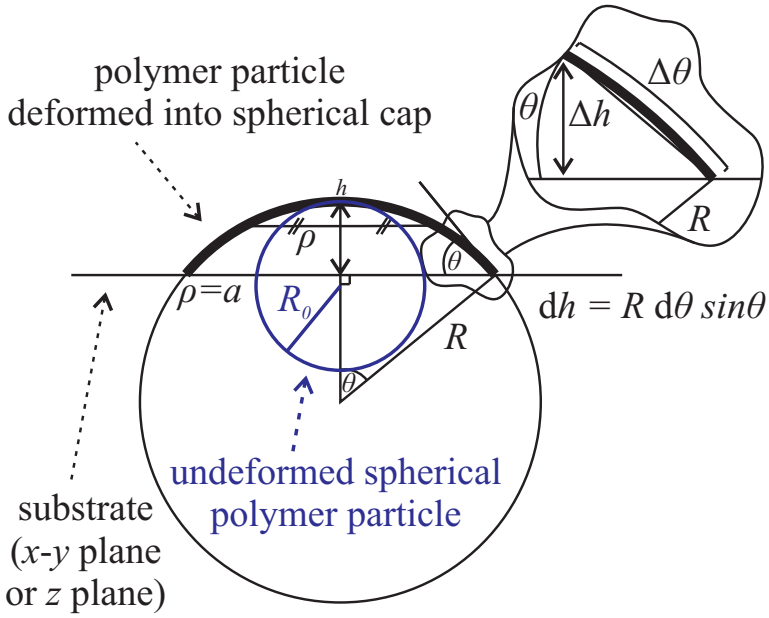

Figure 3.1: Undeformed spherical polymer droplet (blue; not to scale) superimposed on deformed spherical polymer cap (black) adsorbed on substrate. R_0 is radius of curvature in undeformed state; R is the radius of curvature in adsorbed state; ρ is the the horizontal radius of the cap; h is the height at apex; θ is the contact angle between solid-polymer and polymer-air interfaces.

that $\theta \in (0, \pi)$, so that infinities are avoided):

$$R^3 = \frac{4R_0^3}{\cos^3\theta - 3\cos\theta + 2}, \tag{3.2}$$

giving R as $R(R_0, \theta)$, or,

$$R = \frac{4R_0^3 + h^3}{3h^2}, \tag{3.3}$$

giving R as $R(R_0, h)$, from the geometric fact of $\cos\theta = (R - h)/R$, which, itself, may be re-expressed as

$$\cos\theta = \frac{4R_0^3 - 2h^3}{4R_0^3 + h^3}, \tag{3.4}$$

if Eq. (3.3) is applied to it.

It is important to realize that Eqs. (3.2) and (3.3) are basically geometric relations, bearing sphericality and incompressibility as the only physical assumptions. They relate a sphere and spherical cap of equal volumes. Incompressibility, viewed as a constraint in the context of the above geometrical construction, reduces the degrees of freedom associated with the adsorbed state by one: given an initial R_0, a compressible droplet's adsorbed shape and size can be fully specified given R and h (or θ, equivalently), which can be seen mathematically by Eq. (3.1), whereas an incompressible droplet's adsorbed shape and size can be fully specified given only h (or θ, equivalently), seen by Eq. (3.4), which then becomes a measure of the deformation suffered upon adsorption. Here, h is directly measured experimentally by AFM.

3.2 Physical considerations

For our system, the polymer droplet residing on the solid and surrounded by air, we write the condition for equilibrium in terms of the Gibbs free energy differential:

$$dG = dU_{\mathrm{E}} + dU_{\mathrm{I}} = 0 \tag{3.5}$$

dU_{E} represents contributions from elastic deformation and dU_{I} from interfaces, with fluctuations about the equilibrium state. For a simple liquid droplet, $dU_{\mathrm{E}} = 0$, and (3.5) becomes the classical Young's law. Clearly, a polymer droplet behaves differently, for any elastic deformation induced by interfacial effects results in stress development across the bulk in opposition to that deformation, due to the material's elastic nature. In what follows expressions are constructed for U_{E} and U_{I} in terms

of parameters which physically characterize the system and its interactions with the environment.

To construct U_{E} the normal to the surface (z) component of the adsorption-induced deformation field of the droplet, $u_z(\rho)$, is first considered as a function of the radial distance, ρ, from the centre of the (circular) area of contact between the droplet and the substrate:

$$u_z(\rho) = \delta - R_0\left[1 - \sqrt{1-(\rho/R_0)^2}\right] \simeq \delta\left(1 - \frac{\rho^2}{2\delta R_0}\right) \tag{3.6}$$

$\delta \equiv 2R_0 - h$ is the magnitude of deformation at the centre. The middle section of Eq. (3.6) follows by geometry,[2] while the right-hand side is simply a first-order binomial approximation. Equation (3.3) allows one to express the contact radius, $\rho = a$, as a function of the undeformed radius, R_0, and the height of the cap, h:

$$\begin{aligned} a &= R\sin\theta \\ &= \left(\frac{4R_0^3 + h^3}{3h^2}\right)\left(1 - \left(\frac{R-h}{R}\right)^2\right)^{1/2} \\ &= \left(\frac{8R_0^3}{3h} - \frac{h^2}{3}\right)^{1/2} \end{aligned} \tag{3.7}$$

From contact mechanics (Johnson [1985]), application of an external stress of the form

$$\sigma(\rho) = \sigma_0(1-\rho^2/a^2)^{-1/2} + \sigma_1(1-\rho^2/a^2)^{1/2}, \quad \rho < a, \tag{3.8}$$

on the surface of a semi-infinite half-space elastic medium, creates the displacement field

$$u_z(\rho) = \frac{\pi a}{K_{\mathrm{P}}}\left[\sigma_0 + \frac{1}{2}\sigma_1\left(1-\rho^2/a^2\right)\right], \tag{3.9}$$

which is of the form of Eq. (3.6), where $K_{\mathrm{P}} \equiv \frac{E_{\mathrm{D}}}{(1-\nu^2)}$ is a measure of stiffness, E_{D} is Young's modulus, and ν is Poisson's ratio. An advantage of considering a theoretical stress field comprising terms of the form $\sigma(\rho) = \sigma_i(1-\rho^2/a^2)^n$ is that it allows one to calculate analytic solutions for $u_z(\rho)$. The particular values of $n = -1/2$ and $n = 1/2$ correspond to *uniform normal displacement* of the loaded circle and *Hertz pressure*, respectively. The former is the pressure that would arise on the face of a flat-ended, frictionless cylindrical punch pressed squarely against an elastic half-space, while the latter is the pressure exerted between two frictionless

[2] Detailed derivation in Appendix A.

elastic solids of revolution (Johnson [1985]). Comparing the geometrical argument for the displacement field, Eq. (3.6), with the elasticity theory result, Eq. (3.9), in terms of powers of ρ allows us to determine values for the coefficients σ_0 and σ_1:

$$\begin{aligned} \sigma_0 &= \frac{K_{\mathrm{P}}}{\pi}\left(\frac{\delta}{a} - \frac{a}{2R_0}\right) \\ \sigma_1 &= \frac{K_{\mathrm{P}}}{\pi}\left(\frac{a}{R_0}\right) \end{aligned} \tag{3.10}$$

From a generic definition of work an expression can be formed for the elastic energy of deformation due to a stress field $\sigma_z(\mathbf{x})$ in the z-direction inducing a deformation field $u_z(\mathbf{x})$ over an area D. $\mathbf{x}$ represents any point in the z plane, and k is a proportionality constant (in keeping with linear elasticity):

$$\begin{aligned} U_E &= \int_D \int_{\text{strain}} \sigma_z(\mathbf{x}) \\ &= \int_D \int_0^{u_z} \sigma_z(\mathbf{x}) du_z \\ &= \int_D \int_0^{u_z} k u_z(\mathbf{x}) du_z \\ &= \frac{1}{2}\int_D k u_z^2(\mathbf{x}) = \frac{1}{2}\int_D \sigma_z(\mathbf{x}) u_z(\mathbf{x}) \end{aligned} \tag{3.11}$$

The above can be used as general formulae for the elastic energy required to attain $u_z(\mathbf{x})$ given k or $\sigma_z(\mathbf{x})$. With D being the circular contact area between droplet and substrate, Eq. (3.11) can be conveniently re-expressed in polar coordinates:

$$\begin{aligned} U_E &= \frac{1}{2}\int_{\rho=0}^{a}\int_{\phi=0}^{2\pi} \sigma_z(\rho) u_z(\rho) \rho d\phi d\rho \\ &= \pi \int_0^a \sigma_z(\rho) u_z(\rho) \rho d\rho. \end{aligned}$$

Using Eqs. (3.6) and (3.8) (or (3.9)) and by change of variables[3]

$$\begin{aligned} U_E &= \pi \int_0^a \rho d\rho \left[\sigma_0 \left(1 - \rho^2/a^2\right)^{-1/2} + \sigma_1 \left(1 - \rho^2/a^2\right)^{1/2}\right] \delta\left(1 - \rho^2/(2R_0)\right) \\ &= \pi a^2 \delta \sigma_0 - \frac{\pi a^4 \sigma_0}{3R_0} + \frac{\pi a^2 \delta \sigma_1}{3} - \frac{\pi a^4 \sigma_1}{15 R_0}. \end{aligned} \tag{3.12}$$

[3]Detailed Derivation in Appendix A.

Substituting in coefficients (3.10)

$$U_{\mathrm{E}} = \pi a^2 \delta \frac{K_{\mathrm{P}}}{\pi}\left[\frac{\delta}{a} - \frac{a}{2R_0}\right] - \frac{\pi a^4}{3R_0}\frac{K_{\mathrm{P}}}{\pi}\left[\frac{\delta}{a} - \frac{a}{2R_0}\right] + \frac{\pi a^2 \delta}{3}\frac{K_{\mathrm{P}}}{\pi}\left[\frac{a}{R_0}\right] - \frac{\pi a^4}{15R_0}\frac{K_{\mathrm{P}}}{\pi}\left[\frac{a}{R_0}\right]$$

$$= K_{\mathrm{P}}\left[\delta^2 a - \frac{\delta}{2}\frac{a^3}{R_0} + \frac{1}{10}\frac{a^5}{R_0^2}\right]. \tag{3.13}$$

Ultimately, substituting Eq. (3.7), K_{P}, and δ into the above gives U_E in terms of R_0, h, E_{D}, and ν:

$$\Rightarrow U_{\mathrm{E}} = \frac{E_{\mathrm{PG}}}{(1-\nu^2)}\left[(2R_0 - h)^2\left(\frac{8R_0^3}{3h} - \frac{h^2}{3}\right)^{1/2} - \frac{(2R_0 - h)}{2}\frac{\left(\left(\frac{8R_0^3}{3h} - \frac{h^2}{3}\right)^{1/2}\right)^3}{R_0} + \frac{1}{10}\frac{\left(\left(\frac{8R_0^3}{3h} - \frac{h^2}{3}\right)^{1/2}\right)^5}{R_0^2}\right] \tag{3.14}$$

(3.14) expresses the contribution to free energy due to the droplet experiencing deformation quantified by h, given R_0.

To construct U_{I} we firstly note that the excess free energy contribution due to all interfaces can be expressed in an additive manner:

$$U_{\mathrm{I}} = \gamma_{\mathrm{P}} A + (\gamma_{\mathrm{SP}} - \gamma_{\mathrm{S}})O \tag{3.15}$$

A is the polymer-gas interfacial area with associated interfacial tension γ_{P}, and O

is the polymer-substrate interfacial area with associated interfacial tension γ_{SP}.

$$\begin{aligned} A &= \int_{\theta=0}^{\theta=\theta} 2\pi\rho(\theta)Rd\theta \\ &= 2\pi\int_0^{\theta} R\sin\theta Rd\theta \\ &= 2\pi R^2\int_0^{\theta}\sin\theta d\theta \\ \Rightarrow A &= 2\pi R^2[-cos\theta]_0^{\theta} \\ &= 2\pi R^2(1-\cos\theta), \end{aligned}$$

and

$$O = \pi(R\sin\theta)^2.$$

Using Eq. (3.3) and geometry (Fig. 3.1) enables one to re-express the above in terms of the undeformed radius, R_0, and the cap height, h:

$$\begin{aligned} A &= 2\pi\left(\frac{4R_0^3+h^3}{3h^2}\right)^2(1-\cos\theta) \\ O &= \pi\left(\frac{4R_0^3+h^3}{3h^2}\right)^2\sin^2\theta \end{aligned}$$

$$\begin{aligned} \Rightarrow A &= 2\pi\left(\frac{4R_0^3+h^3}{3h^2}\right)^2\left(1-\frac{R-h}{R}\right) \\ O &= \pi\left(\frac{4R_0^3+h^3}{3h^2}\right)^2\left(1-\left(\frac{R-h}{R}\right)^2\right) \end{aligned}$$

$$\begin{aligned} \Rightarrow A &= 2\pi\left(\frac{4R_0^3+h^3}{3h^2}\right)^2\left(1-\frac{\left(\frac{4R_0^3+h^3}{3h^2}\right)-h}{\left(\frac{4R_0^3+h^3}{3h^2}\right)}\right) \\ O &= \pi\left(\frac{4R_0^3+h^3}{3h^2}\right)^2\left(\frac{2\left(\frac{4R_0^3+h^3}{3h^2}\right)h-h^2}{\left(\frac{4R_0^3+h^3}{3h^2}\right)^2}\right) \end{aligned}$$

$$\Rightarrow A = 2\pi \left[\left(\frac{4R_0^3 + h^3}{3h^2} \right)^2 - \left(\left(\frac{4R_0^3 + h^3}{3h^2} \right)^2 - h \left(\frac{4R_0^3 + h^3}{3h^2} \right) \right) \right]$$

$$O = 2\pi \left(\frac{4R_0^3 + h^3}{3h^2} \right) h - \pi h^2$$

$$\Rightarrow A = \frac{8\pi R_0^3}{3h} + \frac{2\pi h^2}{3}$$

$$O = \frac{8\pi R_0^3}{3h} - \frac{\pi h^2}{3}$$

Finally, substituting A and O back into Eq. (3.15) yields

$$U_{\mathrm{I}} = \left(\frac{8\pi R_0^3}{3h} + \frac{2\pi h^2}{3} \right) \gamma_{\mathrm{PG}} + \left(\frac{8\pi R_0^3}{3h} - \frac{\pi h^2}{3} \right) \gamma_{\mathrm{SP}} - \left(\frac{8\pi R_0^3}{3h} - \frac{\pi h^2}{3} \right) \gamma_{\mathrm{SG}}$$

$$= \left(\frac{8\pi R_0^3}{3h} \right) \gamma_{\mathrm{PG}} + \left(\frac{\pi h^2}{3} \right) \gamma_{\mathrm{PG}} + \left(\frac{8\pi R_0^3}{3h} \right) \gamma_{\mathrm{SP}}$$

$$= -\left(\frac{\pi h^2}{3} \right) \gamma_{\mathrm{SP}} + \left(\frac{\pi h^2}{3} \right) \gamma_{\mathrm{SG}} - \left(\frac{8\pi R_0^3}{3h} \right) \gamma_{\mathrm{SG}}$$

$$= -\frac{8\pi R_0^3}{3h} \left(-\gamma_{\mathrm{PG}} - \gamma_{\mathrm{SP}} + \gamma_{\mathrm{SG}} \right) + \frac{\pi h^2}{3} \left(2\gamma_{\mathrm{s}} - \gamma_{\mathrm{SP}} + \gamma_{\mathrm{SG}} \right)$$

$$= -\frac{8\pi R_0^3}{3h} (S) + \frac{\pi h^2}{3} (3\gamma_{\mathrm{PG}} + S)$$

$$= -\frac{4\pi}{3} R_0^2 S \left(\frac{2R_0}{h} \right) + \frac{4\pi}{3} R_0^2 (3\gamma_{\mathrm{PG}} + S) \left(\frac{h}{2R_0} \right)^2, \tag{3.16}$$

where $S = \gamma_{\mathrm{S}} - (\gamma_{\mathrm{SP}} + \gamma_{\mathrm{P}})$ is the spreading parameter defined in Subsection 2.1.5. Equation (3.16) expresses the excess contribution to free energy due to the existence of interfaces. U_{I} depends on the chemical nature of the interfaces involved, quantified through γ_{P} and S, and also, being an extensive quantity, on the interface sizes, quantified through R_0 and h.

3.3 Minimization

As the system approaches equilibrium, fluctuations of the droplet's height, h, progressively decrease about an equilibrium value which minimizes free energy, expressed in terms of a set of parameters. We, therefore, minimize Eq. (3.5) with respect to h, after inserting Eq. (3.14) and Eq. (3.16), to recover an expression relating the equilibrium value of h to parameters R_0, γ_{P}, S, E_{D}, ν:

$$\frac{d\Phi}{dh} = \frac{E_{\mathrm{D}}}{(1-\nu^2)} \left[\frac{(2R_0-h)^2 \left(-\frac{2h}{3} - \frac{8R_0^3}{3h^2}\right)}{2\left(-\frac{h^2}{3} + \frac{8R_0^3}{3h}\right)^{1/2}} - 2(2R_0-h)\left(-\frac{h^2}{3} + \frac{8R_0^3}{3h}\right)^{1/2} - \frac{3(2R_0-h)\left(-\frac{2h}{3} - \frac{8R_0^3}{3h^2}\right)\left(-\frac{h^2}{3} + \frac{8R_0^3}{3h}\right)^{1/2}}{4R_0} + \frac{\left(-\frac{h^2}{3} + \frac{8R_0^3}{3h}\right)^{3/2}}{2R_0} + \frac{\left(-\frac{2h}{3} - \frac{8R_0^3}{3h^2}\right)\left(-\frac{h^2}{3} + \frac{8R_0^3}{3h}\right)^{3/2}}{4R_0^2} \right] + \frac{8\pi R_0^3 S}{3h^2} + \frac{2}{3}h\pi(S+3\gamma_{\mathrm{P}}) = 0 \tag{3.17}$$

As mentioned earlier, when some geometrical facts were established, given R_0, h uniquely specifies the geometry of an adsorbed state. In the physical context, R_0 may depend on the length and number of chains in a droplet, its density, and the solvent conditions, while h depends (according to the present framework) on the set of physical parameters γ_{P}, S, E_{D}, and ν. For experimental situations where h was measured reliably (AFM-measured) and γ_{P}, S, and ν were known or estimated, Eq. (3.17) was solved for E_{D}. Findings are presented in Chapters 4 and 5.

Following up from Eq. (3.9), where E_{D} was defined as Young's modulus in the context of the specific contact mechanics theory, it should be noted that in real terms and in the context of the present experiments E_{D} can be interpreted as a relaxation modulus. Upon adsorption, the viscoelastic polymer droplets are given time to relax, during which the internal stress decreases. E_{D} will, therefore, represent a relaxation modulus relevant to the time scale of each experiment.

Chapter 4

$\sim$ 100 nm – sized droplets

4.1 Experiments of Lau et al. [2002]

4.1.1 Description

Lau et al. [2002] performed an experimental investigation of the spreading of $\sim$ 100 nm-sized isolated latex droplets on a silicon substrate at room temperature. Using an AFM in contact mode, the equilibrium height of the adsorbed latex droplets was measured. The latexes used were formed by a soft core of partially crosslinked styrene-butadiene copolymer molecules, surrounded by a stiffer shell made of carboxylic comonomers. The ratio of styrene to butadiene comonomers in the core allowed for adjustment of the glass transition temperature, T_{g}, of the latex, while the degree of crosslinking, quantified through the gel fraction, GF, allowed for adjustment of the elastic modulus of the core, though the relation between GF and elastic modulus is not quantitative, because the crosslinking reaction is accompanied by chain scission.

Table 4.1 contains data provided by Lau et al. [2002] that were used in the present investigation. Columns, from left to right, display: name of latex, in the form SB-(T_{g})-GF; gel fraction, GF; glass transition temperature, T_{g}; adsorbed droplet height, h; droplet radius in the undeformed state, R_0; polymer surface tension in air, γ_{P}; elastic modulus, E_{M}, of a polymer film of macroscopic dimensions, formed by slow evaporation of the water of the latex suspension and exposing an array of close-packed droplets adhering together by their shells.

Latex	GF (%)	T_g (°C)	h (nm)	R_0 (nm)	γ_P (mJ · m^{-2})	E_M (MPa)
SB-(-2)-75	75	−2	26	87.5	53	0.63
SB-(11)-75	75	11	39	83.5	46	1.35
SB-(28)-75	75	28	49.5	83.5	48	1.92
SB-(-2)-92	92	−2	46	74.0	54	0.6
SB-(-8)-43	43	−8	15.8	82.0	48	2.02

GF : gel fraction
T_g : glass transition temperature
h : maximum height of adsorbed droplet
R_0 : radius of droplet in undeformed state
γ_P : surface tension of polymer in air
E_M : elastic modulus of macroscopic film

Table 4.1: Latexes in the form SB-(T_g)-GF with properties as reported by Lau et al. [2002].

4.1.2 Results

In order for our model, (3.17), to be employed for the prediction of the elastic modulus, E_D, of the polymer droplets we also required values for the spreading parameter, S, and Poisson's ratio, ν. As far as the Poisson ratio is concerned, a good approximation is $\nu = 0.5$ for rubbery polymers (Riande et al. [2000]). As far as the spreading parameter is concerned, it can be seen from its definition, Eq. (2.5), that it was required to individually predict the surface tension of the silicon substrate, γ_S, and the substrate-polymer interfacial tension, γ_{SP}.

Classical liquid-drop-on-surface and immersion calorimetry experiments (Busscher et al. [1986], Douillard et al. [1995], Malandrini et al. [1997], Médout-Marère et al. [1998]) lead to an estimate of $\gamma_S = 254$ mJ/m^2 for the surface tension of a freshly prepared, clean silicon surface, with a native oxide coating, always forming on bare silicon exposed to oxygen-containing environment. This value is also compatible with Portigliatti et al. [2000], where there is reference to the same experimental system as with Lau et al. [2002].

To estimate the substrate-polymer interfacial tension, γ_{SP}, a mechanism is required that allows prediction of interfacial tension based on the respective surface

tensions of the surfaces comprising the interface. There exist three basic semi-empirical candidate models: the model of Girifalco and Good [1957], the oldest and dating back to 1957; the model of Fowkes [1961, 1963], which came only a few years later; and the model of van Oss, Chaudhury, and Good (van Oss et al. [1987]) (vOCG), a more modern take, of the late eighties. All three are based on the assumption that surface tension is a direct measure of intermolecular interactions in a given material, while the last two further assume surface tension as consisting of independent additive components, each corresponding to a different type of intermolecular interaction, for which reason they are known as surface tension component (STC) models (for completeness, we ought to mention the most recent improvement of the vOCG model (van Oss et al. [1987]) by Lee (Lee [2001]) in 2001, whereby the basicity catastrophe is cured and the adsorbed vapour film pressure is taken into account). Throughout this study all three will be used, each depending on the available data for each set of experiments under examination (Lau et al. [2002], Engqvist et al. [2007], and Glynos (Evangelopoulos et al. [2012])). For the present case we employed the model of Girifalco and Good [1957]. It essentially sums up the independent work of many authors (Freundlich [1922], Fowler [1937], Fowler and Guggenheim [1939], Kirkwood and Buff [1949], Donahue and Bartell [1952]) in the following statement:

$$\gamma_{12} = \gamma_1 + \gamma_2 - 2\Phi(\gamma_1\gamma_2)^{1/2}, \tag{4.1}$$

where Φ (precisely defined therein) is a ratio involving the energies of adhesion and cohesion for the two phases involved, equal to a constant, and characteristic of the system. In simpler terms, Φ translates into a correction factor deviating from unity to account for mismatch in intermolecular interaction type between the two media. Carboxyl groups of the droplets' shells carry both a basic (H-bond accepting) and an acidic (H-bond donating) group, while styrene-butadiene of the soft core is somewhat basic due to the π-bonds of the aromatic ring double bonds and of the carbon-carbon double bond of the alkene group. Its cohesion is then brought about by dispersive interactions as well as acid/base ones, which explains its fairly high surface tension compared to most polymers. External carboxyl groups will tend to bury themselves into the core so as to minimize the surface energy but probably not all groups will have a chance to do that. The naturally oxidized silicon substrate carries SiO, Si_2O_3 and other oxides, and is surrounded by a great many silanol ($OH-$) and siloxane (R_2SiO-) groups that make it acidic and basic in the Lewis sense. As a result, the latex droplets will adhere well through H-

Latex	S (mJ · m^{-2})	E_{D} (MPa)
SB-(-2)-75	124.2	1.04
SB-(11)-75	122.5	3.07
SB-(28)-75	123.1	5.10
SB-(-2)-92	124.4	6.37
SB-(-8)-43	123.1	0.44

S : spreading parameter
E_{D} : elastic modulus of nanoscopic droplet

Table 4.2: Calculated data from our theory using Table 4.1 and literature-based data.

bonds, dispersive and polar van der Waals forces, utilizing all of their intermolecular force mechanisms, and the same will be true for silica. This means that we can approximately set $\Phi = 1$ in (4.1) and express that as $\gamma_{\mathrm{SP}} = \gamma_{\mathrm{S}} + \gamma_{\mathrm{P}} - 2(\gamma_{\mathrm{S}}\gamma_{\mathrm{P}})^{1/2}$. Rewriting the spreading parameter, Eq. (2.5), in terms of the above gives $S = -2\gamma_{\mathrm{P}} + 2(\gamma_{\mathrm{S}}\gamma_{\mathrm{P}})^{1/2}$, which was evaluated upon numerical substitution of γ_{S} and γ_{P} for each droplet type (Table 4.1).

Having established all required parameters, h, R_0, γ_{P}, S, and ν were substituted into (3.17), which was solved with respect to E_{D}, for a prediction of the adsorbed droplet's elastic modulus. Table 4.2 summarizes all calculated data. Columns, left to right, display: name of latex; spreading parameter, S; elastic modulus of the droplet, E_{D}.

4.1.3 Discussion

As a preliminary test, Eq. (3.7) was employed to geometrically deduce the contact radii of the adsorbed droplets, a_{geo}, given their corresponding undeformed radii, R_0, and heights, h, as reported in Table 4.1. The geometrical predictions, a_{geo}, are compared against the AFM-measured contact radii, a, of Lau et al. [2002] in Fig. 4.1. For a tip considerably smaller than the object mapped, the AFM topography will contain minimal artifacts revealing almost the real profile of the object.

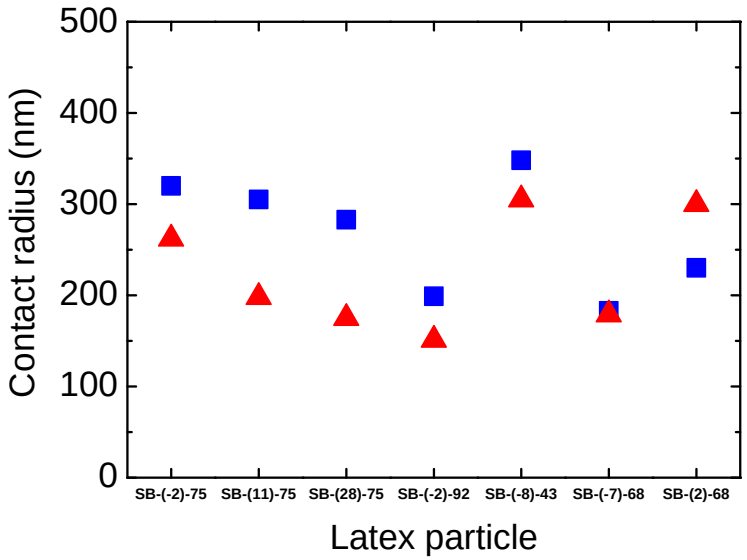

Figure 4.1: Comparison between geometrical predictions, a_{geo} (triangles), and AFM-measured contact radii of Lau et al. [2002], a (squares), in support of spherical geometry assumption for the adsorbed latex droplets.

However, in this case the tip radius of curvature is reported as 35 ± 5nm (Portigliatti et al. [2000]), which is comparable in size to the measured nanodroplets, and will, therefore, induce a significant convolution effect making apparent lateral sizes larger. While the systematically larger (except one case, out of seven) experimentally determined radii are attributed to the convolution effect, the clear qualitative agreement supports the assumption of the spherical geometry of the adsorbed cap-shaped droplet, precisely because the function $a_{\text{geo}} = a_{\text{geo}}(R_0, h)$ (Eq. (3.7)) is constructed based on that assumption. Viewing sphericality as a necessary, but not sufficient, condition for equilibrium, the results of Fig. 4.1 suggest that equilibrium is likely.

From the E_{M} and E_{D} columns of Table 4.1 and Table 4.2, respectively, Fig. 4.2 can be generated. In comparing the two data sets, it is seen that the elastic moduli of the macroscopic strips generally lie, in value, below those of the nanoscopic droplets. The structure of the single droplet is different from that of the film, which is made up of an array of close-packed droplets adhering together by their shells, and one should not anticipate a direct comparison between E_{M} and E_{D}.

Both E_{M} and E_{D} lie within the expected range for rubbery materials in general, $10 - 10,000$ kPa, to account for a range of chemical compositions, material formation processes, ambient conditions, etc. As far as E_{D} is concerned, this is encouraging because it means the model returns reasonable estimates. Kan and

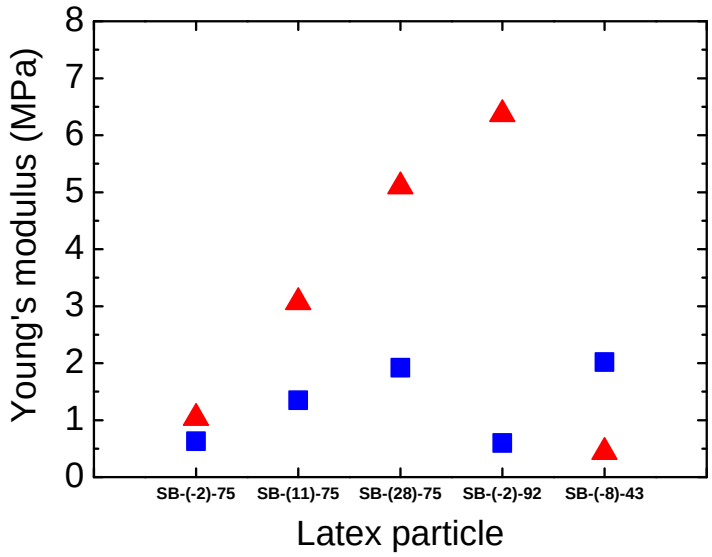

Figure 4.2: Comparison between E_{M} (squares) and E_{D} (triangles).

Blackson [1996] have specifically measured elastic moduli for a series of carboxylated styrene-butadiene latex films and found it to be monotonically decreasing from 1 GPa to 0.1 MPa with a temperature increase from -10°C to 150°C, a range covering temperatures both below and above the glass transition temperature of the latex.

The trend exhibited by E_{M} as measured by Lau et al. [2002] is *only generally* supported by the gel fraction, GF, and glass transition temperature, T_{g}, data for the latexes, while the trend exhibited by E_{D} as calculated with the present model is in *complete agreement* with GF and T_{g}. GF corresponds to the degree of crosslinking in the core, and is defined as the ratio of insoluble species remaining after swelling of the droplets in a good solvent of styrene-butadiene copolymers (Lau et al. [2002]). The larger the GF, the higher the degree of crosslinking and, hence, the stiffness of the material, however not in a known quantitative fashion, because the crosslinking reaction is accompanied by chain scission (Lau et al. [2002]). A higher T_{g} also increases stiffness. SB-(-2)-75, SB-(11)-75, and SB-(28)-75, all share the same GF, therefore we can say that the increasing T_{g} is in accord with both E_{M} and E_{D} increasing. A comparison between SB-(-2)-75 and SB-(-2)-92 should require the latter to exhibit a higher elastic modulus. This is not seen with the measured E_{M} of Lau et al. [2002], but agrees with the prediction of E_{D}. As far as SB-(-8)-43 is concerned, having the both the lowest T_{g} and GF, it is expected to be the least stiff.

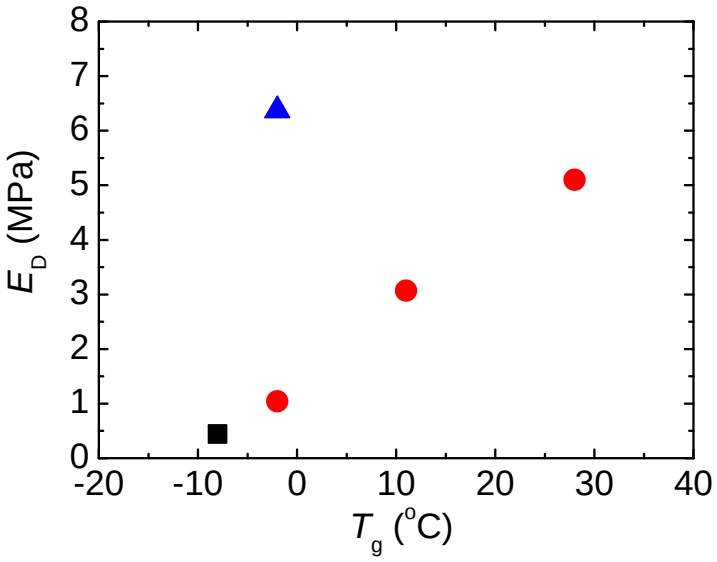

Figure 4.3: Predicted moduli for the adsorbed polymer droplets plotted against glass transition temperature for three structural classes: GF=43% (square), GF=75% (circles), and GF=92% (triangle).

Indeed, this is observed with the smallest calculated modulus of $E_{\mathrm{D}} = 0.44$ MPa, but does not agree with Lau et al. [2002] $E_{\mathrm{M}} = 2.02$ MPa. These inconsistencies regarding SB-(-2)-92 and SB-(-8)-43 are attributed to the fact that E_{M} refers to the corresponding film, which, by construction, contains interface between the close-packed constituent droplets, while the E_{D} calculated directly from AFM data is completely compatible with the materials' properties.

In Fig. 4.3, we offer E_{D} against T_{g}, where we have divided points into three classes based on GF. In the presence of more data we would expect GF=43% points to generally lie in an area below GF=75% points, and GF=75% below GF=92% points. This is generally observed with the few data at our disposal. Also, we would expect a monotonic increase of E_{D} with increasing T_{g} within the same GF class, which is observed with the few data of GF=75%.

All in all, data support that the equilibrium shape of a polymer droplet does not depend only on surface forces, as for the simple liquid case, but is greatly affected by the elastic modulus of the material. Data pertaining to the polymeric droplets' structure and material properties are in good numerical agreement with the present model's predictions. As a final remark following from the introductory note concerning line tension, incorporating that as a one-dimensional analogue of surface tension (Gibbs [1961]) in the present model while keeping the elastic modulus constant at its bulk value resulted in unreasonably high predicted values,

of the order of $10^{-8}\mathrm{Jm}^{-1}$, 3 to 5 orders of magnitude larger than expected for similar systems (Vandecan and Indekeu [2008], Seemann et al. [2001]).

4.2 Experiments of Engqvist et al. [2007]

4.2.1 Description

Engqvist et al. [2007] investigated the effects of temperature, time, and preparation method on the adsorption of isolated styrene-acrylic latex droplets on a silicon substrate. Three types of styrene-acrylic latexes were used: L_{-20}, L_{20}, and L_{60}, the subscripts denoting glass transition temperatures of -20°C, 20°C, and 60°C, respectively. Following evaporation of the solvent, these latexes received different treatments during adsorption. One sample of L_{-20} was left for 1 week at room temperature (RT), another was additionally ultrafiltrated (UF), while a third ultrafiltrated and left for 7 weeks at room temperature. One sample of L_{20} was given 48 hours to adsorb at room temperature, while a second a night at 105°C. L_{60} was left at 70°C for 60 hours. AFM imaging was performed at 23°C and 50% RH.

Samples, treatments, and all data provided by Engqvist et al. [2007] that we use are summarized in Table 4.3. Columns, left to right, display: name of latex, in the form $\mathrm{L}_{T_\mathrm{g}}$, where T_g is the glass transition temperature, followed by treatment description; glass transition temperature, T_g; adsorbed droplet height, h; droplet radius in the undeformed state, R_0; polymer surface tension in air, γ_P; Poisson's ratio, ν; elastic modulus, E_M, of a polymer film of macroscopic dimensions, formed by slowly evaporating the water of the latex suspension and exposing an array of close-packed droplets adhering together by their shells, *measured exclusively at room temperature* (as opposed to the droplet spreading experiments, performed at various temperatures). It is noted that the R_0 values have come from dynamic light scattering measurements of the droplets in diluted dispersions, where a reported 5% swelling compared to the dry state occurs, resulting in R_0 carrying a small positive error.

4.2.2 Results

In order for the continuum theory model, Eq. (3.17), to be employed for the prediction of the modulus E_D, a value for the spreading parameter, S, was required. To that end, the STC model of vOCG (van Oss et al. [1987, 1988a]) was employed, which the available data in this case deemed as appropriate. This model

Latex	T_g (°C)	h (nm)	R_0 (nm)	γ_P (mJ · m^{-2})	ν	E_M (MPa) (RT)
L_{-20} RT, 1 week	−20	39	98	40	0.5	0.2
L_{-20} UF, RT, 1 week	−20	38	98	40	0.5	0.2
L_{-20} UF, RT, 7 weeks	−20	36	98	40	0.5	0.2
L_{20} RT, 12 h	20	97 †	89	40	0.5	12
L_{20} RT, 48 h	20	86 †	89	40	0.5	12
L_{20} 105°C, overnight	20	51	89	40	0.5	12
L_{60} 70°C, 60h	60	59	107	40	0.5	1243

RT : room temperature
T_g : glass transition temperature
h : maximum height of adsorbed droplet
R_0 : radius of droplet in the non-adsorbed state
γ_P : surface tension of polymer in air
ν : Poisson's ratio of polymer material
E_M : elastic modulus of macroscopic film
† From contact angles reported in Figure 2 of Engqvist et al. [2007], converted to heights through our (3.4).

Table 4.3: Latexes in the form L_{T_g} and treatment (adsorption) conditions with properties as reported by Engqvist et al. [2007].

combines London dispersion, Keesom (dipole-dipole), and Debye (dipole-induced dipole) forces into a single term, "LW" (Lifshitz-van der Waals), resulting in the surface tension component γ^{LW}. Remaining surface tension contributions are attributed to acid-base, "AB", interactions, defined through $\gamma = \gamma^{\mathrm{LW}} + \gamma^{\mathrm{AB}}$ and comprising two complementary kinds of behaviour, from acidic, γ^+, and basic, γ^-, groups, of which γ^{AB} is the geometric mean: $\gamma^{\mathrm{AB}} = 2(\gamma^+\gamma^-)^{1/2}$. Given that an interface composed of two adjacent interfacial regions will have an associated interfacial tension equal to the sum of the surface tensions of those regions as part of the interface (Fowkes [1963]),

$$\gamma_{12} = \gamma_1 + \gamma_2 - 2\left[(\gamma_1^{\mathrm{LW}}\gamma_2^{\mathrm{LW}})^{1/2} + (\gamma_1^+\gamma_2^-)^{1/2} + (\gamma_1^-\gamma_2^+)^{1/2}\right]. \tag{4.2}$$

Regarding the substrate, the relevant literature is the same as with Lau et al. [2002], who also used a silica substrate (Busscher et al. [1986], Douillard et al. [1995], Malandrini et al. [1997], Médout-Marère et al. [1998]), leading to the following values of surface tension components and total surface tension: $\gamma_{\mathrm{S}}^{\mathrm{LW}} = 39\ \mathrm{mJ}\cdot\mathrm{m}^{-2}; \gamma_{\mathrm{S}}^+ = 172\ \mathrm{mJ}\cdot\mathrm{m}^{-2}$; $\gamma_{\mathrm{S}}^- = 78\ \mathrm{mJ}\cdot\mathrm{m}^{-2}; \gamma_{\mathrm{S}} = 254\ \mathrm{mJ}\cdot\mathrm{m}^{-2}$.

Styrene-acrylic latex of the droplets, on the other hand, suggests almost exclusively basic behaviour: the aromatic ring and double bond of styrene are slightly basic, whereas the carbonyl groups of acrylate strongly basic. In this sense, the latex should resemble a mix of poly(methyl methacrylate) (PMMA), polystyrene (PS), or poly(tert-butyl-acrylate) (PtBA), and its γ^- should be significant, while γ^+ should be next to zero (Lee [1996], Madani [2005]). Given the total surface tension (Engqvist et al. [2007]) and an average γ^-/γ ratio of like polymers (Lee [1996]), we have: $\gamma_{\mathrm{P}}^{\mathrm{LW}} = 40\ \mathrm{mJ}\cdot\mathrm{m}^{-2}; \gamma_{\mathrm{P}}^+ \simeq 0\ \mathrm{mJ}\cdot\mathrm{m}^{-2}$; $\gamma_{\mathrm{P}}^- = 9\ \mathrm{mJ}\cdot\mathrm{m}^{-2}; \gamma_{\mathrm{P}} = 40\ \mathrm{mJ}\cdot\mathrm{m}^{-2}$. Rewriting the spreading parameter, (2.5), in terms of the vOCG model, (4.2), gives $S = -2\gamma_{\mathrm{P}} + 2\left[(\gamma_{\mathrm{S}}^{\mathrm{LW}}\gamma_{\mathrm{P}}^{\mathrm{LW}})^{1/2} + (\gamma_{\mathrm{S}}^+\gamma_{\mathrm{P}}^-)^{1/2} + (\gamma_{\mathrm{S}}^-\gamma_{\mathrm{P}}^+)^{1/2}\right]$, which can be evaluated after numerical substitution of the aforementioned tensions.

Having established all required parameters, h, R_0, γ_{P}, S, and ν were substituted into (3.17), and solved with respect to E_{D}, for a prediction of the adsorbed droplet's elastic modulus. Table 4.4 summarizes all calculated data. Columns, left to right, display: name of latex, in the form L_{-20}; spreading parameter, S; modulus of the polymer droplet, E_{D}.

Latex	S (mJ · m^{-2})	E_{D} (MPa)
L_{-20} RT, 1 week	78	1.15
L_{-20} UF, RT, 1 week	78	1.08
L_{-20} UF, RT, 7 weeks	78	0.95
L_{20} RT, 12 h	78	6.62
L_{20} RT, 48 h	78	5.72
L_{20} 105°C, overnight	78	2.89
L_{60} 70°C, 60h	78	2.22

S : spreading parameter
E_{D} : elastic modulus of nanoscopic droplet at treatment temperature

Table 4.4: Calculated data from our theory using Table 4.3 and literature-based data. N.B.: E_{D} refers to treatment temperature and time scale.

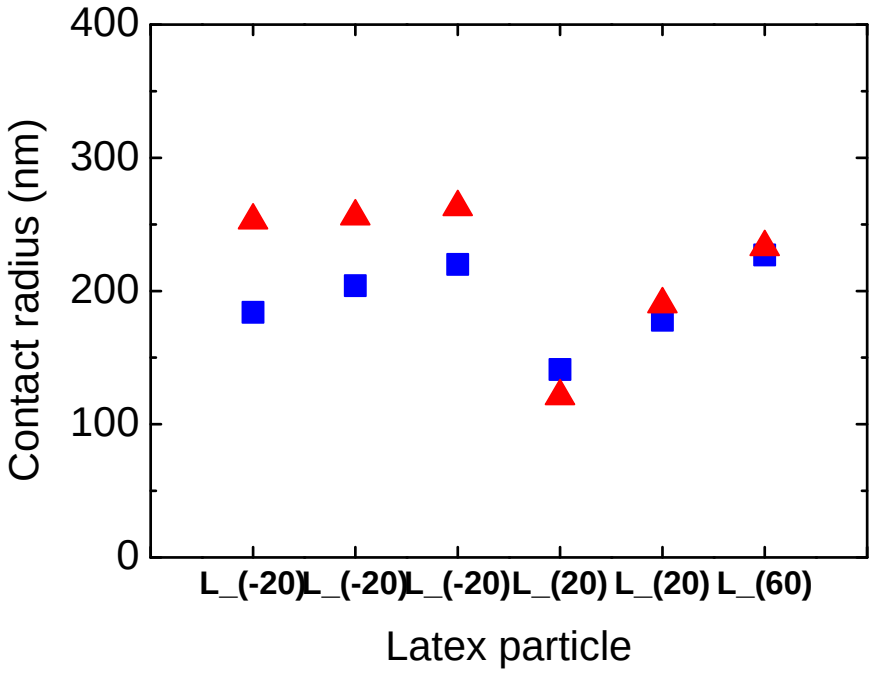

Figure 4.4: Comparison between geometrical predictions, a_{geo} (triangles), and AFM-measured contact radii, a (squares), of Engqvist et al. [2007] in support of spherical geometry assumption for the adsorbed latex droplets.

4.2.3 Discussion

In the same spirit as with the analysis of experiments of Lau et al. [2002], (3.7) was used to geometrically deduce the contact radii of the adsorbed droplets, given their corresponding undeformed radii, R_0, and heights, h, reported in Table 4.3. Our geometrical predictions, a_{geo}, are compared against the AFM-measured contact radii, a, of Engqvist et al. [2007] in Fig. 4.4 (we omit the 'L_{20} RT 12 h' sample, for which no measured contact radius is provided). As was the case with the experimental data of Lau et al. [2002], the clear qualitative agreement supports our assumption of spherical geometry of the adsorbed cap-shaped droplets.

R_0, h, E_{M}, and E_{D} data are collected in Table 4.5 for convenience of comparison. As previously mentioned, a reported 5% swelling compared to the dry state occurs in dispersions, resulting in R_0 carrying a small positive error. This means that for a given measured h the calculated E_{D} carries a small negative error, as the calculations assume larger strain under given surface forces. We, therefore, expect the droplets to be slightly stiffer than what we report. Specifically for the present range of sizes, $+5\%$ systematic error in R_0 will result to about -5% to -10%

Latex	h (nm)	R_0 (nm)	E_{M} (MPa) (RT)	E_{D} (MPa)
L_{-20} RT, 1 week	39	98	0.2	1.15
L_{-20} UF, RT, 1 week	38	98	0.2	1.08
L_{-20} UF, RT, 7 weeks	36	98	0.2	0.95
L_{20} RT, 12 h	97	89	12	6.62
L_{20} RT, 48 h	86	89	12	5.72
L_{20} 105°C, overnight	51	89	12	2.89
L_{60} 70°C 60h	59	107	1243	2.22

h : maximum height of adsorbed droplet
R_0 : radius of droplet in the non-adsorbed state
E_{M} : elastic modulus of macroscopic film at RT
E_{D} : elastic modulus of nanoscopic droplet at treatment temperature

Table 4.5: Collecting data from Engqvist et al. [2007] and our calculations. N.B.: E_{M} refers to RT, whereas E_{D} to the treatment temperature and time scale.

systematic error in our calculated E_{D}. Bearing that in mind, all calculated moduli fall within the expected range for rubbery materials in general, $10 - 10,000$ kPa.

At this point it ought to be stressed that polymeric systems can never be purely elastic or purely viscous, and their modulus will in fact be associated with a time scale (Ferry [1991]). Some observations discussed in the following paragraph relate to that fact. Also to be noted is that, whereas the actual AFM measurements were performed at RT, the adsorbed conformations and all AFM data for that matter correspond to the (higher) treatment temperatures, at which the conformations "froze" upon return to RT in a time frame much shorter than the material's relaxation time.

In the L_{-20} series of 1 week, the ultrafiltration process leads to lower moduli, i.e. samples filtered from surfactants will adsorb more spontaneously, seen from a slightly reduced E_{D}. Comparison of the heights of the two ultrafiltrated L_{-20} samples indicates the existence of viscous effects, though weak, even for as long as 7 weeks after initial deposition of the sample, bringing about a very slow change of conformation towards a state of increased wetting, and portraying the association of larger time scales to lower elastic moduli. The effect is more prominent with the L_{20} sample of RT, pertaining to much shorter time scales of 12 and 48 hours, which resulted in the calculated 6.62 MPa and 5.72 MPa elastic moduli, respectively.

Investigating the effect of temperature, the L_{20} of 12 hours at RT may be compared to that of overnight exposure at 105°C. The substantial impact of exposing a sample to an environment of 85°C above its T_{g} is only evident. Within a time scale of the order of 10 hours, the elastic modulus is brought down to 2.89 MPa, compared to the 6.62 MPa of the RT treatment.

Comparisons can also be made between droplets across different samples. For example, comparing L_{20} to L_{-20} on the basis of them having similar R_0, the higher E_{D} of L_{20} is in agreement with the higher measured h. In a similar spirit, the L_{20} of 105°C may be compared to L_{60} on the basis of their similar h. L_{60} being of greater R_0 implies more spreading, which is in agreement with our calculated lower E_{D}. These comparisons illustrate the mathematical consistency of our model.

A comparison incorporating both temperature and time effects could be made between L_{-20} and L_{60}. The former is treated at over 40°C above its T_{g}, compared to 10°C for the latter, and for much longer periods, justifying its lower E_{D}. Given that the two samples are not very dissimilar in size, their difference in E_{D} is also manifested through their difference in h, L_{-20} experiencing more spreading.

Regarding a comparison between E_{M} measured by Engqvist et al. [2007] and E_{D} calculated from the present model, such can only be made for the L_{-20} sample, since

the relevant experiments for the derivation of both quantities have been performed at equal temperatures. It is seen from Table 4.5 that the droplet appears stiffer than the film, in consistency with the trend observed with Lau et al. [2002] experiments, where almost all droplets appeared stiffer than their corresponding films.

Chapter 5

5–50 nm – sized droplets

5.1 Experiments of Glynos (Evangelopoulos et al. [2012])

5.1.1 Description

Linear polybutadiene (PB) polymer chains of two different molecular weights, 79 kg/mol and 962 kg/mol were dissolved in an appropriate volume of toluene in order for the solutions to maintain concentrations well below the critical overlap concentration, c^* ($c/c^* \simeq 0.3$). Toluene was used as received (Fisher Scientific, Loughborough, UK). In a typical experiment, a freshly cleaved mica surface (Agar Scientific, Essex, UK) was incubated to a polymer solution for several hours. The mica surface was removed from the solution and placed in 100 ml toluene bath for 24 h and then rinsed exhaustively with 100 ml toluene to ensure the removal of non-adsorbed PB chains. Subsequently, the samples were dried gently with a stream of nitrogen. The resulting polymer structures were investigated by atomic force microscopy. The PicoSPM (Agilent Technologies, California, USA) was used operating in tapping mode in air. Commercially available Si_3N_4 (MikroMasch, Talinn, Estonia), rectangular cantilevers, with a spring constant of 1.75 N/m and resonance frequency of $130 - 160$ kHz were used. The cantilevers were oscillated 5% below their natural resonant frequency and during imaging moved in a raster fashion. Each sample was imaged at several different areas.

The size of the polymeric islands was determined by using the grain analysis of the software Scanning Probe Image Processor (SPIP, Image Metrology, Hørsholm, Denmark). It is well known that the AFM tip can make an object lying on a surface to look wider due to the convolution of the geometry of the tip and the shape of

the object being imaged. Glynos [2007] extensively discussed the influence of the tip geometry on the apparent dimensions of an object imaged with AFM. Using similar geometrical arguments and assuming again that the object is a spherical cap (substantiated through AFM measurement of its profile) the real volume of the object imaged was estimated from its apparent height, apparent volume, and radius of the probe tip. Samples were repeatedly imaged at room temperature over the course of weeks and significant changes in the adsorbed state were not observed, i.e. the contact angle did not change. Figure 5.1 contains representative AFM images.

5.1.2 Results

The PB of molar masses $M_{\mathrm{w}} = 78$ kg/mol and $M_{\mathrm{w}} = 962$ kg/mol corresponded to measured volumes of $V = 159\,\mathrm{nm}^3$ and $V = 1937\,\mathrm{nm}^3$, respectively (density $\sim 0.83\,\mathrm{gcm}^{-3}$). The range of heights of adsorbed PB droplets was measured to be approximately $1 - 25$ nm, corresponding to a range of volumes of $1,000 - 1,000,000\,\mathrm{nm}^3$ and a range of undeformed radii $5 - 50$ nm, spanned through polydispersity and a variable number of chains in the aggregates. Volumes were converted into undeformed radii ($V = 4/3\pi R_0^3$), which, combined with AFM-measured adsorbed heights, returned the E_{D} moduli through the theoretical model, Eq. (3.17), given also: the surface tension of the polymer in air, γ_{P}, the spreading parameter, S, and Poisson's ratio, ν. As far as the latter is concerned, a good approximation is 0.5 for rubbery polymers (Riande et al. [2000]). γ_{P} is obtained from literature (van Krevelen and Hoftyzer [1976], Falsafi et al. [2007]) and S estimated through Fowkes's model (Fowkes [1961, 1963]). This is similar in spirit to the vOCG (van Oss et al. [1987]) model, yet considers an alternative force repartition, specifically $\gamma = \gamma^{\mathrm{d}} + \gamma^{\mathrm{p}}$, where γ^{d} refers to the dispersion interaction contribution ("apolar") and γ^{p} collectively to hydrogen bond (γ^{h}), dipolar, etc. contributions ("polar"). The alternative to the vOCG model, (4.2), now is

$$\begin{aligned}\gamma_{12} &= \gamma_1 + \gamma_2 - 2(\gamma_1^{\mathrm{d}}\gamma_2^{\mathrm{d}})^{1/2} - 2(\gamma_1^{\mathrm{p}}\gamma_2^{\mathrm{p}})^{1/2} \\ &= \gamma_1 + \gamma_2 - 2(\gamma_1^{\mathrm{d}}\gamma_2^{\mathrm{d}})^{1/2} - 2(\gamma_1^{\mathrm{h}}\gamma_2^{\mathrm{h}})^{1/2} - \ldots \end{aligned} \tag{5.1}$$

PB is formed by polymerization of the monomer 1,3-butadiene, a hydrocarbon diene molecule. The derived polymer contains single and occasional double covalent bonds along the backbone, and consists exclusively of C and H atoms. Due to the small difference in electronegativity between C and H (0.35 in the Pauling scale)

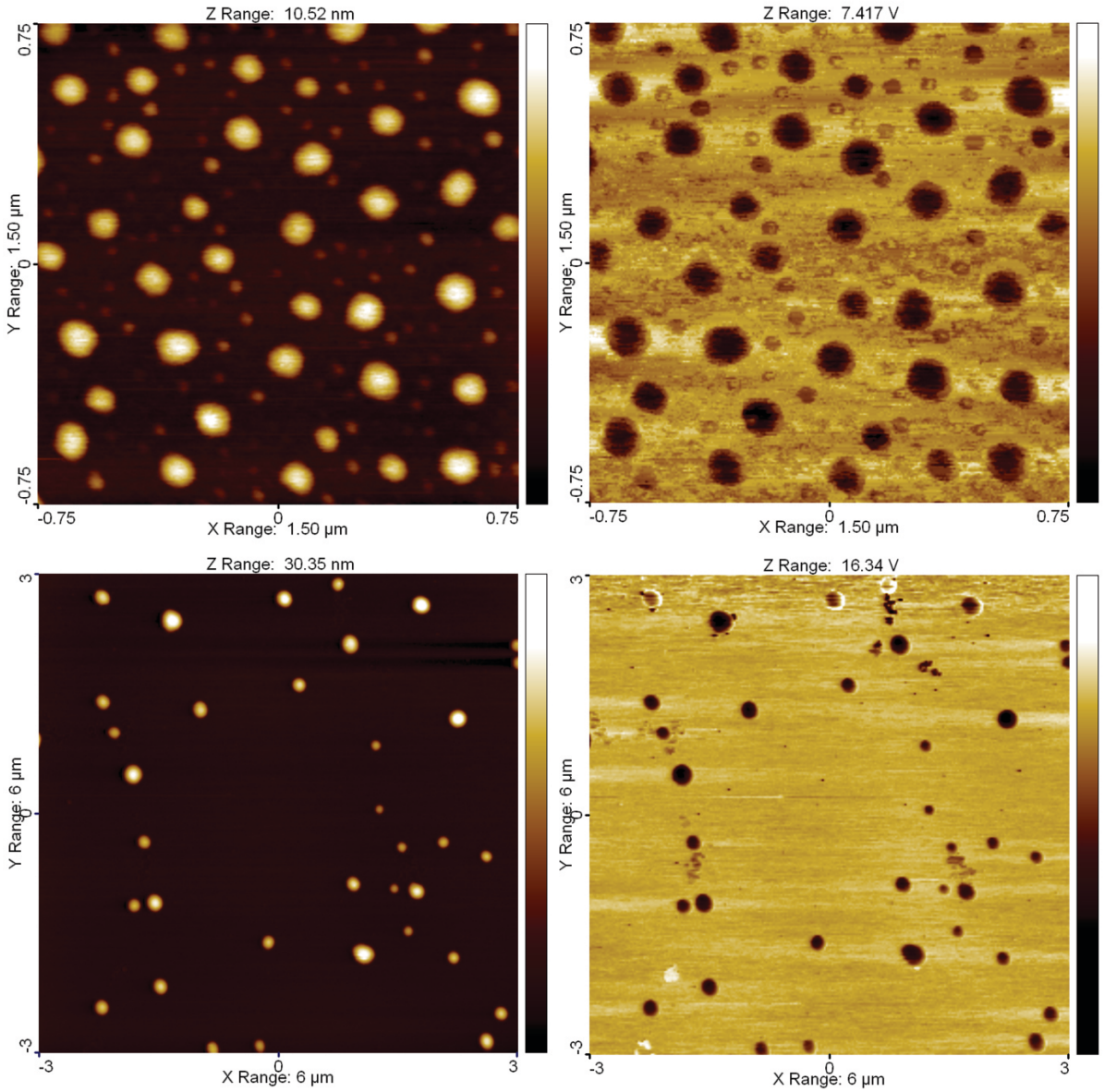

Figure 5.1: Representative topography (left) and phase (right) tapping mode AFM images of linear PB particles on mica, which was freshly cleaved and immediately exposed to the PB solution. Top: $M_w = 78$ kg/mol; bottom: $M_w = 962$ kg/mol.

we consider the polymer approximately non-polar, therefore interacting mainly via dispersion forces with the environment. In the context of Fowkes's theory this can be stated as $\gamma_{\mathrm{P}} \simeq \gamma_{\mathrm{P}}^{\mathrm{d}}$. Specifically, $\gamma_{\mathrm{P}} = 32$ mJ/m^2 (van Krevelen and Hoftyzer [1976], Falsafi et al. [2007]), a value typical of hydrocarbons.

For mica (an extensive account of its surface properties can be found in the work of Hu et al. [1995]), $\gamma_{\mathrm{S}}^{\mathrm{d}} = 30$ mJ/m^2; $\gamma_{\mathrm{S}}^{\mathrm{p}} = 90$ mJ/m^2; $\gamma_{\mathrm{S}} = 120$ mJ/m^2, with γ_{S} simply being the sum of the dispersion (Schultz et al. [1977a], Bailey and Kay [1967], Bailey and Price [1970]) and polar (Schultz et al. [1977b]) contributions, in fair agreement with independently reported values of mica's total surface tension (Bailey and Kay [1967], Bailey and Price [1970], Christenson [1993]).

The spreading parameter, (2.5), written in terms of Fowkes's model, (5.1), and the previous assumption $\gamma_{\mathrm{P}} \simeq \gamma_{\mathrm{P}}^{\mathrm{d}}$, illustrates that the interaction between mica and PB is governed by dispersion forces: $S = -2\gamma_{\mathrm{P}}^{\mathrm{d}} + 2(\gamma_{\mathrm{S}}^{\mathrm{d}}\gamma_{\mathrm{P}}^{\mathrm{d}})^{1/2}$. A similar conclusion would be the product of an analysis from the perspective of the vOCG (van Oss et al. [1987]) model (developed later in this article): the occasional double bond of PB would render it with an ever-so-slightly basic character, while siloxane and other groups make the mica surface mostly basic (van Oss et al. [1988b]), meaning that any acid-base interaction cross terms between the two will be negligible compared to the dominant Lifshitz-van der Waals terms. This fact also makes the value of S more reliable in the context of contamination, which is hard to precisely take into account: build-up of contaminants on a freshly cleaved mica surface would initially mainly screen acid-base interactions, making the present analysis more tolerant on contamination uncertainties. S can be evaluated following substitution of the aforementioned surface tensions and components to give $S \simeq 0$ mJ/m^2.

Experimental data are graphically presented in Fig. 5.2, while calculated moduli in Fig. 5.3. Multi-chain aggregates of $M_{\mathrm{w}} = 78.8$ kg/mol are represented by the filled circular points, while multi-chain aggregates of $M_{\mathrm{w}} = 962$ kg/mol are represented by the unfilled circular points.

5.1.3 Discussion

Overall, the multi-chain aggregates returned reasonable predictions for the elastic modulus of PB. Points lie in the range from a few MPa to a few tens of kPa, the majority being within 100 kPa $-$ 1 MPa, exhibiting a decreasing trend with increasing size. Dossin and Graessley [1979] report a stress relaxation plateau modulus of 1.16 MPa at $T = 298$ K corresponding to a time-scale of a few days. Similarly, Hvidt et al. [1980] reports 0.66 MPa, Colby et al. [1987] 1.20 MPa, Fetters

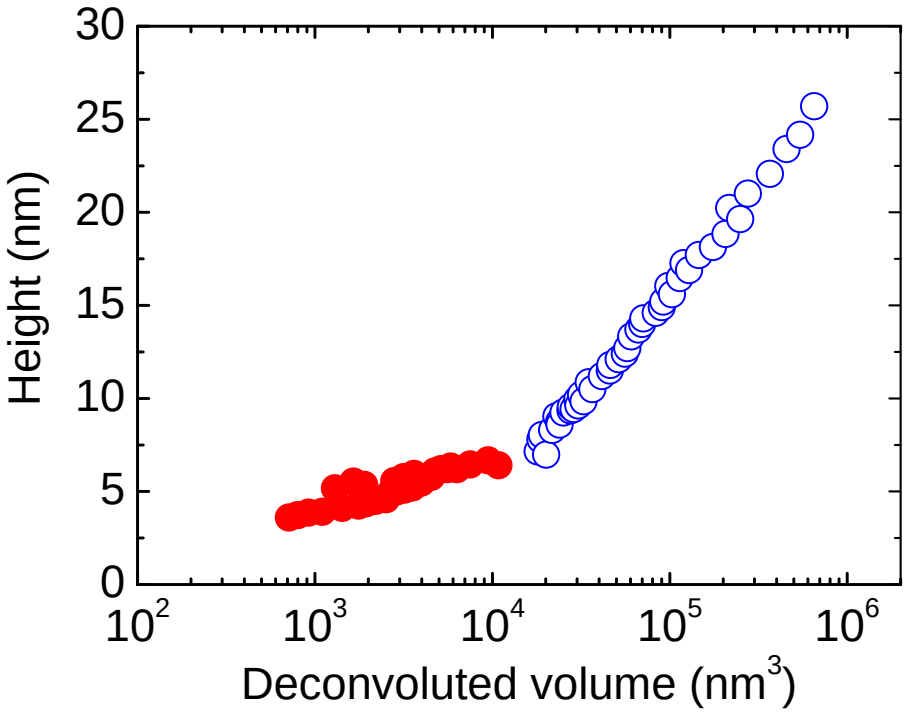

Figure 5.2: Height versus deconvoluted volume for 78.8 kg/mol multi-chain droplets (filled circles) and 962 kg/mol multi-chain droplets (empty circles).

et al. [1994] 1.1 MPa, Carella and Graessley [1984] and Aranguren and Macosko [1988] $\sim$ 1 MPa, and Byutner and Smith [2002] a modulus in the range $10^5 - 10^6$ Pa for time scales in the range $0.001 - 0.1$ s for the melt state. It is expected that the PB modulus bulk value is recovered for large enough droplet sizes where the surface-to-volume ratio becomes negligible and the effective properties are governed by classical bulk elastic strain energy (Sharma et al. [2002]). The reported elastic moduli of Ishikawa et al. [2004], in the range of $10 - 25$ MPa for polymer aggregates of a size range of $15 - 20$ nm, are also an indication of what one should anticipate in the relevant size range, however not to be compared directly against calculated values for the experiments of Glynos (Evangelopoulos et al. [2012]), because the polymer of Ishikawa et al. [2004] consists of hydroxystyrene as base and its modulus has been measured by mechanical testing.

It should be noted that some values of the physical quantities used in the present model (e.g. surface tension) come from literature without mention of the corresponding uncertainty. Also, assumptions have been made (e.g. perfectly spherical caps) of which the uncertainty is not obvious to quantify. Therefore, associating error bars with the calculated E_{D} moduli is rather unreliable. However, judging

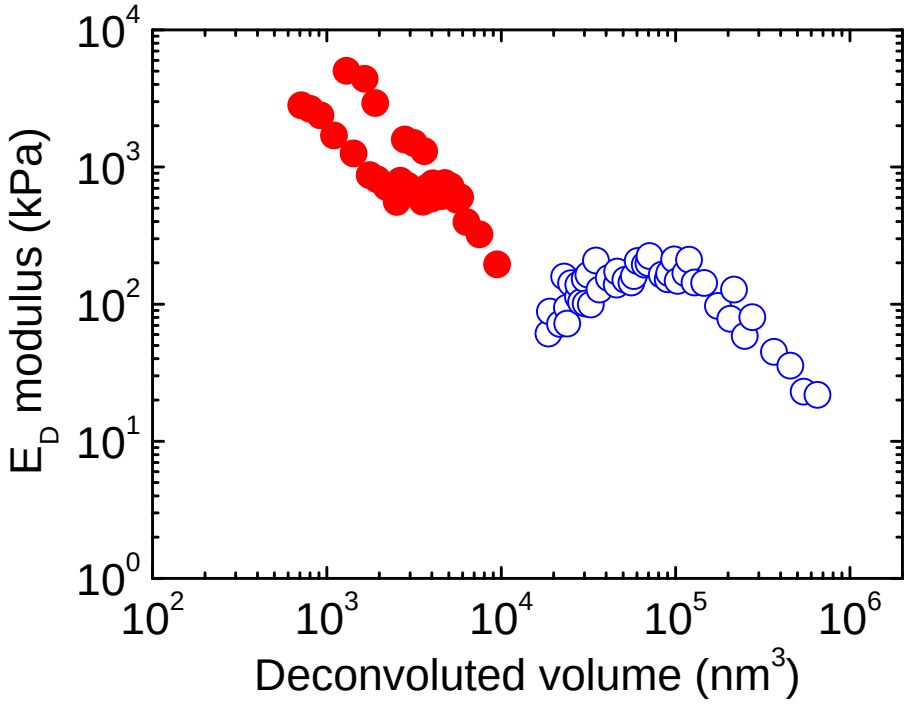

Figure 5.3: Elastic modulus versus deconvoluted volume for 78.8 kg/mol multi-chain droplets (filled circles) and 962 kg/mol multi-chain droplets (empty circles).

from the results, it is anticipated that the accuracy of the predicted elastic moduli is at least within the order of magnitude. In this context, much significance is not attributed to the local maximum of the 962 kg/mol data.

In the PB experiments no change was observed in the adsorbed state even after very long times (months in some cases). Given an entanglement molecular weight of $M_{\mathrm{we}} = 1.9$kg/mol for PB (Rubinstein and Colby [2003]), it is argued that the droplets of $M_{\mathrm{w}} = 78.8$kg/mol and $M_{\mathrm{w}} = 962$kg/mol statistically contain 41 and 506 entanglement strands, respectively, held together by physical crosslinks which prevent the material from flowing and lead to the observed elastic behaviour. One manifestation of entanglement in long chains ($M_{\mathrm{w}} >> M_{\mathrm{we}}$) is the near constancy of the modulus in a stress relaxation experiment (Rubinstein and Colby [2003]). The PB rubbery plateau region has a reported corresponding plateau modulus of 1MPa (Rubinstein and Colby [2003]), in agreement with the calculated range in Fig. 5.3. The presence of more than one chains in an aggregate (approx. $6 - 70$ chains in the 78.8kg/mol aggregates and $10 - 500$ chains in the 962kg/mol aggregates) reinforces the entanglement argument. An additional argument that supports elastic as opposed to purely liquid behaviour of the PB nanodroplets relates to chain packing and entropic elasticity. When a chain is stretched to dimensions larger that its naturally attained root-mean-square end-to-end distance, R_0, it reacts through an entropic force resisting stretching, due to its tendency to increase its entropy. Similarly, when a chain is packed in dimensions smaller than R_0 it resists compression and exhibits effective elasticity (de Gennes [1979]). Given an estimated Kuhn length of $b = 9.6\mathring{A}$ for PB, corresponding to $M_{\mathrm{w}_0} = 105$g/mol (Rubinstein and Colby [2003]), simple division gives $N = 750$ and $N = 9162$ Kuhn segments making up the 78.8kg/mol and 962kg/mol chains, respectively, while the end-to-end expression, $R_0 \sim bN^{1/2}$, gives approximate characteristic sizes of 720 nm and 8800 nm, respectively. These by far exceed the undeformed dimensions of the PB nanodroplets, $5 - 50$ nm, containing few to many chains within (see above). Therefore, the effective elasticity is also supported through the argument of packing. As a last point in the discussion for the legitimacy of treating the PB droplets as elastic objects, the relaxation time of this polymer is discussed (Rubinstein and Colby [2003]). The concept refers to the time it takes for a chain or segment thereof to diffuse out of a tube-like region into which it is confined by its environment (e.g. surrounding chains in a melt). The relaxation time is significant, because it refers to a time-scale within which the chain's motion is topologically hindered by the surroundings and the material does not flow. Specifically for PB, the relaxation time for a Kuhn monomer is $\xi_0 = 0.3$ ns (Rubinstein and Colby

[2003]). The relaxation time for an entanglement strand, ξ_e, scales as the square of its length relative to the Kuhn monomer (Rubinstein and Colby [2003]), thus for an entanglement strand containing $N_e = M_{we}/M_{w0} = 18$ Kuhn monomers that will be $\xi_e = \xi_0 \cdot N_e^2 \cong 0.1\,\mu s$. The whole chain will relax in a time given by $\xi = \xi_e \cdot (N/N_e)^3$ (Rubinstein and Colby [2003], Milner and McLeish [1997]), therefore the $N = 750$ ($M_w = 78.8$kg/mol) chain will require $\xi \cong 7\,\mu s$ to relax, while the $N = 9162$ ($M_w = 962$kg/mol) chain will require $\xi \cong 13$ s to relax. Both of these relaxation time estimates refer to scales shorter than those relevant to the PB experiments (Evangelopoulos et al. [2012]). As these values refer to the bulk of a melt, it is indicated that the effect of the substrate interactions (pinning) introduces chain conformations that are difficult to disentangle, considerably increasing the relaxation time near the substrate interface, due to confinement (Priestley et al. [2005]).

Several sources in the literature are in agreement with the observed trend of an increasing modulus with decreasing size: Miyake et al. [2006] evaluated the surface and bulk elastic modulus of thick and thin polystyrene films, by AFM indentation. Having eliminated the influence from the substrate material by indenting thick films, they measured a surface modulus smaller than the bulk, one possible explanation of which can be the existence of free space presented to the polymer segments at the surface. For thin films, they found that the surface modulus increased considerably with increasing deformation, suggesting an increased influence from the substrate. This was explained by potential trapping/pinning of monomers against the substrate, affecting the rest of the thin film above, which is a good candidate explanation for the present observations also, where trapping would occur due to the adhesion process itself. This pinning effect was also identified in the experiments of Ge et al. [2000]. O'Connell and McKenna [2005] took the bubble inflation of thin membranes biaxial test method (Green and Adkins [1970]) and scaled it so that films of nanometer thickness can be tested. The important aspect of what they did was the use of the imaging capability of the AFM to perform the measurement of the deformation but not the indentation itself, thus avoiding contact mechanics problems when the AFM is used as an indentation machine (VanLandingham et al. [2001]). That work and a follow-up investigation (O'Connell and McKenna [2006]) of supported polymer films of thicknesses from 276 nm to 13 nm revealed an increase of stiffness by over two orders of magnitude at the smallest thickness, recovering the bulk value at around 200 nm to 300 nm. A smooth transition towards the bulk value was observed with experiments of Tweedie et al. [2007], in agreement with the trend in Fig. 5.3. Tweedie et al. [2007] applied contact loads over 5

to 200 nm from the surface of amorphous polystyrene, poly(methyl methacrylate), and polycarbonate. They observed that the apparent stiffness exceeded that of the bulk by up to 200% independent of processing scheme, macromolecular structural characteristics, and relative humidity, and attributed that to contact stress-induced formation of a mechanically confined phase at the probe polymer interface. More specifically, attraction toward and repulsion from the probe material would restrict molecular mobility in the vicinity of mechanical contact with the probe. Balazs et al. [2007] analyze this effect in terms of an enthalpic (intermolecular interactions) and an entropic (stretching/alignment of chains with respect to the contact surface) component. Recognizing that there was no probe-induced deformation in the experiments performed by Glynos (Evangelopoulos et al. [2012]), it is argued that the deformation due to adsorption on a substrate induces a very similar mechanism to the aforementioned. Lastly, an example of experiments indirectly related to the elastic modulus size effect is provided: Priestley et al. [2005] analyzed the structural relaxation of polymers near surfaces and interfaces. Relative to that of the bulk, the rate of structural relaxation at the substrate interface was reduced by a factor of 15, exhibiting a nearly complete arresting of relaxation, and implying an increase of the effective stiffness.

Referring the reader back to Fig. 5.1, a relation between particle size and phase signal is pointed out: Larger particles appear darker in phase image than smaller particles. The phase signal is dependent on a number of factors, including viscoelasticity, adhesion, long-range forces and contact area (Cleveland et al. [1998], Tamayo and García [1996]), however the observation is compatible with the finding of a decreasing elastic modulus with increasing size, through the contribution of (visco-)elastic properties to the phase signal (Magonov et al. [1997]).

For single-chain droplets $\leq$ 5 nm (data not shown), the present continuum theory fails. Structures obtain a pancake-like shape.de Gennes [1976] Monomers then become trapped / pinned against the surface, and, while the "modulus" (if it be assumed legitimate for a moment to talk about modulus at that length scale) ought to, therefore, be high, the theory predicts nonsensical values. This might potentially be more than simply a limitation in size, that is revealed. It appears that the presence of several, as opposed to one, chains in a droplet makes a difference in its adsorption behaviour, as discrepancy is observed between multi- and single-chain droplets of similar size: in the size range of 2.5×10^3 nm^3 $-$ -4×10^3 nm^3, aggregates consisting of M_w = 78.8 kg/mol chains exhibited adsorbed heights in the range 4.5 nm $-$ $-$5.4 nm (Fig. 5.2) with corresponding moduli shown in Fig. 5.2, while single chains of molecular weight M_w = 962 kg/mol exhibited adsorbed heights in

the range 1 nm $-$ -4 nm (data not shown in graphs), which returned nonsensical modulus values. This distinction between single chains and chain aggregates of similar size is reinforced by the MC simulation results of Part II. The reader is referred to Subsection 9.3.2 for the relevant discussion.

For completeness, reference is made to the effect of droplet size on surface tension, introduced theoretically by Tolman [1948]. The surface tension of a droplet of a single pure substance can be expected to decrease with decreasing droplet size. This idea has not been taken on board for the following reasons: Firstly, a decrease of the fluid-air interface tension means that spreading becomes more energetically favourable, opposing our observed trend of increased de-wetting with decreasing size (explained with an increased elastic modulus). Inclusion of a size-dependent surface tension would, therefore, demand an even higher predicted elastic modulus or some other effect to compensate for an increased wetting tendency. Secondly, the effect of droplet size on surface tension becomes significant only when the droplet size approaches or reaches the order 10^{-9}m and the decreasing surface tension function becomes steep only below 5nm (Xue et al. [2011]), which is the lower limit in terms of the droplet sizes investigated in the experiments of Glynos (Evangelopoulos et al. [2012]). It is thus justifiable to presently ignore the effect of a varying surface tension. Perhaps, once the role of line tension is disambiguated, it could be used in conjunction with a variable surface tension, as a future refinement.

As a final remark following from the introductory note concerning line tension, incorporating that as a one-dimensional analogue (Gibbs [1961]) of surface tension in the present model while keeping the elastic modulus constant at its bulk value resulted in a size dependent line tension (increasing with decreasing size), a fact nowhere reported in the literature to the best of my knowledge, except in one case (Furuta et al. [2009]) where the opposite trend is observed (decreasing with decreasing size).

Chapter 6

Conclusions

A theoretical treatment of the spreading of a polymer droplet on a substrate has been considered. It was illustrated that the theoretical model under investigation can be used as a non-invasive method of extracting an elastic modulus for the droplet when an experimental measurement of its adsorbed height is available. As an advantage, one avoids errors and complications involved in direct mechanical testing. The significance of both surface and elasticity effects in the adsorption behaviour of a polymer droplet was established, and the model's limitations were illustrated. All available experimental data supported the theoretical predictions. Specifically: The experiments of Lau et al. [2002] dealt with styrene-butadiene latex droplets of various gel fractions and glass transition temperatures in the ~ 100 nm regime adsorbed on silica. The AFM-measured adsorbed heights confirmed the assumed spherical shape and led to predicted elastic moduli of the anticipated magnitude, given the material. Furthermore, these predictions and their trend were in complete agreement with the gel fraction and the glass transition temperature properties. The experiments of Engqvist et al. [2007] took into account different glass transition and treatment temperatures, as well as treatment times in the spreading of their styrene-acrylic latex droplets. All three parameters came into agreement with the moduli predicted by the present model. The predicted moduli pertaining to droplets of the work of both Lau et al. [2002] and Engqvist et al. [2007] were, on the whole, of higher value than the moduli of macroscopic strips of corresponding consistency. This was attributed to the difference in structure, the strips being made up of an array of close-packed droplets adhering together by their shells. As far as the experiments of Glynos (Evangelopoulos et al. [2012]) are concerned, AFM-measured adsorbed heights of PB on mica revealed a trend of decreasing elastic modulus with increasing droplet size, progressively tending

towards the bulk material value. This size effect is supported by the literature for related systems, though a consensus has not yet been reached (Yang et al. [2010]). It was the experiments of Glynos (Evangelopoulos et al. [2012]) that illustrated the theory's limitations. For droplets of radius $\sim$ 5 nm or less, the theory predicted nonsensical values. Also, between aggregates and single chains of similar size, the former exhibited reasonable moduli, while the latter returned nonsensical values, suggesting a difference in adsorption behaviour between such systems, and, hence, the inapplicability of the present theoretical model for the single-chain type.

It was explained in the introductory note that consideration of a line tension contribution in our model would go beyond the work of this article. However, it is interesting to note at this point that the experimental nanoscale results were shown to be interpretable by a moderate increase of modulus (as expected for these nanometer-scale sizes) without the incorporation of line tension.

Part II

Computer Simulation

Abstract

Polymer nanodroplets interacting with attractive substrates under poor solvent conditions are investigated by means of a Monte Carlo (MC) simulation. Droplets comprised single- and multi-chain architectures in different sizes. Different architectures of equal size were juxtaposed in terms of their state of adsorption for both weakly and strongly attractive substrates. The simulations illustrated architectural effects which brought out a distinction between single- and multi-chain droplets in terms of their adsorbed dimensions.

Chapter 7

Introduction

7.1 Background Theory

7.1.1 Physical Concepts

The size of linear chains can be characterized by their square radius of gyration, defined as the mean square distance between monomers and their centre of mass:

$$R_{\mathrm{g}}^2 = \frac{1}{N}\sum_{i=1}^{N}(\vec{R}_i - \vec{R}_{\mathrm{CM}})^2, \tag{7.1}$$

where i is an index denoting the monomer.

In environments known as solvents, suspended polymer chains attain an isotropic globular conformation with a radius of gyration which scales with the number of monomer units, N, as $R_{\mathrm{g}} \sim N^{\mu}$, where μ is the Flory exponent, characteristic of the solvent quality and equal to 1/3 in poor solvent, 1/2 in theta solvent, and 3/5 in good solvent (Rubinstein and Colby [2003]). The solvent quality is characterized by μ and determined by the chemical specificity of the solvent molecules with respect to the chemical specificity of the polymer at a given temperature. This is understood from the fact that the actual size that a chain attains in a given solvent is determined by the competition between self-attraction (monomer-monomer interaction in the solvent field) and thermal motion, in other words between the lower potential energy of a compact conformation and the higher entropy of an extended/swollen configuration. This competition is present in every thermodynamic system and is formulated through the minimization of the potential $\Phi = I - TS_{\mathrm{E}}$, known as Gibbs free energy and previously defined in Section 2.1. The limiting cases of poor and good solvents are called non-solvents and athermal solvents,

respectively. Also, at some special temperature, called the Θ-temperature, the potential energy - thermal motion competition creates an environment that emulates theta-solvent statistics ($\mu = 1/2$). These statistics also coincide with those in a melt, i.e. a solvent whose molecules are identical to the polymer which is dissolves.

If the solvent quality deteriorates enough, a collapse transition from an extended (Fig. 7.1(a)) to a compact (Fig. 7.1(b)) conformation may occur. Given that in good solvent the monomer-monomer interaction is dominated by short-range repulsion, while in poor solvent the short-range repulsion competes with the monomer-monomer attraction (in a given separation range), the transition from the extended to the compact globular state can be viewed as a gas-to-liquid transition. If the presence of an attractive substrate is also considered, competition between the lower potential energy near the substrate and the higher entropy away from it may result in a transition from a desorbed (Fig. 7.2(a)) to an adsorbed (Fig. 7.2(b)) state (Fleer et al. [1993], Jones and Richards [1999]). All in all, we have an interplay between two possible transitions: from an extended to a compact configuration, induced by varying the chain's effective self-attraction (through the solvent quality), and from a desorbed to an adsorbed configuration, induced by varying the chain's attraction towards the substrate (through the substrate type). In three-dimensional space, the interplay between these possible transitions gives rise to five[1] phases: desorbed extended (DE), desorbed collapsed (DC), adsorbed extended (AE), adsorbed collapsed (AC), and surface attached/adsorbed globule (SAG) (Bouchaud and Vannimenus [1989], Kumar and Singh [1993], Singh et al. [1999]).

In order to make the above description more concrete, we introduce a parametrization through the reduced variables $\omega = e^{\beta E}$ and $\omega_{\mathrm{w}} = e^{\beta E_{\mathrm{w}}}$ (Mishra et al. [2003], Rajesh et al. [2002], Singh et al. [2001]). If β is an inverse temperature, E the attractive potential energy between two non-consecutive monomers, and E_{w} the attractive potential energy between the surface and a monomer (both defined so that greater values imply stronger attraction), then ω and ω_{w} are probabilities for collapse and adsorption, respectively (N.B.: we define energies E and E_{w} so that greater values imply stronger attraction). As a consequence, a lower temperature (greater β) and a stronger monomer-monomer attraction (greater E) result in a statistically more compact configuration, while a lower temperature (greater β) and a stronger monomer-substrate attraction (greater E_{w}) result in a statistically more adsorbed configuration. At a given temperature, the interplay between E and E_{w}

[1] Four in two dimensions, where the surface becomes a line and the adsorbed collapsed (AC) state does not occur (Mishra et al. [2003]).

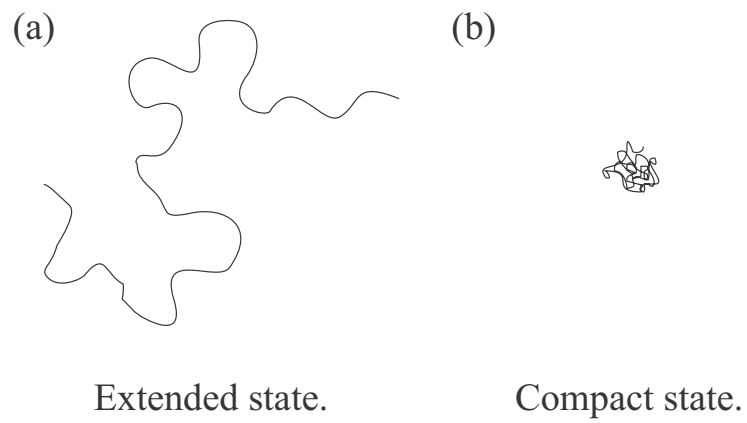

Figure 7.1: (a) Extended and (b) compact states of a polymer chain.

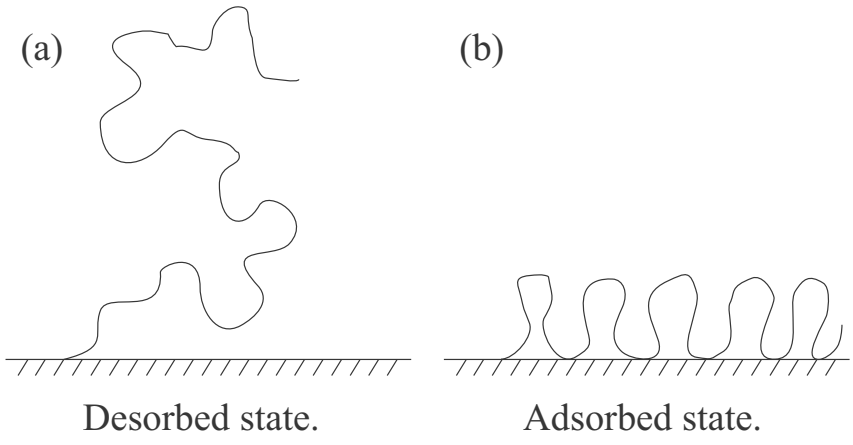

Figure 7.2: (a) Desorbed and (b) adsorbed states of a polymer chain.

alone determines which of the aforementioned five phases the polymer chain will be in, as all physicochemical properties, such as the chemical nature of the solution's constituents, are parameterized by these two energies. Specifically: if E and $E_{\rm w}$ are both small in magnitude, the polymer assumes a swollen, random-coil configuration (DE phase) with $R_{\rm g} \sim N^{\mu}$ and $\mu = 3/5$; if $E_{\rm w}$ is small and E large, the polymer assumes a compact globule configuration away from the substrate (DC phase) with $R_{\rm g} \sim N^{\mu}$ and $\mu = 1/d$ in d-dimensional space; if $E_{\rm w}$ is large, the polymer sticks close to the surface, with a finite fraction of its monomers attached on it, while the rest transversely extend away from it. In this case, depending on whether E is small or large, the polymer can be found in either the AE or AC phase, respectively. In the former case, the size in the transverse to the substrate direction scales as $\sim N^{\mu'}$, where μ' is the Flory exponent mentioned earlier in $d-1$ dimensions; in the latter case, the transverse size scales as $\sim N^{1/(d-1)}$, in d-dimensional space (Rajesh et al. [2002]) —the AC phase does not exist for $d < 3$ (Mishra et al. [2003]). In three-dimensional space, such as with our simulations, $\mu' = 3/4$, therefore the polymer growth rate transversely to the attractive surface is lower in the AC than in the AE case, as expected. Lastly, the SAG phase is to be thought of as intermediate between the DC and AC phases in terms of the degree of affinity with the surface. Here, the polymer exists as a collapsed globule of finite density attached to the surface. Its size in both the parallel and perpendicular to surface directions scales as $N^{1/d}$, while the number of monomers in contact with the surface scales as $N^{(d-1)/d}$, in d dimensions. It is important to note that even though the SAG is considered a separate phase, its surface energy density scales as $N^{-1/2}$, and, therefore, vanishes in the thermodynamic limit, leaving it with the same free energy per monomer as the DC phase (Singh et al. [2001], Mishra et al. [2003]). This makes the transition between the SAG and the DC a surface transition. A qualitative phase diagram relevant to 3-dimensional space is presented in Fig. 7.3.

As mentioned earlier, the solvent quality is dependent not only on the chemistry between solvent and polymer, but also on the temperature of the system. In real experiments, phase transitions may, therefore, be induced either by a change of environment, such as evaporation of the solvent or introduction of an interface near the polymer, or by a change in temperature. In computer experiments, such changes are simulated by fluctuating E and $E_{\rm w}$, which parameterize not only monomer-monomer and monomer-substrate interaction, but temperature, also. This is possible through an effective equivalence between E and β, and $E_{\rm w}$ and β, which can be seen mathematically from the products βE and $\beta E_{\rm w}$ in the expressions of ω and

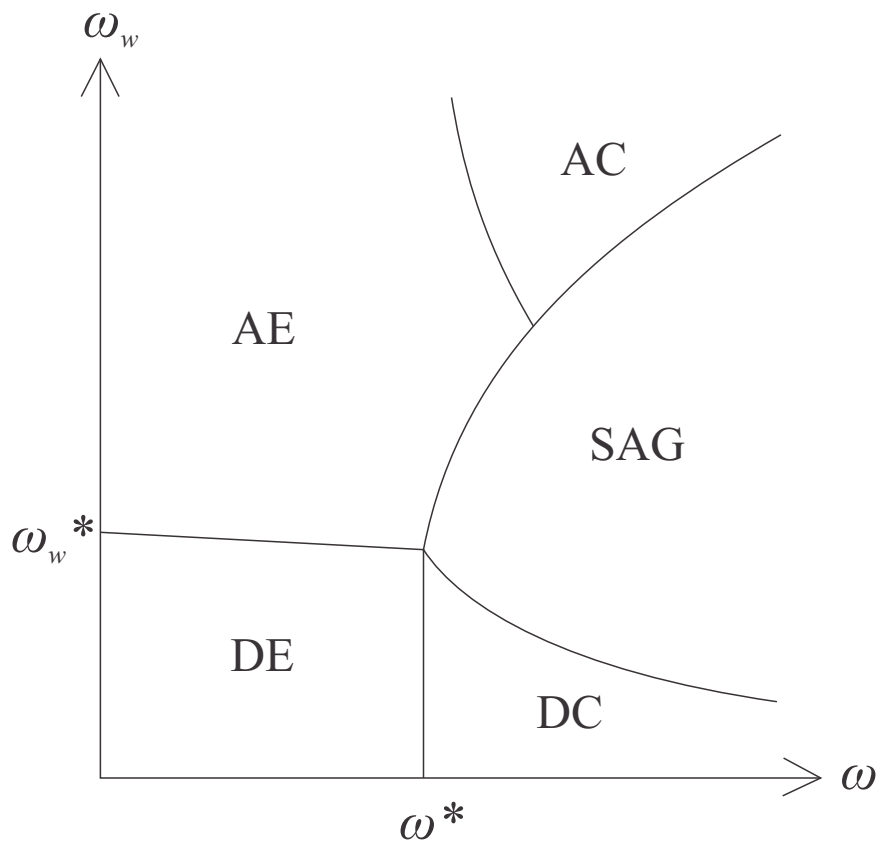

Figure 7.3: Qualitative phase diagram depicting the five distinct available states, desorbed extended (DE), desorbed collapsed (DC), adsorbed extended (AE), adsorbed collapsed (AC), and surface adsorbed globule (SAG), for a polymer chain in 3-dimensional space. Asterisks (*) denote critical values at which transitions occur.

ω_{w}, respectively. This means that neither E should be associated strictly with the probability of collapse, ω, nor E_{w} strictly with the probability of adsorption, ω_{w}. Through their equivalence with temperature, varying E can also have an effect on ω_{w}, while varying E_{w} can also have an effect on ω. For example, an increase in E (poorer solvent) will result not only in a more compact conformation but also in a more adsorbed one, a fact observed in both real and computer experiments.

The parametrization in terms of E and E_{w} explained in this Section conveniently makes the connection with the parametrization employed in the present work's MC simulation, where the context of a specific random walk model allows for a quantitative interpretation of ω and ω_{w} in Section 8.

7.1.2 Computer Simulations and the Monte Carlo Algorithm

Computer simulations have become an accepted form of experimentation in a similar way that literal experimental investigation became an accepted form of research following the historical period of science when the scientific process featured a purely philosophical-theoretical character. Interestingly enough, and in contrast to literal experimentation, the computer simulation plays a double role. The first role is to serve as an experiment to be compared with theory, and there are a few reasons that can make a simulation preferable to a real experiment. High complexity of a real system is one: The ability to independently regulate different physical effects that come into play during the course of an experiment is an advantage of the simulation which is difficult to be had when dealing with a real system. Other reasons that can make a simulation more appealing than a real experiment can be cost, as well as the non-desirability of a real experiment. The results of a nuclear reactor meltdown might be of interest, however the consequences of the corresponding experiment not quite sought after. Lastly, some experiments are simply not possible. We cannot reproduce the internal workings of a star or recreate the universe. The second role of a computer simulation is that of a model to be tested against experimental results. In case the model is proven successful, the simulation can further offer insights towards the discovery of new results. The relationship between theory, simulation, and experiment is depicted in Fig. 7.4. Given the increasing sophistication, processing capacity, and availability of computers, the all-important role of simulations in the scientific method is more evident than ever.

A main advantage of computer simulations is an environment free from inessen-

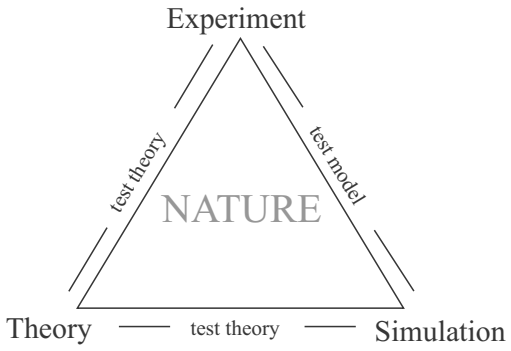

Figure 7.4: Relationship between theory, simulation, and experiment.

tial details of real systems which may disguise essential features of the phenomena under study. One can reduce the unnecessary complexity of a real situation to an idealized model situation, where the fundamental features become evident. In the present work's context, an ideally flat, rigid, defect-free substrate of a simulated experiment will allow a polymer chain to freely adsorb and attain equilibrium conformation, whereas a rough, chemically heterogeneous substrate might hinder or prevent equilibration altogether. For another example, a polydisperse polymer sample in a real solution might introduce molecular-weight–dependent behaviour, while a simulation can allow a perfectly monodisperse sample. It is not to be assumed, however, that simulations are free of shortcomings. For example, only short time-scales are available for equilibration and accessible length scales are in the 10 nm range (Binder [1995]). What is more, not all properties of real systems can be directly measured in a simulation. Conversely, most of the quantities that can be measured in a simulation do not correspond to experimental data, for example the instantaneous positions and velocities of all molecules of a liquid. The bridge between computer data and useful data is statistical mechanics, which also lies at the heart of a MC simulation. In what follows, we present the fundamental algorithm.

In a MC simulation the evolution of a system is developed in such a way that it does not proceed according to some pre-determined dynamical fashion (e.g. according to Newton's laws of motion), rather in a stochastic manner which depends on a sequence of randomly generated numbers (relevant to Step 2 in the algorithm that follows).[2] With a second, different sequence of random numbers, the simulation

[2]Of course, truly random numbers are unpredictable in advance and can, therefore, not be generated by any pre-composed algorithm; they can only be produced by some physical process,

does not give identical results but yields values which agree with those obtained from the first sequence to within some 'statistical error'. The ultimate goal of the MC method is to evolve the system to its thermodynamical equilibrium state. It is emphasized that the stochastic manner by which equilibrium is approached renders the meaning of time differently from, say, a MD-simulation context, where simulation time corresponds to physical time. With MC, the system explores different coordinates (microstates) of its phase space (Landau and Lifshitz [1980]) under the requirement that transition to a future coordinate abides by the laws of statistical mechanics.

It is simplest to introduce the fundamental algorithm (Metropolis et al. [1953]) through the example of a polymer chain. If $\mathbf{r}^N$ are the position vectors of all monomers and $\mathcal{U}(\mathbf{r}^N)$ the energy of the corresponding configuration, then the probability of the system attaining that configuration is proportional to the Boltzmann factor $\exp[-\beta\mathcal{U}(\mathbf{r}^N)]$ (Landau and Lifshitz [1980], Frenkel and Smit [2002]).

- Step 1: Calculate the energy of the configuration, $\mathcal{U}(\mathbf{r}^N)$.
- Step 2: Select a particle at random and give it a random displacement, $\mathbf{r}' = \mathbf{r} + \Delta$.
- Step 3: Calculate the energy of the new configuration, $\mathcal{U}(\mathbf{r}'^N)$.
- Step 4: Accept the new configuration with probability

$$\min\left(1, \exp\{-\beta[\mathcal{U}(\mathbf{r}'^N) - \mathcal{U}(\mathbf{r}^N)]\}\right). \tag{7.2}$$

In terms of the MC code of this Thesis, $\mathcal{U}$ is determined by the monomer-monomer and monomer-substrate interactions as defined in Section 8, while the displacement may be any of the four types of local MC moves defined therein.

7.2 Literature Review

Macromolecules adsorbed on surfaces have and still receive a lot of interest. A brief overview of computer simulation treatments of this topic is given through influential references (in approximate chronological order), which are by no means exhaustive of the literature.

such as radioactive decay. Series of truly random numbers have been recorded but would be very cumbersome to use for Monte Carlo simulations. It is left to be said that the pseudo-randomness of a numerical sequence produced by a computer is, indeed, one source of error in the simulation's results (James [1990]).

One of the first documented simulations is that of DiMarzio and McCrackin [1965]. One-dimensional chains without excluded-volume interactions in two-dimensional space (square lattice) were treated using the MC method. The reflecting-boundary method generated initial configurations of 50-, 100-, and 200-monomer chains, large numbers of which were required in order to calculate reliable averages of the number of segments on the surface and the coordinates of the ends of the chains. These quantities were studied as functions of the adsorption energy, and a main conclusion of that early work was that an adsorbed polymer can belong to either of two classes of behaviour: for strong adsorption, the molecule lies flat on the surface with perpendicular dimensions independent of molecular weight; for weak adsorption, the molecule desorbs altogether. A year later, Bluestone and Cronan [1966] performed a similar investigation of the adsorbed chain thickness as a function of the adsorption potential, this time in three-dimensional space, where the monomers were confined on the sites of a cubic lattice. McCrackin [1967] also extended his previous work (DiMarzio and McCrackin [1965]) to three dimensions, further adding the excluded-volume effect along chains which now comprise up to 300 segments. The number of segments on the surface and the coordinates of the ends of the chains calculated in McCrackin's previous work alter, here, considerably under strong adsorption conditions, due to the excluded-volume effect: the fraction of segments on the surface is reduced by a factor of about 2 and the average distance of the end of the molecule from the surface is increased by a factor of about 2 for the longest of chains. Clark et al. [1975] considered a lattice with a square-well potential to describe the monomer-monomer and monomer-surface interactions. The effect of solvent quality on the chain conformation was studied, revealing a tendency for long tail formation protruding into the solution phase when the solvent is good, and loop formation when the solvent is bad. Clark and Lal [1978] evaluated the effect of surface coverage (regulated through the monomer-monomer and monomer-substrate potential) on the configurational properties of adsorbed chains. Properties considered included the dimensions of the adsorbate chains, thickness of the adsorbed layer, fraction of the segments attached to the adsorbent plane, and the density distributions of segments in the layer. Their study revealed only a small dependence in the low and medium coverage regime, but a dramatic dependence in the high regime. Eisenriegler et al. [1982] studied the influence of a hard wall on the configurations of both ideal and non-ideal long flexible chains. Linear dimensions parallel and perpendicular to the wall and the chains' probability distributions were studied, as well as the behaviour of monomers as a function from their distance from the wall. In this seminal work, it was shown that polymer adsorption

is related to a surface phase transition in magnetism, and that, in order to describe the situation correctly, novel surface exponents must be taken into account. These results were later used in scaling theory arguments (de Gennes and Pincus [1983]). Kramarenko et al. [1995] investigated the adsorption of single chains of various lengths ($N = 16, 32, 64, 128$) and degrees of stiffness by MD. They calculated the degree of adsorption through the fraction of surface-bound monomers, the radius of gyration, and the average length of loops and tails. Their radius of gyration calculations confirmed the scaling behaviour predicted by Eisenriegler et al. [1982], while loop and tail statistics characterized the adsorbed morphology, to conclude that stiffer chains adsorb more easily. Chremos et al. [2008] employed Langevin MD to study: (a) isolated polymers on surfaces with various solvent qualities; (b) many polymers on surfaces in good solvent; (c) many polymers in bad-solvent conditions. In going from (b) to (c), Langevin dynamics was appropriate for simulation of the good-to-bad-solvent quench that occurred in real experiments upon evaporation of the good solvent. Of particular importance, was the simulated reproduction of the experimentally observed bimodal cluster distribution at low-to-moderate polymer concentrations and over a broad range of adsorption potentials. Calculations included the fraction of monomer units bound to the surface, the height of an adsorbed polymer film, and the radius of gyration of an adsorbed polymer chain consisting of 50, 100, and 200 beads. Ivanov et al. [2009] presented a comparative study of the conformations of flexible and semi-flexible polymer chains under variable solvent conditions tethered to a planar wall with both an adsorption potential incorporating both a short-range square well and a long-range decaying tail ($\sim r^{-3}$). One aim was to construct diagrams of states (similar to Fig. 7.3) as a function of temperature and adsorption strength and compare between the flexible and semi-flexible cases. In general, no differences were found. Another aim was to clarify the effect of flexibility on the adsorption-versus-collapse behaviour. It was found that the effect was considerable, provided the chain was near the adsorbing wall and under poor solvent conditions. The same year, Karaiskos et al. [2009] simulated tethered chains under athermal solvent conditions, where the conformational characteristics and shape of the anchored chains were compared with predictions from SCFT.

Not only the statics, post adsorption, but the kinetics from a desorbed to an adsorbed phase has received interest and revealed information about the adsorbed phase itself. Metzger et al. [2002] studied this transition with a bead-spring model of a polymer chain with one end permanently attached (tethered) to a surface by means of a MC simulation. Chain lengths ranged from 16 to 256 monomers.

The bead-spring interaction between monomers was realized through two Lennard-Jones potentials (9-3 and 10-4). The authors concentrated on the transition from a non-adsorbed configuration, where only one end was attached to the surface ("mushroom configuration"), to a strongly adsorbed configuration, where the majority of the monomers were attached to the surface ("pancake configuration"), through an intermediate adsorption-transition regime. Sikorski [2001] extended the study of the adsorption transition to different molecular architectures. Linear chains were compared to star-branched and ring chains. He found that all architectures obey scaling laws. Also, that weakly adsorbed ring polymers tend to be considerably more adsorbed than linear and star, a difference which becomes less pronounced as the strong-adsorption regime is approached. Morphological details such as trains, loops, and tails, and their distributions for the above geometries were presented subsequently in Sikorski [2002] and Sikorski and Romiszowski [2005]. Descas et al. [2004] focused on the mean number of (linear) chain contacts with the adsorbing wall, on the chain's radius of gyration perpendicular and parallel to the wall, on the probability distribution of the free end, and on the density profile for all monomers. This time by means of isothermal MD simulations, Liu and Chakrabarti [2009] considered both homopolymer chain and "protein-like" copolymer chain adsorption. Their results indicated that when adsorption was strong enough, a scaling description of the adsorption mechanism worked well for both good and poor solvent conditions. When, on the other hand, adsorption was not strong enough, the chains adsorbed partially, and one needed to consider effects of this partial adsorption in the scaling description. Heine et al. [2003], using MD, studied the kinetics of spreading of very large hemispherical droplets of $200,000$ monomers, containing chains of length 10, 20, and 40 monomers. Such large droplets allowed the simultaneous study of the bulk and precursor foot regions. Starting from a hemispherical droplet, it was found that the precursor foot forms immediately and spreads diffusively for each system where the surface interaction strength is above the wetting–non-wetting transition. The bulk region of the droplet was found to spread at a significantly slower rate. The effect of a higher-N architecture resulted in the transition from non-wetting to wetting occurring at higher adsorption potentials. Samsonov and Ratnikov [2006] also studied spreading kinetics of nanodroplets. The total system size in this case was 3000 monomers, comprising many chains (polymer droplets), but also the extreme of 3000 nonbonded atoms (simple droplet). Kinetic curves for the first (lower) monolayer radius are analyzed for both types of nanodroplets. It was concluded that, similar to macroscopic spreading, nanoscale spreading is characterized by different

regimes. Polymer spreading kinetics are more complex, and different spreading regimes cannot be always identified. A study involving multiple phase transitions was undertaken by Rissanou et al. [2009]. The collapse from an extended to an compact state under the attractive effect of a surface was investigated for rather long chains, up to 5000 monomers (adsorption-versus-collapse transition). It was shown that adsorbed polymer chains assume "globular" or "pancake" configurations depending on the competition between adsorption strength, cohesive energy, and entropy. Also, it was shown that the dependence of the adsorbate thickness on chain length ranges between three-dimensional (hemispheres) and two-dimensional (pancake) objects.

Milchev and Milchev [2001], Milchev and Binder [2001], and Milchev et al. [2002] are of special relevance to the present work: The adsorption of polymer melt sessile droplets, specifically homopolymer chain aggregates, was simulated on a flat, structureless, solid, substrate of variable (attractive) potential, under poor solvent conditions. The system was realized by a MC coarse-grained bead-spring model, where the anharmonic springs representing bonds were described by the finitely extensible nonlinear elastic (FENE) potential and the nonbonded interactions were described by the Morse potential. The attractive substrate potential was an inverse-cube function of distance. Milchev and Milchev [2001] experimented with droplets of 4096 to 512 monomers for chains of length $N = 32$. It was found that at weak adhesion the droplet contact angle grew steadily with the decrease of drop size, ultimately leading to dewetting below a critical size. This led Milchev and Milchev [2001] to incorporate a corrective term in the classical Young's equation. The corrective term is a function of line tension (as defined in Subsection 2.1.3) that increasingly competes with the surface tension terms with diminishing droplet size. This augmented form of the classical Young's equation, known as the Gretz relation, recovers the description of a size-dependent contact angle, as observed with the weakly adsorbed drops of Milchev and Milchev [2001], for an appropriate sign and magnitude of the line tension. For strong adsorption, on the other hand, no size dependence of the contact angle was observed. While a treatment with the Gretz relation is correct for sufficiently large drops, for nanodroplets the discreteness of matter cannot be neglected and this continuum approach becomes questionable. The smallest drops simulated by Milchev and Milchev [2001] contained only 16 chains or 512 monomers and were seen to hover over the substrate. The contact between drop interface and substrate ceased to exist and one could say that the contact angle reached 180°, i.e. complete dewetting (if it is temporarily assumed that it is legitimate to talk about contact angles at such small sizes).

Although the long-range surface forces still kept this droplet in the vicinity of the wall, its spherical shape was distorted and resembled rather a prolate ellipsoid. This deviation from the cap-shaped spherical form suggested that a quantitative description in terms of the Gretz relation is hardly possible. Qualitatively, however, their MC simulations supported a positive value for the line tension. Milchev and Binder [2001] experimented with droplets of 2048 or 4096 monomers for chains of lengths $N = 16$ and $N = 32$. The existence of a dewetting limit found in the previous study was confirmed. Analyzing the capillary wave spectrum of the interfacial fluctuations, the surface tension of the polymer was extracted. Via the anisotropy of the local pressure near the wall, the wall excess free energy of the polymer melt was found, and the Young equation was tested. Milchev et al. [2002] experimented with droplets of 2048 monomers for chains of lengths $N = 32$ and $N = 16$. They derived the surface tension and free energy in the same way as previously. They showed that Tanner's law for the kinetics of drop spreading holds also on nanoscopic scales, and confirmed earlier predictions of the existence of a precursor film with a transition region surrounding the spreading droplet. In spite of the fact that these three works aim at answering different questions from the ones set in this Thesis, a couple of indirect comparisons can be drawn between their results and those of the present work (viz Subsection 9.3.2).

With exceptions such as Clark et al. [1975], Milchev and Milchev [2001], Milchev and Binder [2001], Milchev et al. [2002], Ivanov et al. [2009], and Rissanou et al. [2009], the majority of literature deals with polymer adsorption in good solvent conditions. A principal reason is the deceleration of kinetics in a poor solvent environment (Mukherji et al. [2008]), requiring considerably more simulation time, which is already expensive for large systems such as polymers. The simulations presented in this Thesis contribute to understanding the poor solvent case better. The specific issue regarding the effect of the internal structure of the particle on its state of adsorption (under poor solvent conditions) that this work addresses has, to the best of my knowledge, not been dealt with in the literature.

The following review works are noted: Fleer et al. [1993], Eisenriegler [1993] explain polymers at interfaces through both theoretical and experimental developments up to that date. Baschnagel et al. [2003] present a topical overview of both MD and MC simulations utilizing simplified coarse-grained models. Specifically, the focus is on bead-spring chains and either Lennard-Jones crystalline or smooth impenetrable surfaces. Cases reviewed range from single-chain adsorption from dilute solution, through sub-monolayer monomeric or polymeric lubricants, to crystallization of dense polymer films. Binder and Paul [2008] give a brief overview

of recent methodological advances made with the Monte Carlo sampling of equilibrium properties of simple lattice models of polymer systems with representative applications, one of which involves the adsorption transition and its interplay with the collapse (coil-to-globule) transition. Descas et al. [2008] is another recent review of scaling and computer simulation methods in the study of equilibrium and dynamic properties of chains on surfaces under good solvent conditions. This review concerns chains that are tethered on the surface and emphasizes the role of critical parameters (viz the critical adsorption strength and cross-over exponent) in a correct description and understanding of such polymer adsorption phenomena.

The rest of Part II is structured as follows: A description of the simulation method is given in Chapter 8. Chapter 9 offers, combined, the simulation's results and their discussion. A brief conclusions Chapter 10 brings Part II to a close.

Chapter 8

Simulation Method

An ideal simulation method for polymers at interfaces would consider long chains ($N \gtrsim 10^3$) with potentials being calculated from the simultaneous motion of all nuclei and electrons (the Car-Parrinello method —Galli and Pasquarello [1993]). However, such an approach is not feasible due to the large spread between subatomic and molecular time scales. E.g.: a single chain of $N \sim 10^3$ in good solvent requires a relaxation time of $\sim 10^{-6}$ s, while inclusion of the electrons requires a time step of $\sim 10^{-17}$ s (Baschnagel et al. [2003]). The disparity of 11 orders of magnitude simply cannot be covered by present day computers. What is more, the total number of particles simulated (electrons and nuclei) is limited to some hundreds or thousands.

A typical necessary simplification that was employed in the present simulation is called coarse graining. This general scheme replaces the atomistic description with a lower-resolution coarse-grained model that averages or smooths away fine details. In the present case, each monomer was reduced to a point (though represented by a spherical bead), constrained on the vertices of a three-dimensional cubic lattice, which defined the simulation space, and associated with an effective contact potential which assumed a value depending on whether contact was made with another monomer or the substrate. This choice of coarse graining is justified by the fact that for uncharged linear polymers large-scale behaviour is governed by chain connectivity, excluded volume interactions, monomer-monomer, and monomer-substrate interactions, rather than bond length, bond-angle vibrations, and chemical specificity (Varnik and Binder [2009]). Next follows a description of how each of these important effects were modeled.

The chain connectivity occurred along the cubic lattice, which had unit length equal to the monomer-monomer bond length and can be thought of as an infi-

nite half-space, bounded by the $z = 0$ plane. The polymer chains, however, were constrained inside a simulation box of dimensions $L \times L \times LZ$, as a truly infinite simulation space would require infinite computer capacity. The box's bottom surface, the substrate upon which chains were adsorbed, coincided with the $z = 0$ plane and the box's vertical walls had periodic boundary conditions (PBC) imposed on them in order to avoid confinement effects due to the presence of the walls; the bottom and ceiling were impenetrable. $L, LZ > 8 \sim 10 \times R_{\mathrm{g}}$ is typically required (Rissanou et al. [2009]), in order to avoid self-interaction of the chains through the periodic walls (finite size / self-correlation effects), as well as simultaneous interaction with both the bottom and ceiling (bridge formation). In keeping with the coarse-grained approach, the substrate was also treated at a generic level. The heterogeneity and irregularity of real substrates influences the properties of the material in contact and may destroy an eventual formation of order (Patrykiejew et al. [2000]). The substrate was, therefore, typically treated as a perfect crystal. It was flat, rigid, homogeneous, and impenetrable.

The excluded volume effect was implemented through self-avoidance of the chain, which was "fully flexible" or "freely jointed", i.e. there was no associated potential with bending between bond vectors of adjacent monomers.

Following up from Section 7.1, where the parametrization in terms of E and E_{w} was introduced, the simulation code considered the monomer-monomer potential, E (in units of thermal energy $k_{\mathrm{B}}T$), between non-consecutive monomers located on consecutive lattice sites, and the monomer-substrate potential, E_{w} (in units of thermal energy $k_{\mathrm{B}}T$), between the substrate and any monomer adjacent to it. For a given chain, E quantifies the solvent quality, with increasing absolute values corresponding to decreasing solvent quality, $E = 0$ being the athermal solvent. Each site of the chain adjacent to another non-consecutive site contributes an amount E to the free energy of the system, with a probability for this to happen to be equal to $\omega = \exp^{\beta E}$. Each site of the walk adjacent to the substrate contributes an amount E_{w} to the free energy of the system, with a probability for this to happen to be equal to $\omega_{\mathrm{w}} = \exp^{\beta E_{\mathrm{w}}}$.[1]

Based on the analysis in the bulk (Rissanou et al. [2006]), the choice of $E = 0.45$ throughout all the simulation experiments can be characterized as that of a poor solvent. Based on the analysis near an adsorbing substrate (Rissanou et al. [2009]), the adsorption-desorption threshold is specified around $E_{\mathrm{w}} = 0.25$.

A Monte Carlo step (MCS) was defined as one attempted move.[2] The following

[1] ω and ω_{w} were introduced in Section 7.1.

[2] The alternative common definition of N-attempted moves for an N-constituent system is

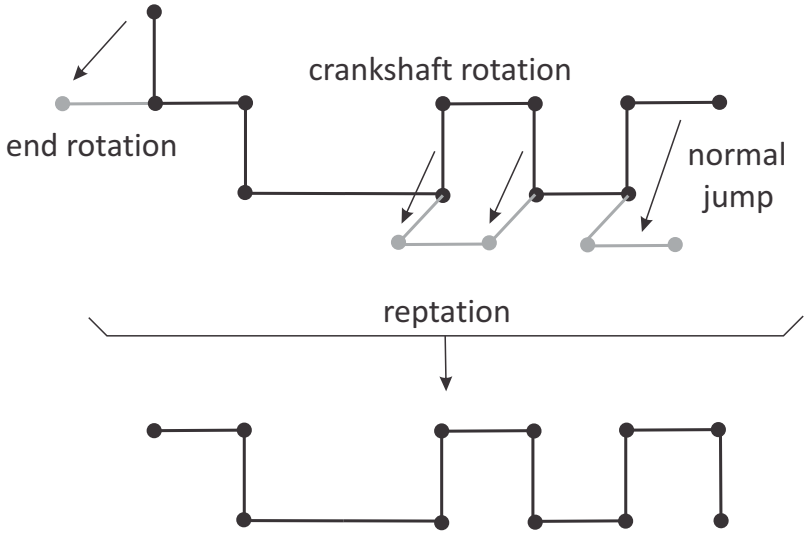

Figure 8.1: Local Monte Carlo (LMC) moves implemented in the algorithm.

types of local (small-scale) Monte Carlo (LMC) moves were employed, respecting lattice positions and chain connectivity: a) end rotation, whereby the last monomer of either end of the chain is free to rotate; b) crankshaft motion, whereby a group of internal monomers may perform a jump from one set of coordinates to another; c) reptation, whereby a monomer from one end of the chain will be transferred to the opposite end, simulating reptation as observed in nature, as the chain seems to essentially flow through a 'tube' of fixed shape; d) normal jump, similar to crankshaft motion, but for the sequence of monomers constituting the chain end. The LMC moves are illustrated in Fig. 8.1. The popular configuration bias Monte Carlo (CBMC) routine (Frenkel and Smit [2002]), involving moves whereby a section of given length constituting one end of the chain is cut off and relocated to the opposite end, was not implemented, as poor solvent conditions rendered the large-scale movements of the CBMC method highly inefficient.

Further to the MC code, a smaller-scale programme was written, which evaluated the radius of gyration, all of its components, and their cumulative averages. To this end, an expression equivalent to Eq. (7.1) was used, which bypasses the necessity of a pre-evaluated centre of mass (Rubinstein and Colby [2003]):

$$R_{\mathrm{g}}^2 = \frac{1}{2N^2} \sum_{i=1}^{N} \sum_{j=1}^{N} (\vec{R}_i - \vec{R}_j)^2, \tag{8.1}$$

often encountered.

where i and j are indices denoting the monomers, each pair entering twice in the double sum. Each component, $R^2_{g_x}$, $R^2_{g_y}$, $R^2_{g_z}$, was separately evaluated from the respective position vector component. Of particular interest were the lateral, $R^2_{g_{xy}} = R^2_{g_x} + R^2_{g_y}$, and perpendicular, $R^2_{g_z}$, to substrate components. All radius of gyration values presented later in the text are root-mean-square quantities, i.e. the square-rooted values of the above expressions.

The rest of this Chapter provides a description of the simulation process, along with results and discussion of those. The simulation process involved three distinct, consecutive phases. Phase I - Initial Conditions involved the creation of suitable conformations (relatively compact and securely adsorbed) from preliminary ones of random shapes and positions. Phase II - Equilibration and Aggregate Formation involved the creation of aggregate structures from the single chains of Phase I and equilibration of all samples under appropriate solvent and adsorption conditions. Phase III - Production Runs was the ultimate phase, during which meaningful statistical data relevant to the samples' equilibrium adsorption states were collected.

As a final note, a system/sample/experiment is uniquely specified by the following complete set of parameters: N_{T} (total monomer number), N (monomers per chain), E (monomer-monomer potential), and E_{w} (monomer-substrate potential). The visual molecular dynamics (VMD) software (Humphrey et al. [1996]) was used for visualization of chains in their simulation boxes. Images have the origin of the coordinates at the corner of the box.

Chapter 9

Results and Discussion

9.1 Phase I: Initial Conditions

Three preliminary single chains of sizes $N = 1000$, $N = 5000$, and $N = 10000$, in random shapes and at random positions relative to the substrate were used to begin the first phase of the simulation with. It was, hence, necessary to manipulate each in appropriate ways to create suitable initial conditions for input into the next phase. This means relatively compact configurations securely adsorbed.

Chains had to be artificially displaced near the attractive substrate in order to maximize the chance of adsorption through brownian motion. A moderately attractive potential ($E_{\mathrm{w}} = 0.3$) had to be used in order to prevent immediate adsorption of the extended configuration in a two-dimensional fashion, which would have made the subsequent formation of a three-dimensional spherical cap a considerably slow process.[1] The three preliminary conformations and the corresponding initial conditions these gave rise to are depicted in Figures 9.1, 9.2, and 9.3.

9.2 Phase II: Equilibration and Aggregate Formation

Prior to any meaningful statistical analysis it is imperative to run a preparatory phase of equilibration, by the end of which appropriate states are generated for input into the last phase, of the production runs. Appropriate states would be spherical-cap–shaped adsorbates that are statistically indistinguishable (i.e. equili-

[1] By trial and error, it was observed that when the transition from the extended to the collapsed state occurs simultaneously with the transition from the desorbed to the adsorbed state, attainment of the desired initial conditions occurs fastest.

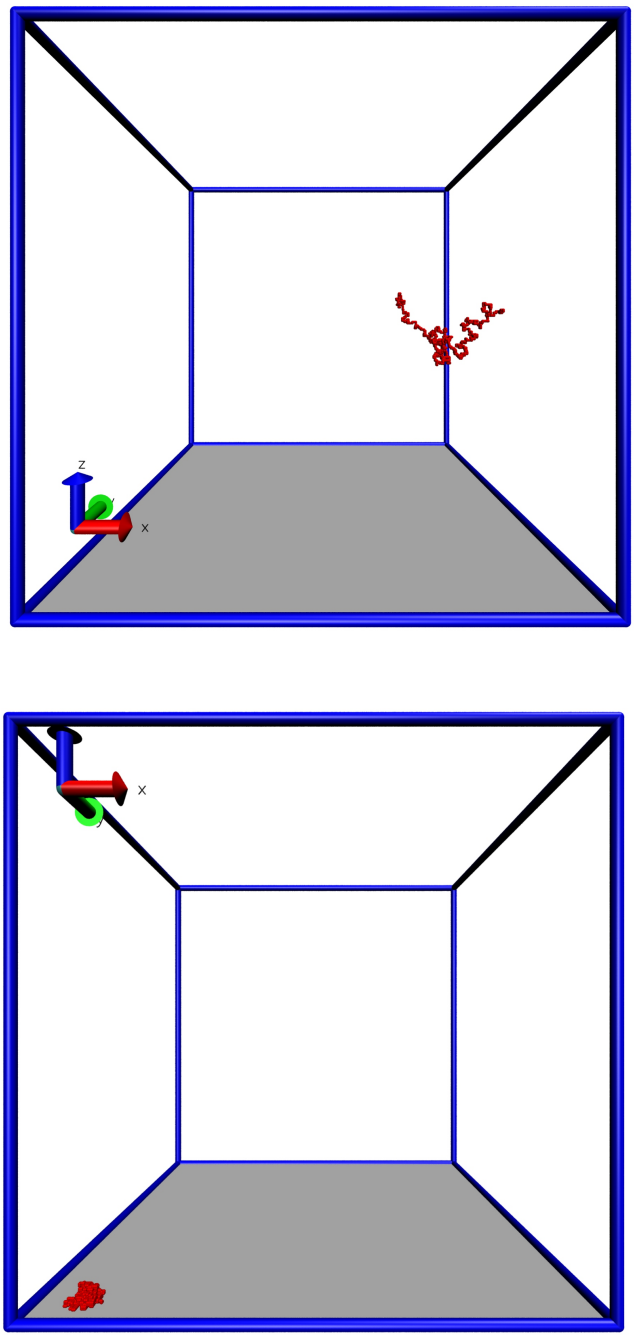

Figure 9.1: Preliminary (top) and initial (bottom) conformation of the $N_{\mathrm{T}} = 1000$ system. Simulation parameters: $E = 0.45$, $E_{\mathrm{w}} = 0.3$; box dimensions: $350 \times 350 \times 350$; duration: 10^7 MCS. (perspective view)

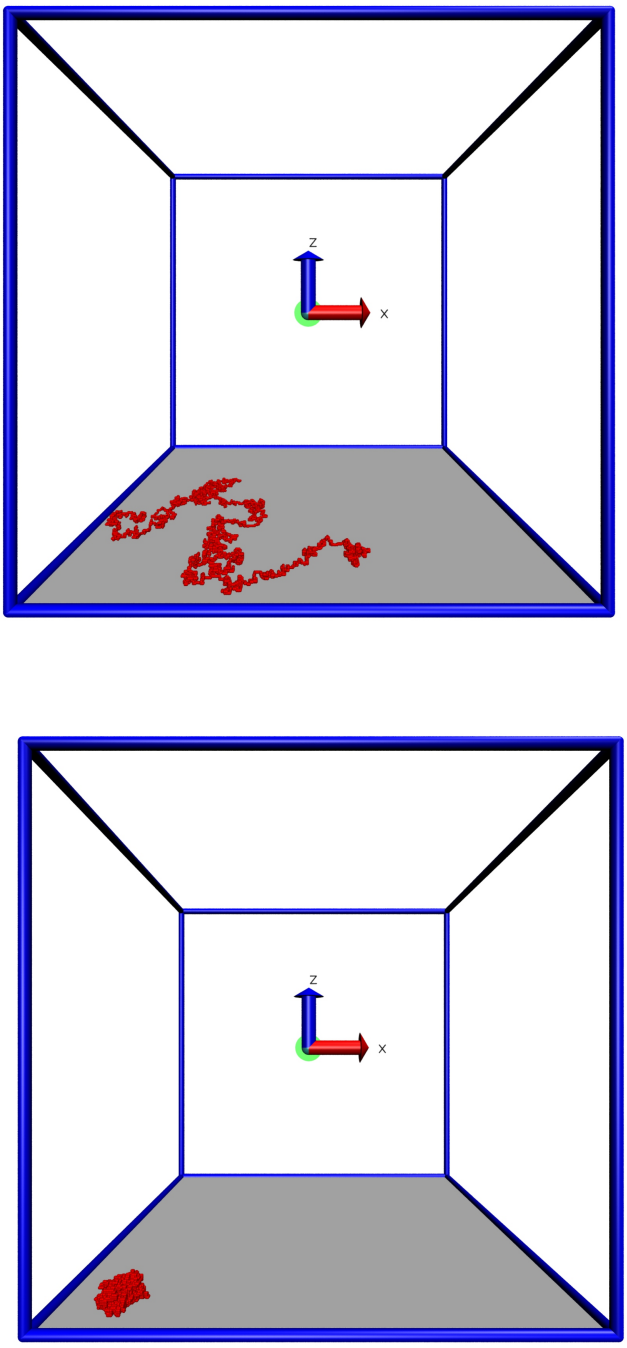

Figure 9.2: Preliminary (top) and initial (bottom) conformation of the $N_{\mathrm{T}} = 5000$ system. Simulation parameters: $E = 0.45$, $E_{\mathrm{w}} = 0.3$; box dimensions: $350 \times 350 \times 350$; duration: 10^7 MCS. (perspective view)

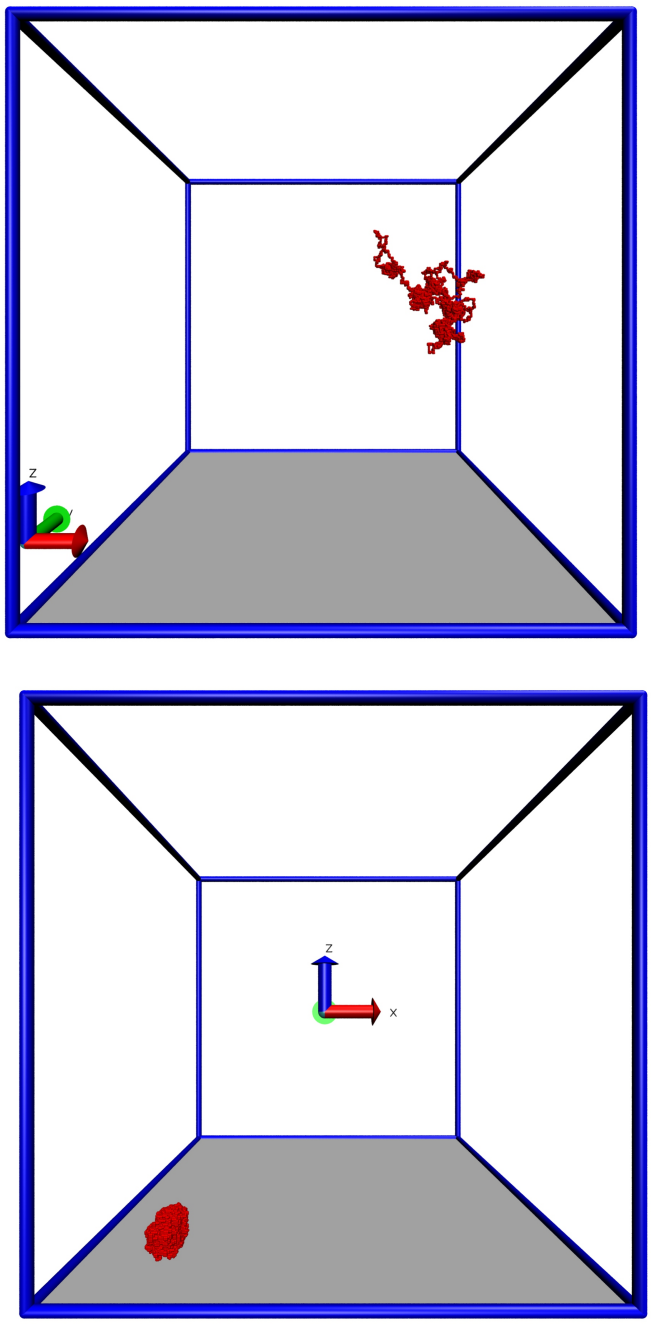

Figure 9.3: Preliminary (top) and initial (bottom) conformation of the $N_{\mathrm{T}} = 10000$ system. Simulation parameters: $E = 0.45$, $E_{\mathrm{w}} = 0.3$; box dimensions: $350 \times 350 \times 350$; duration: 10^8 MCS. (perspective view)

brated) from the conformations that succeed them in the last phase. N.B.: Systems of the size of several atomic diameters only are strongly fluctuating objects and their shape often deviates from the spherical-cap shape expected for mesoscopic droplets, however on average the systems are spherical (Milchev and Binder [2001]). For the specific purposes of the present investigation, phase II also involved formation of aggregates, by "cutting up" the $N = 1000$, $N = 5000$, and $N = 10000$ single chains into smaller ones of length N, while preserving the total monomer number, N_{T}. The procedure is explained next.

Single chains were divided in as many ways possible so that they contained smaller chains of equal length while the total monomer number within the system would be kept constant. The permissible lengths for the internal chains were given by observing the constraint $n = N_{\mathrm{T}}/N \in \mathbb{N}^*$, where n is the number of chains constituting the aggregate, i.e. all chains were required to have equal length. Also, n was constrained (bounded above) by the requirement that N had a lower limit, below which an aggregate suffered scission, i.e. one or more chains or chain aggregates became permanently[2] detached from the original structure. This lower limit varied between different systems and was found to depend on N_{T} and E_{w}. A lowest value of $N = 100$ was attempted for all simulated aggregates. For most aggregates, $N = 100$ was found to lie below the lowest limit of scission. It was, therefore, a good choice of value in that it allowed the simulation to explore that limit. Table 9.1 presents all simulated structures; twenty nine, including single chains.

In phase II, each of the twenty nine structures had to be equilibrated at poor solvent conditions, specifically $E = 0.45$, and under the influence of both a mildly, $E_{\mathrm{w}} = 0.3$, and a more strongly, $E_{\mathrm{w}} = 0.416$, attractive substrate. This entailed a total number of fifty eight systems that had to be equilibrated (hence fifty eight separate computer experiments), before any meaningful statistical data could be collected in phase III. *For convenience and only in relative terms*, $E_{\mathrm{w}} = 0.3$ shall, henceforth, be referred to as weak adsorption and $E_{\mathrm{w}} = 0.416$ as strong adsorption.[3] What is more, it should be clear that the set of $[N_{\mathrm{T}},\ N]$ uniquely specifies the structure, out of the twenty nine, while the set of $[N_{\mathrm{T}},\ N,\ E_{\mathrm{w}}]$ uniquely specifies

[2]Permanent is meant in a statistical sense, because of the nature of the system and the simulation method. An instantaneous or very brief detachment of a sub-structure cannot be considered significant of the thermodynamic stability of the aggregate as a whole. The phenomenon of scission is discussed in Section 9.3.

[3]Indeed, no absolute or of a more general context characterization is intended by those terms. Definitions and uses can vary dramatically across the literature; e.g. Milchev and Binder [1996] consider both 'strong' and 'weak' to lie above $1kT$.

$N_{\mathrm{T}} = 1000$	$N_{\mathrm{T}} = 5000$	$N_{\mathrm{T}} = 10000$
x	x	10000
x	5000	5000
x	2500	2500
x	x	2000
x	1250	1250
1000	1000	1000
x	625	625
500	500	500
x	x	400
250	250	250
200	200	200
125	125	125
100	100	100

Table 9.1: Simulated structures stemming from each of the $N_{\mathrm{T}} = 1000$, $N_{\mathrm{T}} = 5000$, and $N_{\mathrm{T}} = 10000$ single chains. Fields marked with 'x' do not satisfy the requirement of an integer number of chains of equal length contained within each aggregate, leaving a total number of twenty nine different structures under investigation.

the system/experiment, out of the fifty eight. Figure 9.4 illustrates two examples of equilibrated aggregates containing a different number of chains but of equal length.

It is difficult to generally predict how long equilibration takes, the system's rate of response being heavily dependent on its morphology, size, ambient conditions etc. (Allen and Tildeslay [1991]). One can, however, be guided by the general rule of statistical physics which dictates that statistical quantities will fluctuate about steady mean values at equilibrium. Observation of such fluctuations is a good indication of equilibrium. Strictly speaking, this observation is a necessary but not sufficient condition for equilibrium, because meta-stable states deceptively reproduce similar fluctuations in the shorter term. An example of such a statistical quantity is the radius of gyration, R_{g}, as defined in Section 7.1. R_{g} and its components in the lateral, $R_{\mathrm{g}_{xy}}$, and perpendicular, R_{g_z}, to the substrate dimensions were used to monitor equilibration and subsequently characterize the size and proportions of the samples. Though it is difficult to make quantitative predictions on equilibration times, there are a couple of qualitative comparisons that can be made within the context of a simulation environment.

The first and more obvious statement is that larger systems require longer times to equilibrate. This was seen, for example, with the sample of Fig. 9.4, where an aggregate of 20 chains of length $N = 250$ required 10 times the number of MCS an aggregate of 4 chains of length $N = 250$ required.

Also, a structural effect was observed. Within the same N_{T} category, aggregates of lesser N equilibrate faster. This is reasonable if one considers that shorter chains within the aggregate attribute more degrees of freedom. Figures 9.5 and 9.6 illustrate this effect through the evolution of R_{g} and its cumulative average (defined in Section 8), which smooths out the dense fluctuations of the former. Figure 9.5 presents $N = 250$, $N = 625$, and $N = 10000$ systems of the $N_{\mathrm{T}} = 10000$ category under weak adsorption conditions, while Fig. 9.6 presents the same systems under strong adsorption conditions. The $N_{\mathrm{T}} = 10000$ category is chosen because it illustrate this structural effect in a more pronounced manner due to a broader N-range and overall size. The time required to equilibrate the $N = 250$ system of Fig. 9.5 can be directly compared with those of Fig. 9.4, and be found consistent with the aforementioned size-dependent effect.

It is not obvious to comment on the effect of the substrate potential on equilibration time from the available data, because the initial configurations are not equidistant from their respective equilibria, in terms of radius of gyration values (this can be seen in the range covered along the graphs' ordinates). In general,

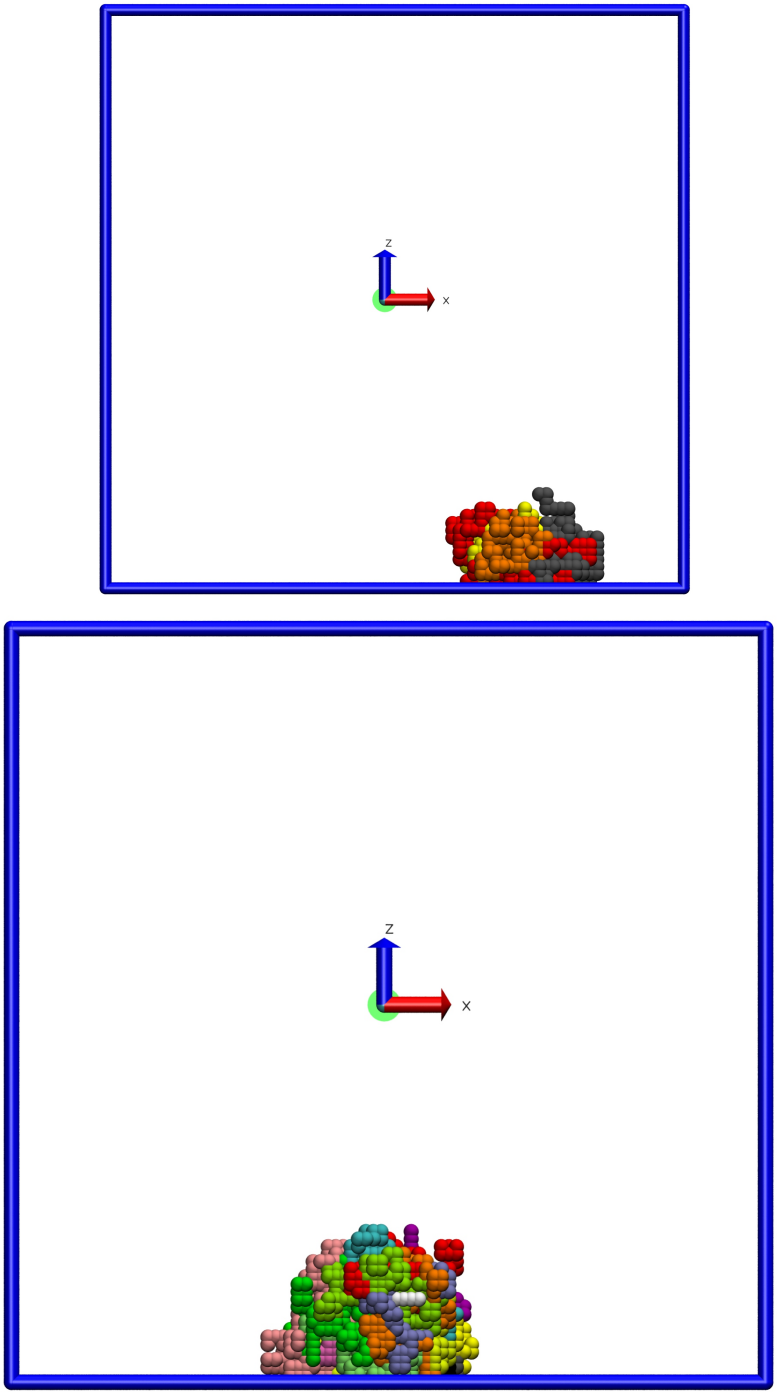

Figure 9.4: Equilibrated, weakly adsorbed ($E_{\mathrm{w}} = 0.3$) aggregates in poor solvent ($E = 0.45$). Top: $N_{\mathrm{T}} = 1000$, $N = 250$; box dimensions: $80 \times 80 \times 80$; equilibration time: 10^7 MCS. Bottom: $N_{\mathrm{T}} = 5000$, $N = 250$; box dimensions: $100 \times 100 \times 100$; equilibration time: 10^8 MCS. At any instant the equilibrated aggregates will appear non-spherical, however on average the structures are spherical caps (orthoscopic view; each colour denotes a different chain; boxes approximately to scale).

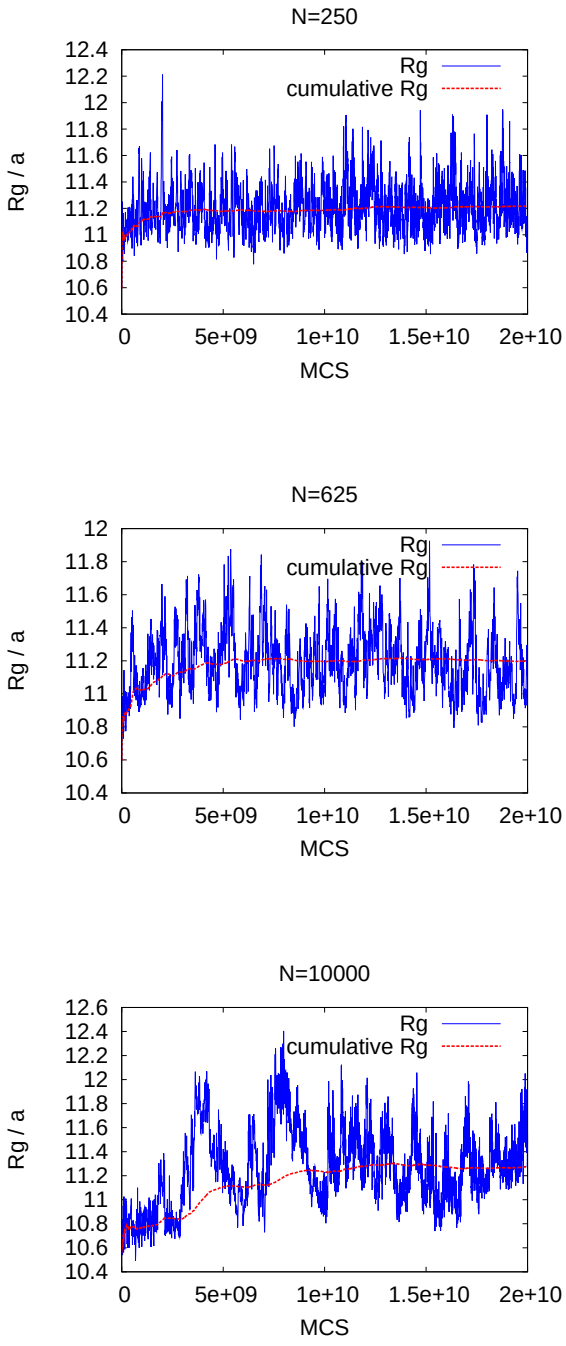

Figure 9.5: Radius of gyration (blue solid line) and cumulative average radius of gyration (red dashed line) vs time, for $N = 250$, $N = 625$, and $N = 10000$ of the $N_{\mathrm{T}} = 10000$ category, illustrating equilibration and the steady state beyond under weak adsorption conditions ($E_{\mathrm{w}} = 0.3$). A progressively slower equilibration rate is seen with increasing N.

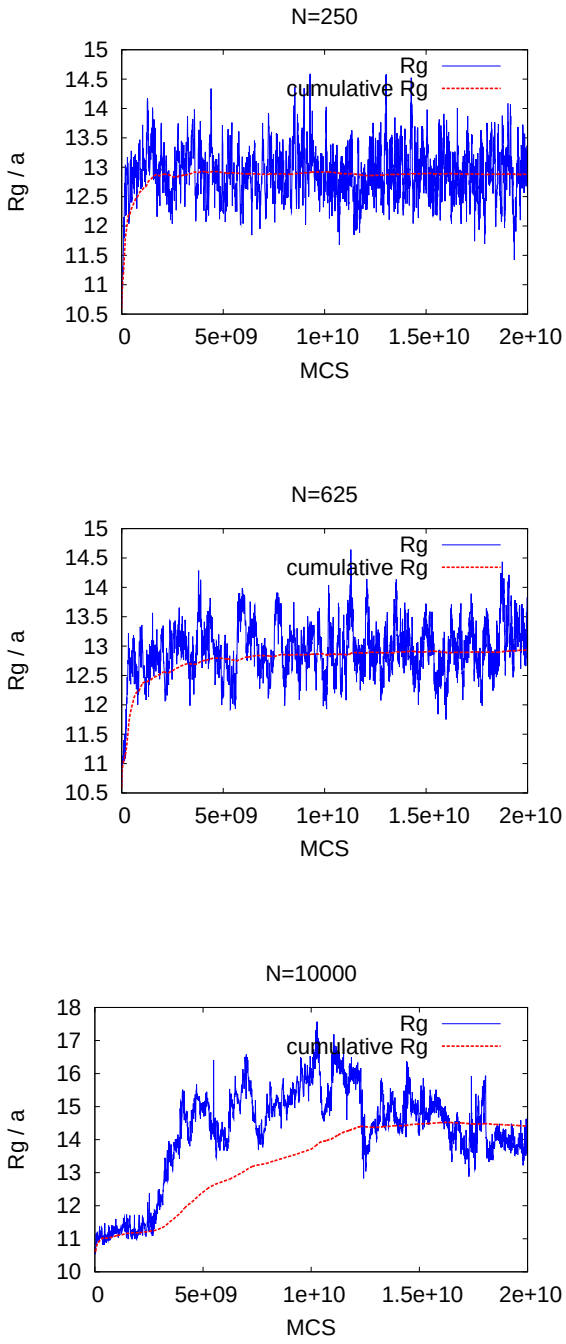

Figure 9.6: Radius of gyration (blue solid line) and cumulative average radius of gyration (red dashed line) vs time, for $N = 250$, $N = 625$, and $N = 10000$ of the $N_{\mathrm{T}} = 10000$ category, illustrating equilibration and the steady state beyond under strong adsorption conditions ($E_{\mathrm{w}} = 0.416$). A progressively slower equilibration rate is seen with increasing N.

however, strongly attractive surfaces require more MCS for equilibration, because kinetics are substantially slower under strong adsorption conditions (Rissanou et al. [2009]).

9.3 Phase III: Production Runs

Following phase II - equilibration and aggregate formation, the production phase of the simulation began, during which meaningful statistical data relevant to the samples' equilibrium adsorption states were collected. For all samples, phase III lasted approximately two to three orders of magnitude longer (in MCS) than phase II. No significant deviations from the mean R_{g} values established from phase II were observed, reinforcing the assumption that phase II successfully equilibrated all structures.

The data collected during phase III for the forty nine simulated systems (fifty eight attempted minus nine that suffered scission) are presented in Figures 9.7–9.18. The points in the graphs represent statistical averages of radius of gyration values and their components in the xy and z directions. Each point corresponds to an average from approximately 1000 to 2000 conformations/microstates intermittently collected during the production runs. The aim was to sample from at least 1000 instances, for the results to be statistically reliable. Where possible (depending on time constraints), up to double that number was reached. Care was taken so that the microstates sampled were as statistically uncorrelated as possible, by allowing a large number of MCS in between.[4] Error bars represent size fluctuations exclusively —as there are no measurement errors involved in a computer experiment. They measure one standard deviation $(+/-\sigma)$ from the sample of data that make up each point.

The radius of gyration data are presented and discussed in the following sequence: To begin with, single chains are exclusively examined (Figures 9.7–9.8). Subsequently, single- and multi-chain structures are juxtaposed in context of the size category in which they belong; $N_{\mathrm{T}} = 1000$ (Figures 9.9–9.10), $N_{\mathrm{T}} = 5000$ (Figures 9.11–9.12), and $N_{\mathrm{T}} = 10000$ (Figures 9.13–9.14). Figures 9.7–9.14 incorporate

[4]It is not trivial to define the statistical correlation between two states as a function of their separation in MCS units and to predict at what separation that correlation tends to zero. Therefore, an ad hoc rule of thumb was considered, whereby enough MCS were allowed so that the majority of the monomers experienced one step of random motion. This, however, should not be a strict rule. Sampling too often might be redundant (the same information being reused), but is not practically wrong. Sampling more densely over a given simulation range is at least as good as sampling less densely.

both weak and strong adsorption conditions, as well as the perpendicular- and lateral-to-surface components of the radius of gyration. Where appropriate, they are presented in logarithmic scale. Figures 9.7–9.14 represent the totality of data collected during phase III. Finally, all data are juxtaposed in context of adsorption potential; weak (Figures 9.15–9.16) and strong (Figures 9.17–9.18).

9.3.1 Single Chains

Figure 9.7 presents the perpendicular, R_{g_z}, and lateral, $R_{g_{xy}}$, components of the radius of gyration for all single chains residing on both a weakly ($E_w = 0.3$) and a strongly ($E_w = 0.416$) adsorbing substrate.

Pertaining to the R_{g_z} graph, the $E_w = 0.416$ data lie below the $E_w = 0.3$ data for all N, as expected, because stronger adsorption conditions flatten the chains more. Also, a relatively small dependence of the chains' perpendicular dimensions on chain length / molecular weight, N, is observed. Namely, for an overall increase of N by one order of magnitude, R_{g_z} of $E_w = 0.3$ increases by approximately 1.7 times and R_{g_z} of $E_w = 0.416$ increases by approximately a factor of 1.4. The R_{g_z} dependence becomes weaker with increasing N (the slope of the graph is less between $N = 5000$ and $N = 10000$ than between $N = 1000$ and $N = 5000$). It is a known fact that as $N \to \infty$ an adsorbate's thickness becomes independent of N. This has been shown theoretically, for example through scaling theory (Rubinstein and Colby [2003]), as well as experimentally. Attention is drawn to recent experiments of Glynos et al., where single chains of molecular weights 38.6 kg/mol, 78.8 kg/mol, and 962 kg/mol were measured at 1.04 nm, 1.15 nm, and 1.84 nm, respectively, in adsorbed height. Once again, height dependence weakened with increasing molecular weight, while, overall, an increase in molecular weight by over an order of magnitude resulted in the adsorbed height changing approximately by a factor of 1.8 (AFM-measurement errors of height are reported around 0.3 nm).

The relative error within each adsorption category decreases with increasing chain length (errors bars remain approximately constant while R_{g_z} increases). This finds its justification in the fact that larger subsystems[5] in statistical physics exhibit more stable equilibria, hence expected to fluctuate less, relative to their size.

Pertaining to the $R_{g_{xy}}$ graph, the $E_w = 0.3$ data lie below the $E_w = 0.416$, mirroring the R_{g_z} graph. The dependence of $R_{g_{xy}}$ on N is slightly greater than of R_{g_z}. This is in agreement with the scaling theory prediction that the adsorbate thickness is independent of molecular weight, implying that molecular weight is

[5] As defined in, for example, Landau and Lifshitz [1980].

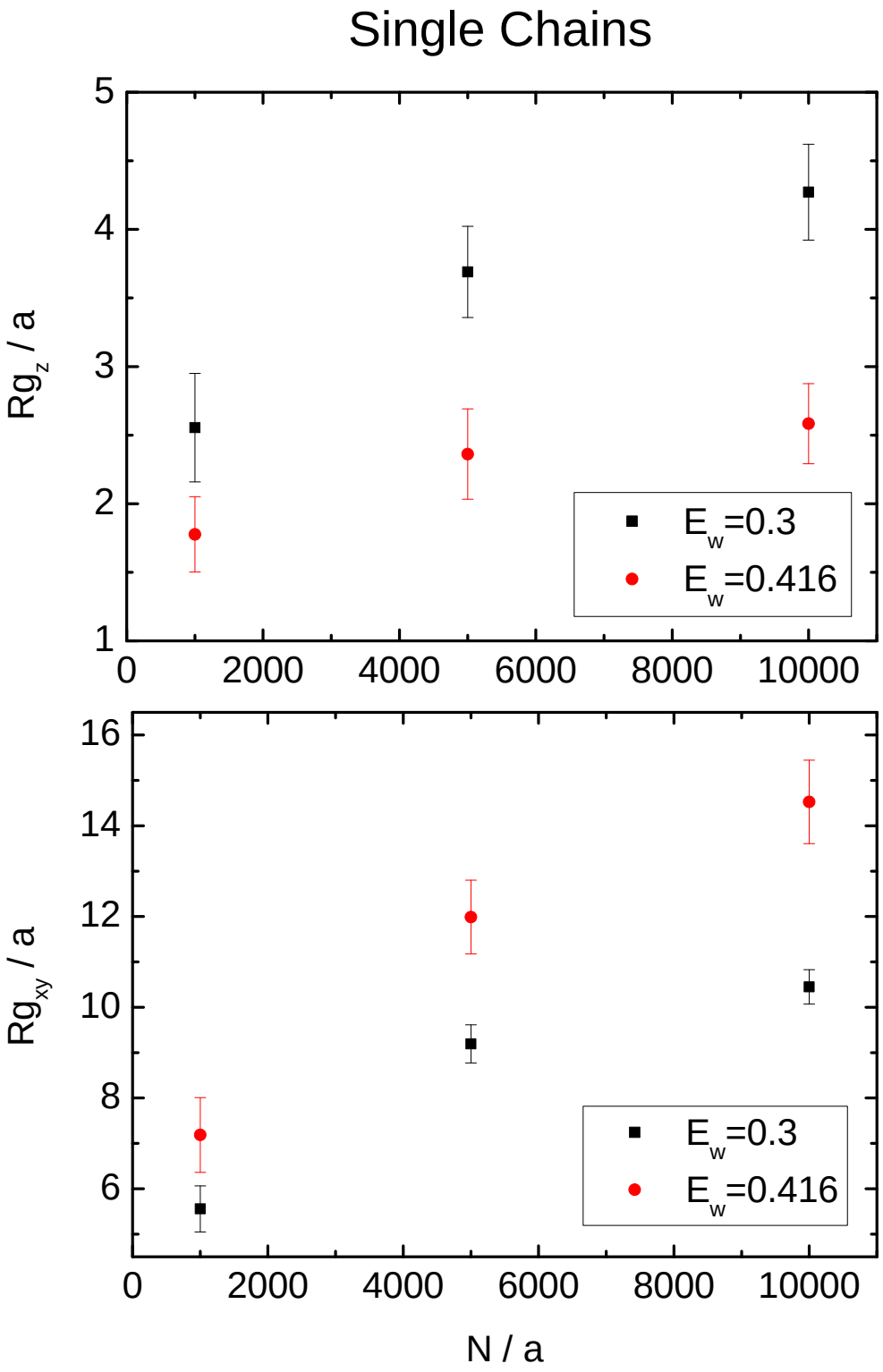

Figure 9.7: Perpendicular (top) and lateral (bottom) components of the radius of gyration, R_{g}, vs chain length, N, for all single chains on a weakly ($E_{\mathrm{w}} = 0.3$) and a strongly ($E_{\mathrm{w}} = 0.416$) adsorbing substrate. a is one lattice unit of length.

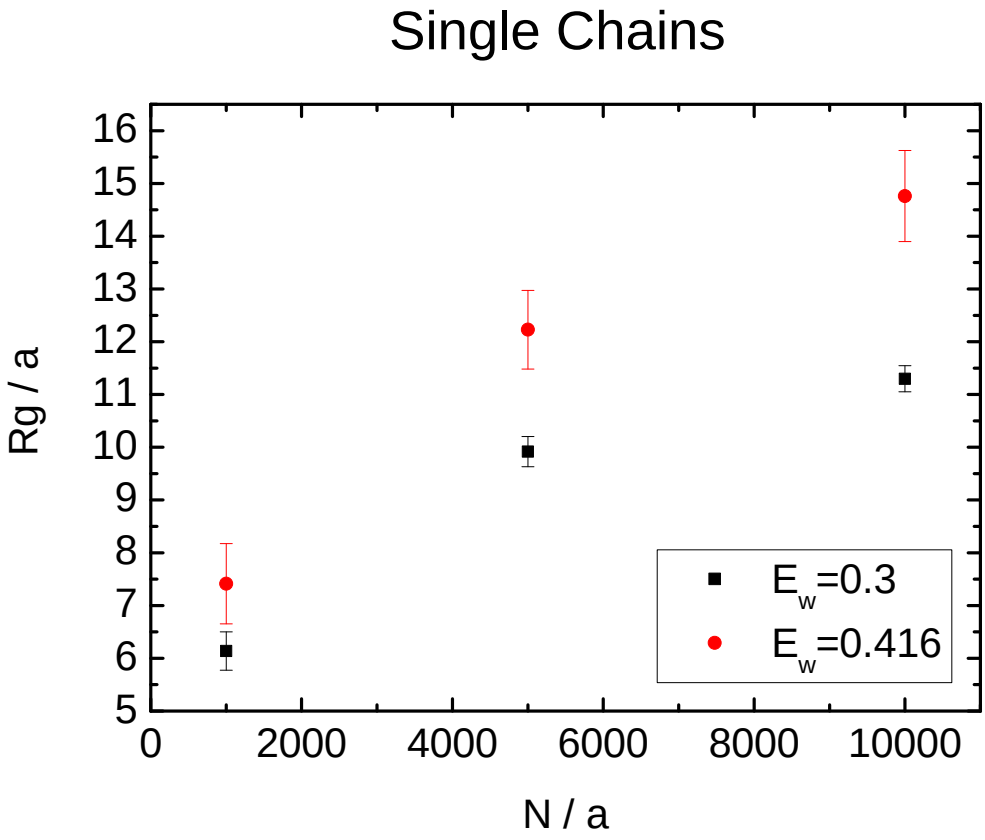

Figure 9.8: Radius of gyration, R_g, vs chain length, N, for all single chains on a weakly ($E_w = 0.3$) and a strongly ($E_w = 0.416$) adsorbing substrate. a is one lattice unit of length.

distributed along the surface rather than on top of existing layers. On the other hand, the $R_{g_{xy}}$ increase might be less than anticipated, because there are two dimensions in which the chain has the freedom to spread —a chain on a one-dimensional substrate would reflect this scaling theory prediction better. The larger spreading tendency and dimensions of the $E_w = 0.416$ chains are reflected in larger error bars compared to the $E_w = 0.3$ chains. The decreasing relative error trend with increasing N is observed similarly to the R_{g_z} graph.

Figure 9.8 presents the total radius of gyration, R_g. R_g follows the trend of $R_{g_{xy}}$, due to the latter's dominant contribution in comparison to that of R_{g_z}. Relative errors for $E_w = 0.416$ are greater than for $E_w = 0.3$. Stronger adsorption slows down kinetics and, as result of this, simulation data tend to be noisier.

9.3.2 Single Chains and Aggregates

Figures 9.9–9.14 present the perpendicular component, R_{g_z}, lateral component, $R_{g_{xy}}$, and total magnitude of the radius of gyration, R_g, of single- and multi-chain structures residing on both weakly ($E_w = 0.3$) and strongly ($E_w = 0.416$) adsorbing substrates. The entirety of single- and multi-chain structures are juxtaposed in context of the size category in which they belong: $N_T = 1000$ (Figures 9.9–9.10), $N_T = 5000$ (Figures 9.11–9.12), and $N_T = 10000$ (Figures 9.13–9.14).

Examination of the R_{g_z} components of the $N_T = 5000$ (Fig. 9.11) and $N_T = 10000$ (Fig. 9.13) systems reveals a feature central to the present results: *There is a distinction between single- and multi-chain systems in regard to their dimensions perpendicularly to the substrate upon which they are adsorbed.* An increase in size is observed from one to many chains, under both weak and strong adsorption conditions, somewhat more pronounced in the latter case. The increase is not gradual but steps up from one to many chains with a common plateau (with the exception of some two-chain aggregates discussed below). This result implies that there is a fundamental difference about the way in which a single chain interacts with an interface compared to the way a chemically identical aggregate of chains of the same total mass does. The following explanation is set forth: In the single chain case, adsorbed monomers / trains will drive their neighbours towards the substrate sheerly by mechanical connectivity. After a single chain is dissected, segments are freed up and settle on average further away from the substrate.

The above result is reinforced by experimental findings of Glynos et al.. As mentioned in Part I, where part of those experiments was presented, single-chain droplets could not be treated by continuum theory due to very low adsorbed height. Structures obtained a pancake-like shape (Fleer et al. [1993]) and monomers became trapped/pinned against the surface. The presence of a single chain, as opposed to several, in a droplet made a difference in its adsorption behavior, as discrepancy was observed between aggregates and single chains of similar size. Specifically, in the size range of 2.5×10^3 nm^3 to 4×10^3 nm^3, single chains of molecular weight $M_w = 962$ kg/mol exhibited adsorbed heights in the range 1 nm $-$ -4 nm, while aggregates consisting of $M_w = 78.8$ kg/mol chains exhibited adsorbed heights in the range 4.5 nm to 5.4 nm. What is more, the smallest single chains (similar-sized aggregates did not exist for comparison) also exhibited adsorbed heights so low as to not be treatable by continuum theory. It is, therefore, suggested that single chains, irrespectively of size, attain a fundamentally different adsorbed state.

Reference can be made to the works of Milchev and Binder [2001] and Milchev

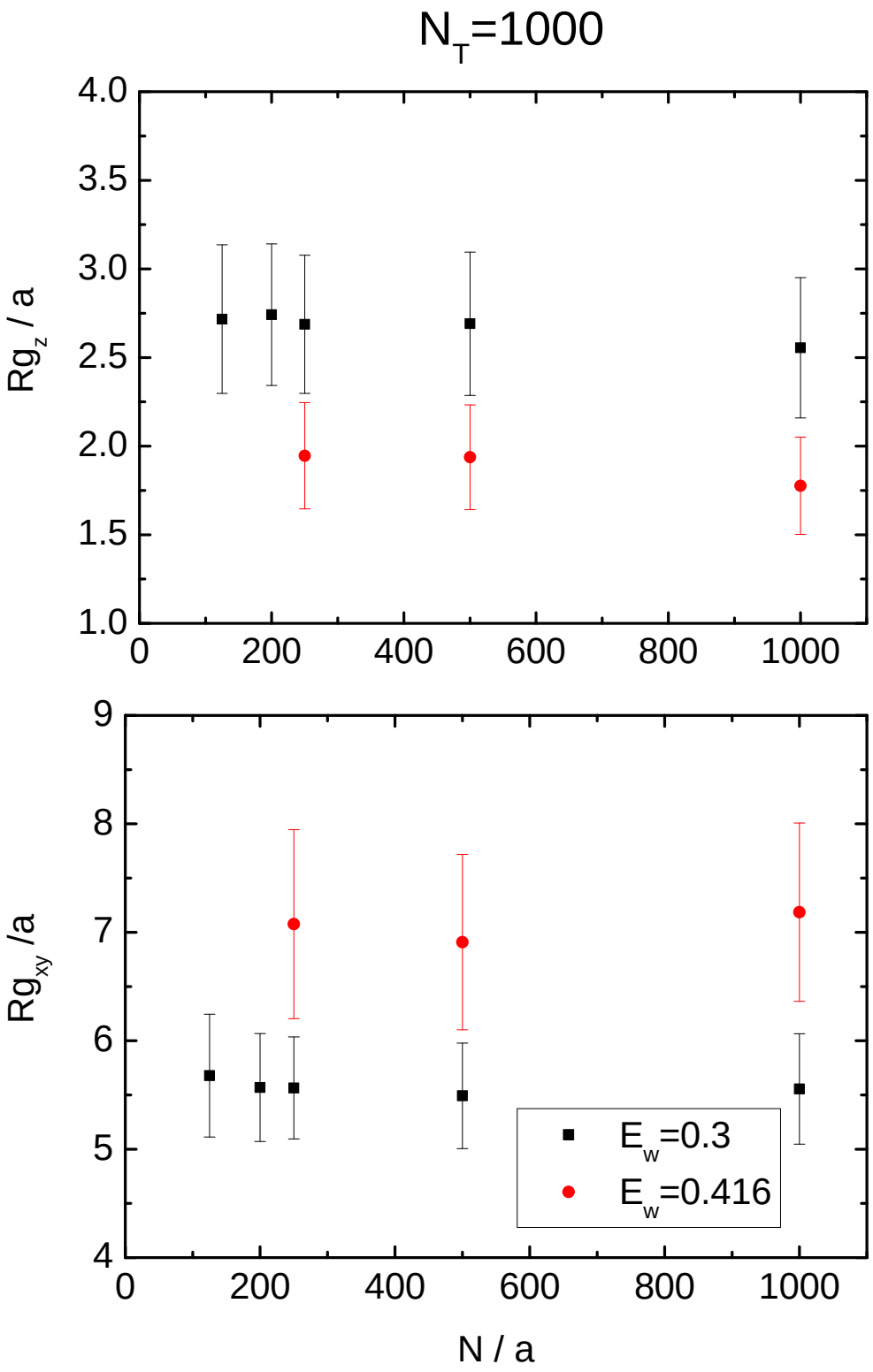

Figure 9.9: Perpendicular (top) and lateral (bottom) components of the radius of gyration, R_g, vs chain length, N, for the single chain and aggregates of $N_T = 1000$ on a weakly ($E_w = 0.3$) and a strongly ($E_w = 0.416$) adsorbing substrate. a is one lattice unit of length.

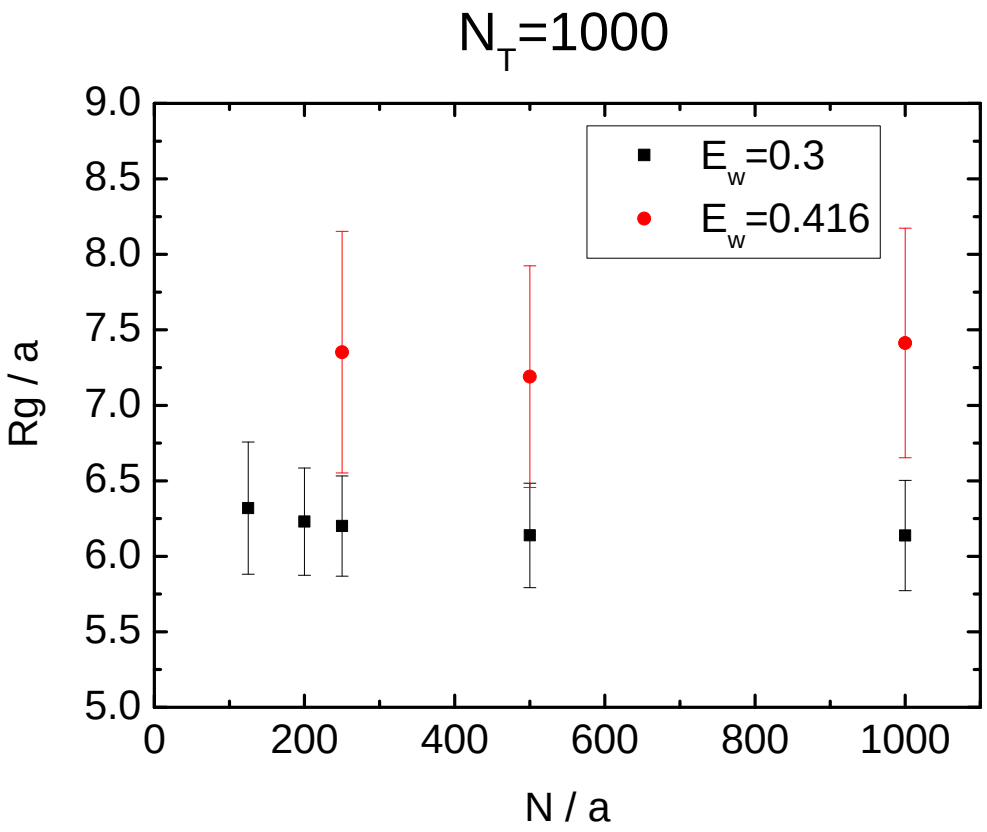

Figure 9.10: Radius of gyration, R_g, vs chain length, N, for the single chain and aggregates of $N_T = 1000$ on a weakly ($E_w = 0.3$) and a strongly ($E_w = 0.416$) adsorbing substrate. a is one lattice unit of length.

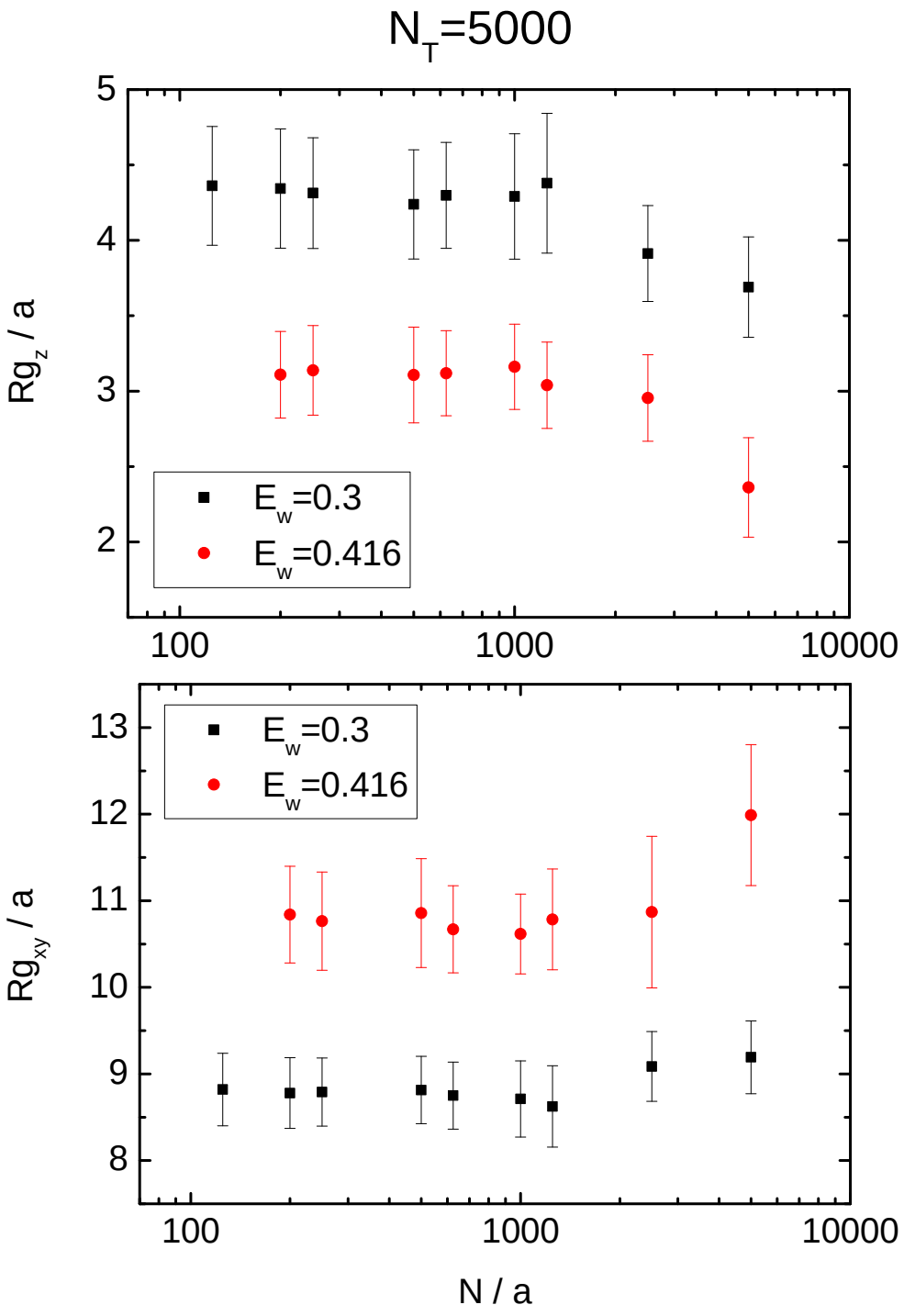

Figure 9.11: Perpendicular (top) and lateral (bottom) components of the radius of gyration, R_g, vs chain length, N, for the single chain and aggregates of $N_T = 5000$ on a weakly ($E_w = 0.3$) and a strongly ($E_w = 0.416$) adsorbing substrate. a is one lattice unit of length.

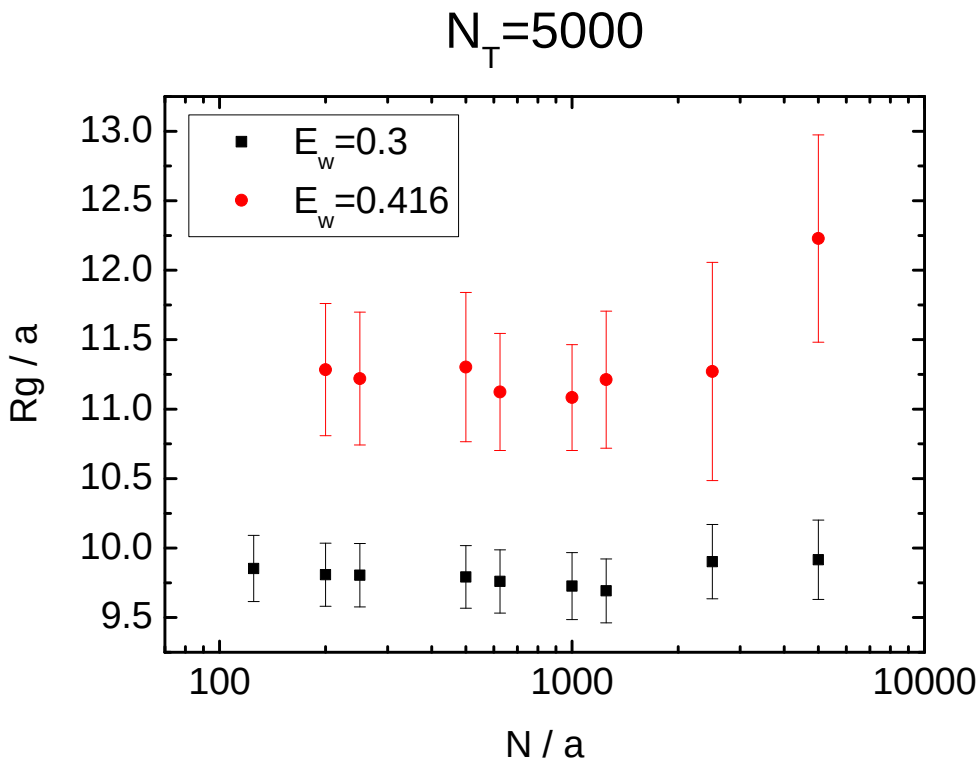

Figure 9.12: Radius of gyration, R_g, vs chain length, N, for the single chain and aggregates of $N_T = 5000$ on a weakly ($E_w = 0.3$) and a strongly ($E_w = 0.416$) adsorbing substrate. a is one lattice unit of length.

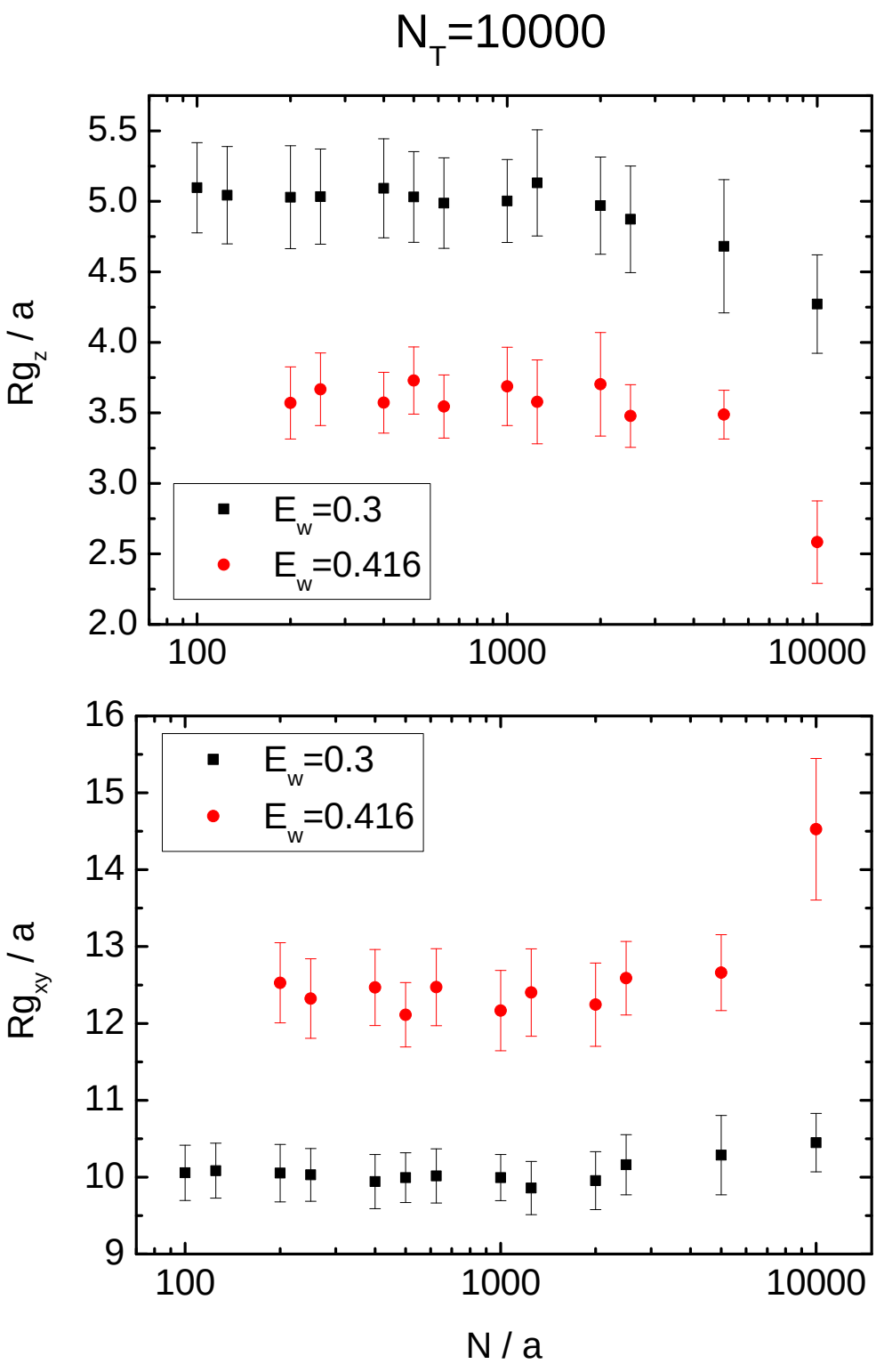

Figure 9.13: Perpendicular (top) and lateral (bottom) components of the radius of gyration, R_g, vs chain length, N, for the single chain and aggregates of $N_T = 10000$ on a weakly ($E_w = 0.3$) and a strongly ($E_w = 0.416$) adsorbing substrate. a is one lattice unit of length.

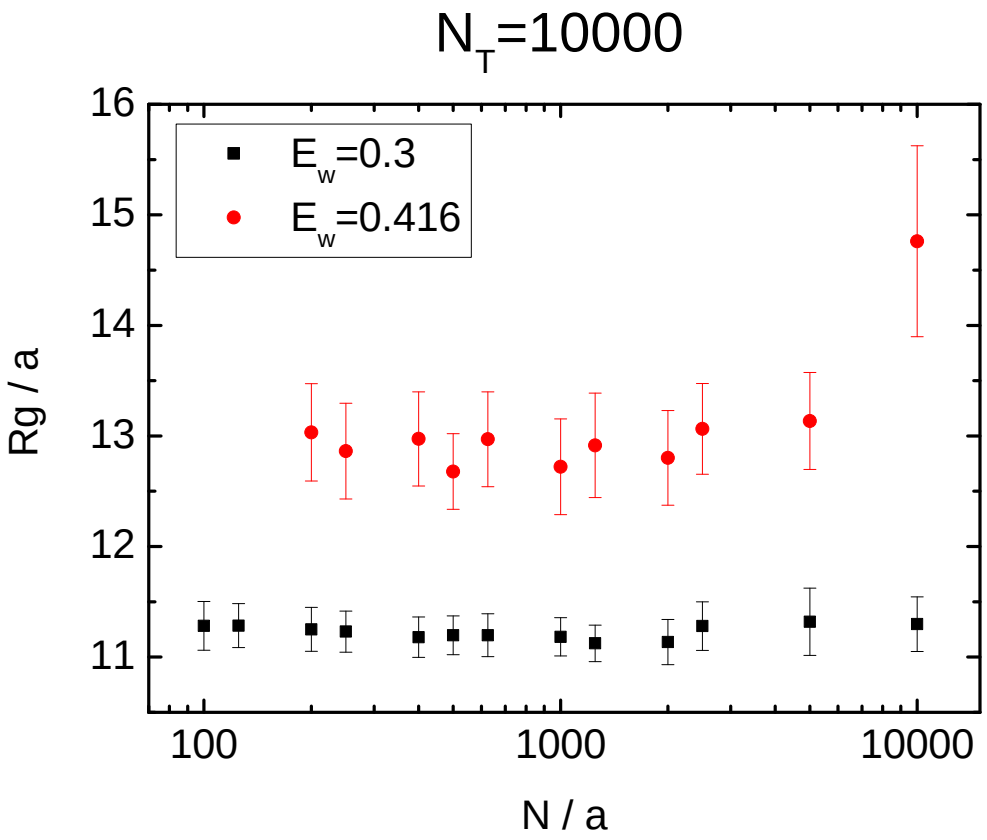

Figure 9.14: Radius of gyration, R_g, vs chain length, N, for the single chain and aggregates of $N_T = 10000$ on a weakly ($E_w = 0.3$) and a strongly ($E_w = 0.416$) adsorbing substrate. a is one lattice unit of length.

et al. [2002], which was introduced in Section 7.2, for an indirect comparison regarding aggregate adsorption. Milchev and Binder [2001] simulated chain aggregates on a substrate of variable (attractive) potential, under poor solvent conditions. Their results included density profiles of the cross section of adsorbed aggregates. Bearing in mind that such small systems may exhibit considerable fluctuations about their equilibrium shape and size, it can be argued from the density profiles that aggregates of 64 chains of length $N = 32$ exhibit a similar adsorbed height with aggregates of 128 chains of length $N = 16$ (equal total monomer number of 2048). Milchev et al. [2002] simulated similar systems and their results included contact angle estimates. It can be seen that aggregates of $N = 32$ and $N = 16$ (equal total monomer number of 2048) exhibit very similar contact angles (for a wide range of adsorbed states, from complete dewetting to complete wetting), implying similar adsorbed heights. Both of these works indirectly support the R_{g_z} plateau shared by multi-chain aggregates.

The contrast between single chains and aggregates is less apparent in the $N_T = 1000$ (Fig. 9.9) data, because the magnitude of the error bars (size fluctuations) is large compared to the data points' difference in value. The single chain's dimensions are still smaller than those of the aggregates, but only by a little. It is speculated that the overall smallness of these systems, being overwhelmed by the substrate attraction, drives them towards a pancake- than droplet-like shape.

There are minor distinctions between the $E_w = 0.3$ and $E_w = 0.416$ systems, in terms of the comparison between single chains and aggregates. Firstly, the increase in R_{g_z} appears proportionately larger for $E_w = 0.416$. Secondly, the location of $E_w = 0.3$ points corresponding to two-chain aggregates, namely $N_T = 5000$, $N = 2500$ (Fig. 9.11) and $N_T = 10000$, $N = 5000$ (Fig. 9.13), potentially implies a narrow transition region between single chains and aggregates. The existence of this region is less obvious in the $E_w = 0.416$ cases, where points corresponding to two-chain aggregates lie much closer to the multi-chain average.

All $R_{g_{xy}}$ data mirror, in trend, their corresponding R_{g_z} data about the horizontal. Where there is an increase in R_{g_z}, there is a decrease in $R_{g_{xy}}$, and vice versa, which is reasonable and means that polymers exhibit a positive Poisson's ratio. The total radius of gyration, R_g, follows the trend of $R_{g_{xy}}$, due to the latter's dominant contribution in comparison with that of R_{g_z}.

As briefly explained in Section 9.2, not all of the aggregates retained their cohesion during the simulation runs. A few underwent scission, that is chains or aggregates of chains became detached from the original structure. Following an event of scission, aggregate constituents recombined if their random walks brought

them sufficiently close together. The probability of recombination was considerably increased by the imposed periodic boundary conditions, which essentially confined motion inside the box. It, then, follows that systems spent a percentage of time in an aggregated state and the rest in a segregated state. Through ergodicity, it can be asserted that these percentages reflect the aggregates' stability. The stability of an aggregate renders it more or less meaningful —and possible— to analyze them. That is to say, a rather unstable aggregate indicates an unlikely observable in a real experiment. Also, an unstable aggregate would require a multiple of simulation time (quite considerable for the larger aggregates) in order for a minimum amount of data pertaining to its aggregated state to be gathered. Structures that appear in Table 9.1 but for which corresponding data points are missing from graphs of this section have been too unstable for a meaningful analysis to have become possible. Namely, these are: $N_{\mathrm{T}} = 1000$, $E_{\mathrm{w}} = 0.3$, $N = 100$; $N_{\mathrm{T}} = 1000$, $E_{\mathrm{w}} = 0.416$, $N = 100$ and $N = 125$ and $N = 200$; $N_{\mathrm{T}} = 5000$, $E_{\mathrm{w}} = 0.3$, $N = 100$; $N_{\mathrm{T}} = 5000$, $E_{\mathrm{w}} = 0.416$, $N = 100$ and $N = 125$; $N_{\mathrm{T}} = 10000$, $E_{\mathrm{w}} = 0.416$, $N = 100$ and $N = 125$.

Based on the above set, it is proposed that the following factors determine the probability of scission: Firstly, the degree of entanglement. Indeed, systems of greater N and N_{T} exhibited higher cohesion. For example, within any N_{T} category, there was not an unstable system of greater N than of a stable one. Also, under weak adsorption, while the $N_{\mathrm{T}} = 1000$, $N = 100$ experienced scission, the $N_{\mathrm{T}} = 10000$, $N = 100$ did not. The effect of N, however, dominates over that of N_{T}. Secondly, the contact area between chains. For a given monomer-monomer potential, corresponding to some probability of attachment of a monomer of one chain to a monomer of another chain, a greater N and N_{T} would increase the overall probability of inter-chain attachment. Though pertaining to the same variables and exhibiting similar trends, physical crosslinking and inter-chain monomer-monomer attachment are distinct mechanisms promoting cohesion. Thirdly, the effect of the substrate. A greater E_{w} increases the likelihood of a sub-part of the aggregate to be detached and be individually adsorbed on the substrate.[6] For example, in the $N_{\mathrm{T}} = 1000$ system, while only the $N = 100$ structure experienced scission under weak adsorption, both the $N = 100$ and $N = 125$ structures experienced scission under strong adsorption.

Figures 9.15–9.18 contain the entirety of data previously shown in Figures 9.9–

[6]Though not explored by the present simulations, the solvent quality, E, would obviously be expected to play a role. Given that $E = 0.45$ for all simulations, it can be asserted that cohesion was promoted, in respect of the solvent conditions.

9.14 re-illustrated in context of the two potentials, $E_{\mathrm{w}} = 0.3$ (Figures 9.15–9.16) and $E_{\mathrm{w}} = 0.416$ (Figures 9.17–9.18), under which polymers adsorbed. If Figures 9.9–9.14 allowed the reader the opportunity to compare between the weakly and strongly adsorbed state, then Figures 9.15–9.18 allow the opportunity to compare between the different size categories. $N_{\mathrm{T}} = 1000$, $N_{\mathrm{T}} = 5000$, and $N_{\mathrm{T}} = 1000$ systems are now superimposed on the same graph, while the sequence of presentation of the perpendicular component, R_{g_z}, followed by the lateral component, $R_{\mathrm{g}_{xy}}$, and, finally, the total magnitude of the radius of gyration, R_{g}, is preserved.

In all graphs, $N_{\mathrm{T}} = 10000$ samples lie above $N_{\mathrm{T}} = 5000$ samples, which lie above $N_{\mathrm{T}} = 1000$ samples, each category occupying a distinct region with virtually no overlap between error bars.

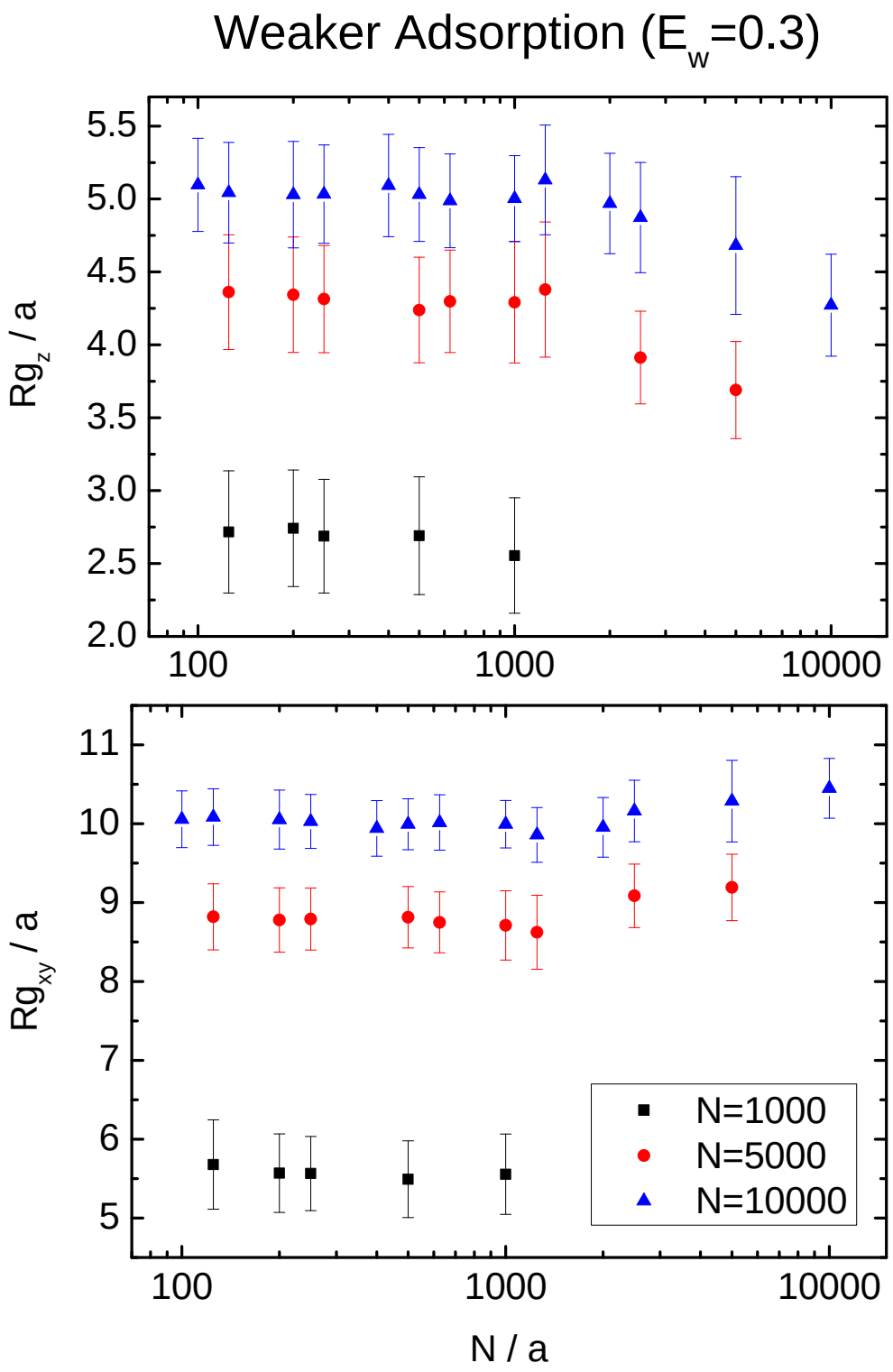

Figure 9.15: Perpendicular (top) and lateral (bottom) components of the radius of gyration, R_g, vs chain length, N, for the single chain and aggregates of $N_T = 1000$, $N_T = 5000$, and $N_T = 1000$ on a weakly adsorbing substrate ($E_w = 0.3$). a is one lattice unit of length.

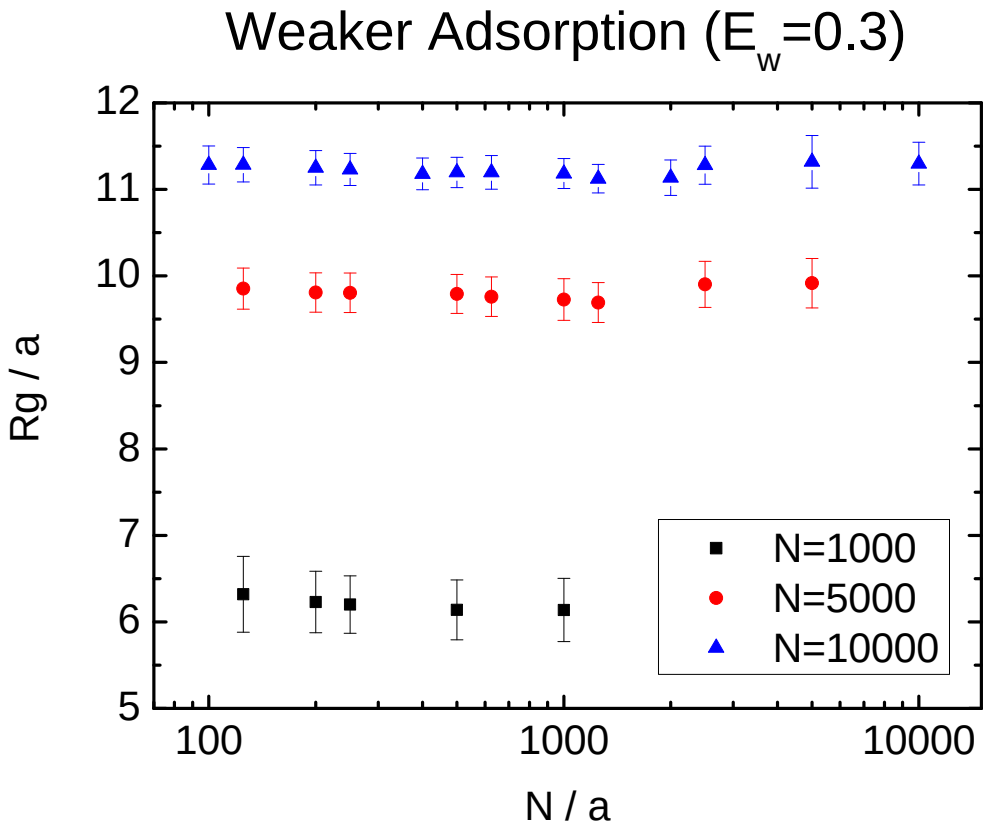

Figure 9.16: Radius of gyration, R_g, vs chain length, N, for the single chain and aggregates of $N_T = 1000$, $N_T = 5000$, and $N_T = 1000$ on a weakly adsorbing substrate ($E_w = 0.3$). a is one lattice unit of length.

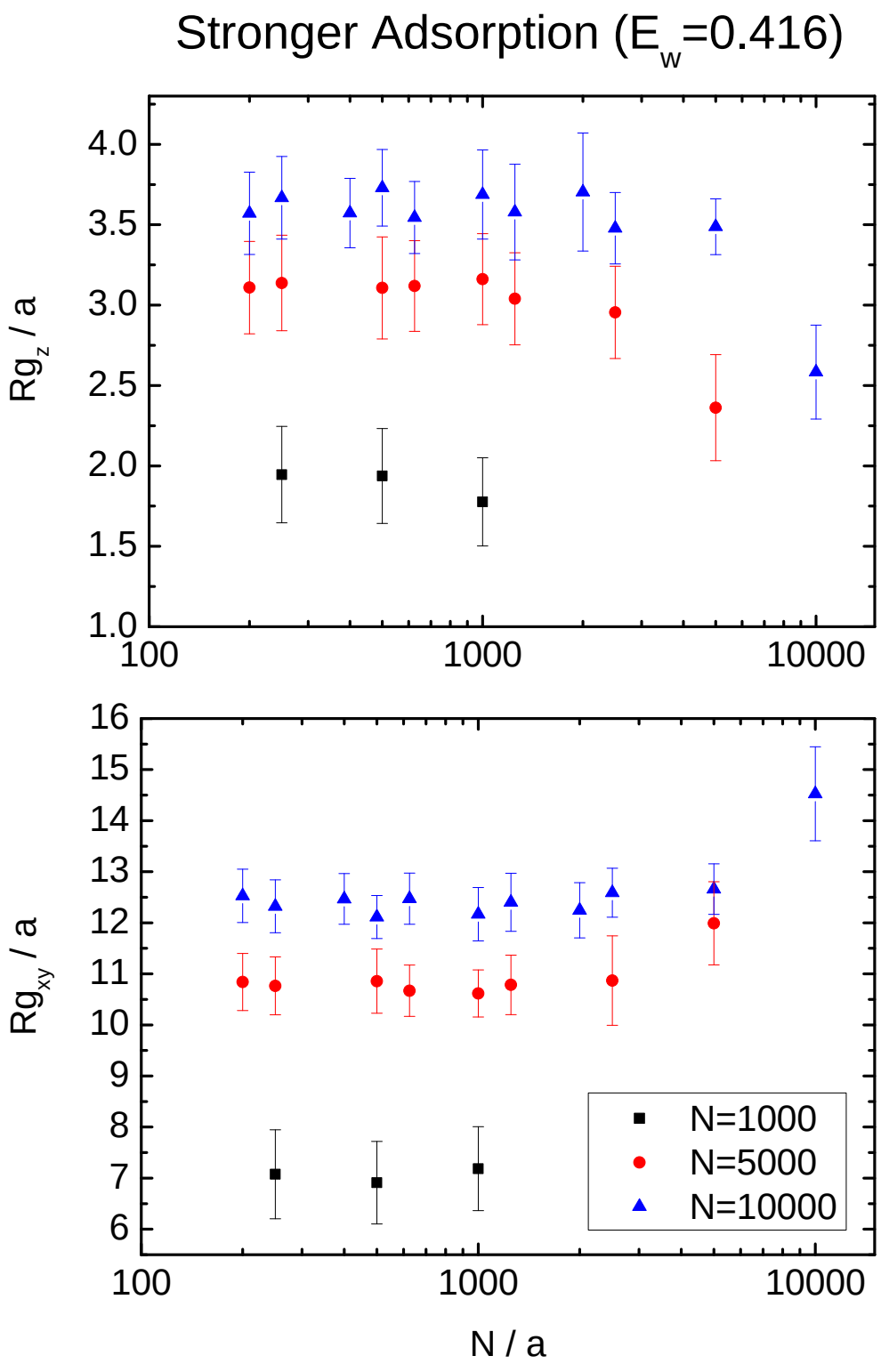

Figure 9.17: Perpendicular (top) and lateral (bottom) components of the radius of gyration, R_g, vs chain length, N, for the single chain and aggregates of $N_T = 1000$, $N_T = 5000$, and $N_T = 1000$ on a strongly adsorbing substrate ($E_w = 0.416$). a is one lattice unit of length.

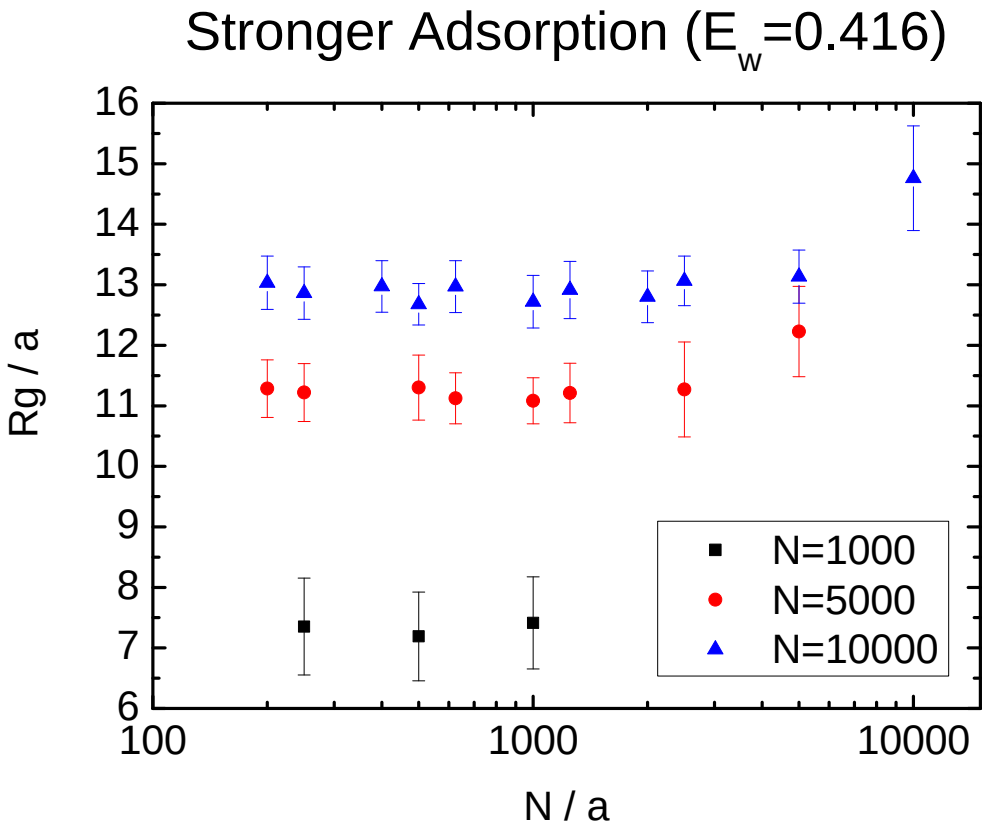

Figure 9.18: Radius of gyration, R_g, vs chain length, N, for the single chain and aggregates of $N_T = 1000$, $N_T = 5000$, and $N_T = 1000$ on a strongly adsorbing substrate ($E_w = 0.416$). a is one lattice unit of length.

Chapter 10

Conclusions

A MC computer simulation of polymer nanodroplets adsorbed on a substrate under poor solvent conditions has been performed. Droplets came in three different size categories, of $N_{\mathrm{T}} = 1000$, $N_{\mathrm{T}} = 5000$, and $N_{\mathrm{T}} = 10000$ total number of monomers. Each category comprised a range of architectures in terms of the length, N, of the chains contained within a droplet, N being constant across chains of the same droplet. Architectures ranged from single-chain droplets of $N = N_{\mathrm{T}}$ to many-chain droplets/aggregates. Both weak and strong adsorption potentials were investigated. The quantity under study was the radius of gyration, R_{g}, and its components along the perpendicular, R_{g_z}, and lateral, $R_{\mathrm{g}_{xy}}$, to the substrate directions, quantifying the droplets' adsorbed dimensions.

Regarding a comparison between single chains only, a relatively small dependence of R_{g_z} on N was observed, which became weaker with increasing N. This finding was supported by both theory and experiment. Regarding aggregates, different architectures of equal N_{T} were juxtaposed. The simulations illustrated a distinction between single- and multi-chain droplets: An increase in R_{g_z} was observed from one to many chains, under both weak and strong adsorption conditions, somewhat more pronounced in the latter case. The increase was generally not gradual but stepped up from one to many chains with a common plateau. This finding was supported by the experiments of Glynos et al. As also mentioned in Part I (where part of these experiments is discussed), in a given size range, single-chain structures obtained a pancake-like shape and monomers became trapped/pinned against the surface, while aggregates obtained a spherical-cap–shaped conformation. Indirect evidence in support of the multi-chain plateau was to be found in Milchev and Binder [2001] and Milchev et al. [2002], where density profiles and contact angle measurements implied similar adsorbed heights between aggregates

of 16 and 64 chains of an equal total monomer number of 2048.

Chapter 11

Summary, General Conclusions, and Further Work

Part I considered a theoretical treatment of the spreading of a polymer droplet on a substrate under poor solvent conditions. It was illustrated how the continuum theoretical model proposed can be used as a non-invasive method of extracting an elastic modulus, E_{D}, for the droplet when an experimental measurement of its adsorbed height is available. For the first time in the literature has such a theory been employed for adsorbed polymer droplets of a range of nanoscopic sizes ($5 - 100$ nm). The advantage of such an implementation is the avoidance of errors and complications involved in direct mechanical testing, allowing one to shed light on the relation between the material's response and intrinsic effects. Another benefit, stemming from the continuum nature of the model, as opposed to a microscopic theory, is that it is not confined to a particular type of polymeric material. This is because different types may be modeled through an according choice of values for macroscopic parameters. Having established all required parameters, h, R_0, γ_{P}, S, and ν, for a droplet, the theoretical model, represented by Eq. (3.17), was solved with respect to E_{D}.

The aforementioned range of droplet sizes was covered by samples in experiments of three different authors: Lau et al. [2002], Engqvist et al. [2007], and Glynos (Evangelopoulos et al. [2012]). Lau et al. [2002] dealt with styrene-butadiene latex droplets of various gel fractions (GF) and glass transition temperatures, T_{g}, in the ~ 100 nm regime adsorbed on silica at room temperature. Using an AFM in contact mode, Lau et al. [2002] measured the equilibrium height of the adsorbed latexes. The AFM-measured adsorbed heights confirmed the assumed spherical shape and led to predicted elastic moduli of the anticipated magnitude, given the

material. Lau et al. [2002] also measured the elastic modulus, E_{M}, of a polymer film of macroscopic dimensions, formed by an array of close-packed droplets like the aforementioned adhering together by their shells. E_{M} as measured by Lau et al. [2002] was *only generally* supported by the GF and T_{g} data for the latexes, while the trend exhibited by E_{D} as calculated with the present model is in *complete agreement* with the GF and T_{g}. This is attributed to the fact that E_{M} refers to the corresponding film, which, by construction, contains interface between the close-packed constituent droplets, while E_{D}, calculated directly from AFM data, is completely compatible with the materials' properties. Engqvist et al. [2007] investigated the effects of temperature, time, and preparation method on the adsorption of isolated styrene-acrylic latex droplets in the ~ 100 nm regime on a silicon substrate. Three types of styrene-acrylic latexes were used: L_{-20}, L_{20}, and L_{60}, the subscripts denoting glass transition temperatures of -20°C, 20°C, and 60°C, respectively. Using an AFM in contact mode, the height of the adsorbed latex droplets was measured. The AFM-measured adsorbed heights again confirmed the assumed spherical shape and led to predicted elastic moduli of the anticipated magnitude, given the material. The experiments of Engqvist et al. [2007] took into account different glass transition and treatment temperatures, as well as treatment times in the spreading of their styrene-acrylic latex droplets. All three parameters came into agreement with the moduli predicted by the present model. Lastly, the experiments of Glynos (Evangelopoulos et al. [2012]) measured heights of PB polymer droplets in the $5-50$ nm range on a mica substrate by AFM at room temperature. In conjunction with the present theoretical model, these experiments revealed a trend of decreasing elastic modulus E_{D} with increasing droplet size, progressively tending towards the bulk material value. This size effect is supported by the literature for related systems, though a consensus has not yet been reached (Yang et al. [2010]). Equally importantly, the experiments of Glynos (Evangelopoulos et al. [2012]) revealed the continuum theory's limitations: For single-chain droplets of (undeformed) radius ~ 5 nm or less, the theory predicted nonsensical values. Also, between aggregates and single chains of similar size, the former exhibited reasonable moduli, while the latter returned nonsensical values, suggesting a difference in adsorption behaviour between such systems, and, hence, the inapplicability of the present theoretical model for the single-chain type.

All in all, the investigation in Part I concluded on the following: the significance of not only surface forces, as for simple liquid droplets, but also of elasticity effects in the adsorption behaviour of a polymer droplets; the extent of a continuum theory's validity as one approaches the nanoscale; a droplet size effect on the elastic

modulus.

The following are set forth as proposed future work: Firstly, to seek experimental data involving chain aggregates of (undeformed) radius ~ 5 nm or less. As mentioned previously, this apparent size limitation might potentially entail more, as single-chain droplets of any size failed to be treated successfully by the theory. As these might be challenging structures to create, a computer simulation might complement in this respect (see later). Secondly, following from the relevant discussion in Subsection 5.1.3, further theoretical investigation on the effects of a size-dependent surface tension and of line tension, independently, or in a combined fashion, for such polymer droplets as those investigated herein, has potential to contribute to the field.

Part II considered a MC computer simulation of a polymer nanodroplet adsorbed on a substrate under poor solvent conditions. Droplets came in three different size categories, of $N_{\mathrm{T}} = 1000$, $N_{\mathrm{T}} = 5000$, and $N_{\mathrm{T}} = 10000$ total number of monomers. Each category comprised a range of architectures in terms of the length, N, of the chains contained within a droplet, N being constant across chains of the same droplet. Architectures ranged from single-chain droplets of $N = N_{\mathrm{T}}$ to multi-chain droplets/aggregates of $N = 100$, with all possible integral combinations in between. Both weak, $E_{\mathrm{w}} = 0.3$ and strong $E_{\mathrm{w}} = 0.416$ adsorption potentials were investigated. The quantity under study was the radius of gyration, R_{g}, and its components along the perpendicular, R_{g_z}, and lateral, $R_{\mathrm{g}_{xy}}$, to the substrate directions, as a means of characterizing the adsorbed dimensions of the droplets.

Single chains were examined first. A relatively small dependence of R_{g_z} on N was observed. Namely, for an overall increase of N by one order of magnitude, R_{g_z} of $E_{\mathrm{w}} = 0.3$ increased by approximately 1.7 times and R_{g_z} of $E_{\mathrm{w}} = 0.416$ increased by approximately a factor of 1.4. The R_{g_z} dependence became weaker with increasing N. These findings are supported by both theory, such as the scaling prediction of an adsorbate's thickness becoming independent of N as $N \to \infty$, and experiment, such as the recent experiments of Glynos et al. Following the investigation on single chains, different aggregate architectures of equal N_{T} were juxtaposed. In the $N_{\mathrm{T}} = 5000$ and $N_{\mathrm{T}} = 10000$ categories, the simulations illustrated a distinction between single- and multi-chain droplets. An increase in R_{g_z} was observed from one to many chains, under both weak and strong adsorption conditions, somewhat more pronounced in the latter case. The increase was generally not gradual but stepped up from one to many chains with a common plateau. It is speculated that in the single chain case, adsorbed monomers / trains will drive their neighbours towards the substrate sheerly by mechanical connectivity. After a single chain is dissected,

segments are freed up and settle on average further away from the substrate. This is a point which brings Part I and II together, as the above result is reinforced by the findings discussed in Subsection 5.1.3, where single-chain droplets could not be treated by the continuum theory model of Part I due to very low adsorbed height. Structures obtained a pancake-like shape and monomers became trapped/pinned against the surface. Equal-sized droplets containing several chains, on the other hand, did attain spherical-cap conformations, for which the theory returned sensible elastic moduli. The distinction between single chains and aggregates was not seen from simulations in the $N_{\mathrm{T}} = 1000$ category.

The above point allows for a further connection with Part I to be made, regarding the nature of the limit of the continuum theory at very small sizes (~ 5 nm), and a way of using lattice simulation as a way to validate the continuum theory can be proposed for future work: If a quantitative correspondence can is made between the unit length of the simulated chain and the unit length of the real PB chain (with the Kuhn segment as the common denominator, for example), then simulating relatively small N_{T} systems might substitute for the lack of real multi-chain structures at those very small sizes. Further to that specific size range, a simulation can offer an alternative to the real experiment more generally, as one can design a system which is not only free of experimental uncertainty and unnecessary features, however also precisely designed. For instance, one of the largest uncertainties in the application of the continuum theory model came from literature-reported surface tension values (Subsection 5.1.3). To the advantage of simulations, several techniques have been developed to calculate surface tension, from a mechanical definition and calculation of pressure components (Walton and Gubbins [1985]), through a thermodynamic definition and calculation of free-energy (Bennett [1976]), to finite-size scaling (Binder [1982]). Further future work ideas could include: Droplet shape analysis as per Rissanou et al. [2009] and Ivanov et al. [2000], for a more complete consideration of the adsorbed state. Calculation of the mean height of a collection of monomers at the top of droplets. This calculation would enable a more direct comparison with AFM-measured heights than the currently used R_{g_z}. There is correlation, of course, between R_{g_z} and the droplet height, measured in a real experiment, however R_{g_z} can more generally be affected by other properties such as the internal distribution of monomers and chains. Therefore, calculation of a mean height would come to much closer correspondence with what the AFM tip measures in reality. In the discussion of the difference between the adsorption behaviour of single- and multi-chain systems in Subsection 9.3.2, the following explanation was set forth: In the single chain case,

adsorbed monomers / trains drive their neighbours towards the substrate sheerly by mechanical connectivity. After a single chain is dissected, segments are freed up and settle on average further away from the substrate. Here a couple methods are proposed as a quantitative verification of this hypothesis: 1. Statistical analysis of the internal structure of a (multi-chain) droplet in terms of the location of its constituent chains and monomers. The analysis could include calculation of the number of chains in contact with substrate, the number of monomers in contact with substrate, and the number of monomers per chain in contact with substrate. 2. Calculation of the stress tensor (Doi and Edwards [1991]) inside the droplet. Deformation of the polymer due to adsorption will give rise to internal stress. Following appropriate definition of a tensor quantifying stress as the ratio of force to cross-sectional area in specified directions, the tensor could be evaluated throughout the volume of the polymer structure and could be compared between the cases of different numbers of chains making up a droplets of equal mass. If the aforementioned hypothesis is correct, then is it anticipated that stress will be higher in a single-chain structure, due to the fact that adsorbed monomers and trains will drag neighbouring segments towards the substrate, manifested in a flatter (more deformed) structure overall. Both the statistical analysis of the internal monomer and chain structure and the calculation of the stress tensor may reveal information that is impossible to measure in a real experiment and potentially clarify the mechanism that drives single chains to adsorb differently from aggregates.

Appendix A

Analytical Derivations

A.1 Derivation of Eq. 3.1

$$
\begin{aligned}
V_{\text{cap}} &= \int_h^0 \pi\rho^2(h)dh \\
&= \int_0^\theta \pi\rho^2(\theta)Rd\theta\sin\theta \\
&= \pi R\int_0^\theta \rho^2(\theta)Rd\theta\sin\theta, \quad \rho(\theta) = R\sin\theta \\
&= \pi R\int_0^\theta (R\sin\theta)^2\sin\theta d\theta \\
&= \pi R^3\int_0^\theta \sin^3\theta d\theta, \\
&= \pi R^3\int_0^\theta (1-\cos^2\theta)\sin\theta d\theta \\
&= \pi R^3\int_0^\theta -(1-y^2)\sin\theta(dy/\sin\theta) \\
&= \pi R^3\int_0^\theta (y^2-1)dy \\
&= \pi R^3\left[y^3/3-y\right]_{\theta=0}^{\theta=\theta} \\
&= \pi R^3\left[\frac{\cos^3\theta}{3}-\cos\theta-\left(\frac{\cos 0}{3}-1\right)\right] \\
&= \frac{\pi R^3}{3}\left[\cos^3\theta-3\cos\theta+2\right] \qquad \text{(A.1)}
\end{aligned}
$$

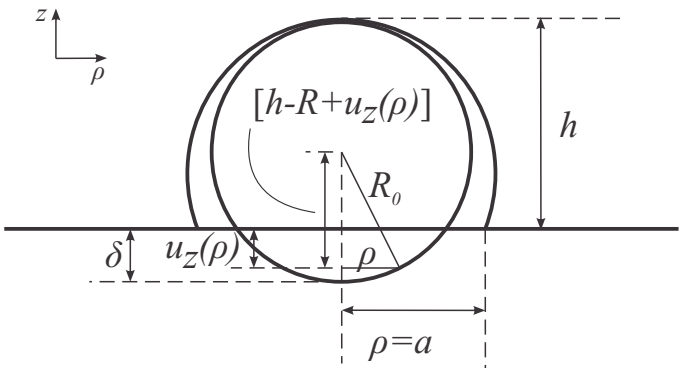

Figure A.1: Geometry of deformation upon adsorption.

A.2 Derivation of Eq. 3.6

Refer to Figure A.1. By superimposing the undeformed onto the deformed state, it can be seen that the extent of deformation in the z direction will equal $u_z(\rho)$, i.e. the magnitude of the undeformed arc coordinate below the substrate. From the Pythagorean theorem,

$$\begin{aligned}
(u_z(\rho) + h - R_0)^2 &= R_0^2 - \rho^2 \\
u_z(\rho) &= R_0 - h + \sqrt{R_0^2 - \rho^2} \\
u_z(\rho) &= 2R_0 - h - R_0 \left[1 - \left(\sqrt{R_0^2 - \rho^2}\right)/R_0\right] \\
u_z(\rho) &= \delta - R_0 \left[1 - \sqrt{1 - (\rho/R_0)^2}\right],
\end{aligned}$$

where $\delta = 2R_0 - h$ is the central deformation.

A.3 Derivation of Eq. 3.12

$$U_E = \pi \int_0^a \rho d\rho \left[\sigma_0 \left(1 - \rho^2/a^2\right)^{-1/2} + \sigma_1 \left(1 - \rho^2/a^2\right)^{1/2}\right] \delta \left(1 - \rho^2/(2R_0)\right).$$

Changing variables $u = (\rho^2/a^2) \Rightarrow d\rho = a^2 du/2\rho$,

$$U_{\rm E} = \frac{\pi a^2}{2} \int_{u=0}^{1} du \left[\left(\delta - a^2 u/(2R_0)\right) \sigma_0 (1-u)^{-1/2} + \left(\delta - a^2 u/(2R_0)\right) \sigma_1 (1-u)^{1/2} \right]$$

$$= \frac{\pi a^2}{2} \int_{0}^{1} du \left[\delta\sigma_0 (1-u)^{-1/2} - \frac{a^2\sigma_0}{2R_0} u'(1-u')^{-1/2} + \delta\sigma_1 (1-u)^{1/2} - \frac{a^2\sigma_1}{2R_0} u(1-u)^{1/2} \right]$$

$$= \frac{\pi a^2 \delta\sigma_0}{2} \left[-2\sqrt{1-u} \right]_0^1 + \frac{\pi a^4 \sigma_0}{4R_0} \left[-\frac{2}{3}(1-u)^{3/2} + 2\sqrt{1-u} \right]_0^1 + \frac{\pi a^2 \delta\sigma_1}{2} \left[-\frac{(1-u)^{3/2}}{3/2} \right]_0^1 - \frac{\pi a^4 \sigma_1}{4R_0} \left[\frac{2}{5}(1-u)^{5/2} - \frac{2}{3}(1-u)^{3/2} \right]_0^1$$

$$= \frac{\pi a^2 \delta\sigma_0}{2} [2] + \frac{\pi a^4 \sigma_0}{4R_0} \left[\frac{2}{3} - 2 \right] + \frac{\pi a^2 \delta\sigma_1}{2} \left[\frac{2}{3} \right] - \frac{\pi a^4 \sigma_1}{4R_0} \left[-\frac{2}{5} + \frac{2}{3} \right]$$

$$= \pi a^2 \delta\sigma_0 - \frac{\pi a^4 \sigma_0}{3R_0} + \frac{\pi a^2 \delta\sigma_1}{3} - \frac{\pi a^4 \sigma_1}{15R_0}.$$

Appendix B

List of Symbols

Latin

E – monomer-monomer potential
E_{D} – elastic modulus of polymer droplet
E_{M} – elastic modulus of macroscopic polymer material
E_{w} – monomer-substrate potential
h – adsorbed droplet height
I – thermodynamic internal energy
K – rigidity
M_{w} – molecular weight
$M_{\mathrm{w_0}}$ – molecular weight of a Kuhn monomer
$M_{\mathrm{w_e}}$ – molecular weight of an entanglement strand
N – chain length (polymerization index)
N_{T} – total number of monomers in a system
$\mathbb{N}$ – set of natural numbers
P – pressure
R_0 – undeformed polymer droplet radius

R_{g} – radius of gyration
S – spreading parameter
S_{E} – entropy
T_{g} – glass transition temperature
T_{Θ} – theta temperature for a polymer solution
U – free energy contribution from the bulk
U_{DEF} – free energy contribution from defects
V – volume
w – Dupré energy of adhesion

Greek

Γ – surface energy
γ – surface tension
μ – Flory exponent
ν – Poisson's ratio
ξ – relaxation time
ξ_0 – relaxation time of a Kuhn monomer
ξ_e – relaxation time of an entanglement strand
τ – line tension
Φ – Gibbs free energy

Appendix C

List of Abbreviations

AC – adsorbed collapsed
AE – adsorbed extended
AFM – atomic force microscopy
CBMC – configuration bias Monte Carlo
DC – desorbed collapsed
DE – desorbed extended
DNA – deoxyribonucleic acid
DPAT – direct peeling with AFM tip
FENE – finitely extensible nonlinear elastic (potential)
GF – gel fraction
HDPE – high density polyethylene
JKR – Johnson-Kendall-Roberts
LDPE – low density polyethylene
LMC – local monte carlo
MC – monte carlo
MCS – monte carlo step

MD – molecular dynamics
MFT – mean-field theory
PBC – periodic boundary conditions
PDMS – polydimethylsiloxane
PMHS – polymethylhydrosiloxane
PS – polystyrene
PVC – polyvinyl chloride
RG – renormalization group
RT – room temperature
SAG – surface attached globule
SAW – self-avoiding walk
SCFT – self-consistent field theory
SEM – scanning electron microscopy
STC – surface tension component
STP – standard temperature and pressure
vOCG – van Oss Chaudhury Good

Bibliography

N. K. Adam. Use of the term 'young's equation' for contact angles. *Nature*, 180 (4590):809–810, 1957.

K. Akabori, K. Tanaka, T. Kajiyama, and A. Takahara. Anomalous surface relaxation process in polystyrene ultrathin films. *Macromolecules*, 36(13):4937–4943, 2003.

G. Alberti, G. Bouchitté, and P. Seppecher. Phase transition with line tension effect. *Arch. Ration. Mech. Anal*, 144(1), 1998.

M. Alcoutlabi and G. B. McKenna. Effects of confinement on material behaviour at the nanometre size scale. *J. Phys.: Condens. Mater*, 17(5):R461–R524, 2005.

B. J. Alder and T. E. Wainwright. Studies in molecular dynamics. i. general method. *The Journal of Chemical Physics*, 31(2):459–466, 1959.

S. Alexander. Adsorption of chain molecules with a polar head - a scaling description. *Journal de Physique*, 38(8):983–987, 1977.

M. P. Allen and D. J. Tildeslay. *Computer Simulation of Liquids*. Oxford University Press, 1991.

A. Amirfazli and A. W. Neumann. Status of the three-phase line tension: a review. *Advances in Colloid and Interface Science*, 110(3):121–141, 2004.

E. Amitay-Sadovsky, B. Ward, G. A. Somorjai, and K. Komvopoulos. Nanomechanical properties and morphology of thick polyurethane films under contact pressure and stretching. *J. Appl. Phys.*, 91(1):375–381, 2002.

M. I. Aranguren and C. W. Macosko. Modulus of polybutadiene networks made by hydrosilation cross-linking. *Macromolecules*, 21(8):2484–2491, 1988.

O. Araujo, L. Brauge, and A. D. Findlay. Modelling polymer particle deformation on mineral surfaces - part i: Validation of initial concepts. *Macromolecular Symposia*, 271:75–82, 2008.

J. B. Avalos, A. D. Mackie, and S. Diez-Orrite. Development of an importance sampling single chain mean field theory for polymer adsorption onto a flat wall. *Macromolecules*, 37(3):1124–1133, 2004.

A. I. Bailey and S. M. Kay. A direct measurement of the influence of vapour, of liquid and of oriented monolayers on the interfacial energy of mica. *Proceedings of the Royal Society A - Mathematical, Physical and Engineering Sciences*, 301 (47):47–56, 1967.

A. I. Bailey and A. G. Price. Interfacial energies of monomolecular films of fatty acids deposited on mica in aqueous and nonaqueous media strength of hydrophobic interactions. *The Journal of Chemical Physics*, 53(9):3421–3427, 1970.

A. C. Balazs, T. Emrick, and T. P. Russell. Nanoparticle polymer composites: Where two small worlds meet. *Science*, 314:1107–1110, 2007.

K. G. Barnett, T. Cosgrove, B. Vincent, D. S. Sissons, and M. Cohen-Stuart. Measurement of the polymer-bound fraction at the solid-liquid interface by pulsed nuclear magnetic-resonance. *Macromolecules*, 14(4):1018–1020, 1981.

K. G. Barnett, T. Cosgrove, B. Vincent, A. N. Burgess, T. L. Crowley, T. King, J. D. Turner, and T. F. Tadros. The configuration of adsorbed polymers at the solid-solution interface. *Symposia of the Faraday Society*, (16), 1982.

J. Baschnagel, H. Meyer, F. Varnik, S. Metzger, M. Aichele, M. Müller, and K. Binder. Computer simulations of polymers close to solid interfaces: some selected topics. *Interface Science*, 11(2):159–173, 2003.

A. Baumgärtner and M. Muthukumar. Effects of surface roughness on adsorbed polymers. *J. Chem. Phys.*, 94:4062–4070, 1991.

C. H. Bennett. Efficient estimation of free-energy differences from monte-carlo data. *Journal of computational physics*, 22:245–268, 1976.

K. Binder. Monte-Carlo calculation of the surface-tension for two-dimensional and 3-dimensional lattice-gas models. *Physical Review A*, 25:1699–1709, 1982.

K. Binder, editor. *Monte Carlo and Molecular Dynamics Simulations in Polymer Science*. Oxford University Press, 1995.

K. Binder and W. Paul. Recent developments in monte carlo simulations of lattice models for polymer systems. *Macromolecules*, 41(13):4537–4550, 2008.

S. Bluestone and C. L. Cronan. Polymer configuration at an adsorbing interface by the Monte Carlo method. *The Journal of Physical Chemistry*, 70(1):306–309, 1966.

E. Bouchaud and J. Vannimenus. Polymer adsorption : bounds on the cross-over exponent and exact results for simple models. *Journal de Physique*, 50(19): 2931–2949, 1989.

F. Bresme and N. Quirke. Computer simulation study of the wetting behavior and line tensions of nanometer size particulates at a liquid-vapor interface. *Physical Review Letters*, 80(17):3791–3794, 1998.

B. J. Briscoe and K. S. Sebastian. The elastoplastic response of poly(methyl methacrylate) to indentation. *Proc. R. Soc. Lond. A*, 452(1996):439–457, 1996.

H. R. Brown. Chain pullout and mobility effects in friction and lubrication. *Science*, 263(5152):1411–1413, 1994.

R. P. Brown. *Handbook of Polymer Testing*. Marcel Dekker, 1999.

M. Burman, A. Arinstein, and E. Zussman. Free flight of an oscillated string pendulum as a tool for the mechanical characterization of an individual polymer nanofiber. *Appl. Phys. Lett.*, 93(19):193118–1–193118–3, 2008.

H. J. Busscher, G. A. M. Kip, A. van Silfhout, and J. Arends. Spreading pressures of water and n-propanol on polymer surfaces. *Journal of Colloid and Interface Science*, 114(2):307–313, 1986.

O. Byutner and G. D. Smith. Viscoelastic properties of polybutadiene in the glassy regime from molecular dynamics simulations. *Macromolecules*, 35:3769–3771, 2002.

N. Cabeo. Philosophia magnetica. Ferrara, 1629. cap. 20.

J. M. Carella and W. M. Graessley. Effects of chain microstructure on the viscoelastic properties of linear polymer melt: Polybutadienes and hydrogenated polybutadienes. *Macromolecules*, 17(12):2775–2786, 1984.

A. Carré, J.-C. Gastel, and M. E. R. Shanahan. Viscoelastic effects in the spreading of liquids. *Nature*, 379:432–434, 1996.

D Chan, D. J. Mitchell, B. W. Ninham, and L. R. White. Conformation of a non-interacting polymer near a sticky wall. *Journal of The Chemical Society - Faraday Transactions II*, 71(2):235–268, 1975.

C. Q. Chen, Y. Shi, Y. S. Zhang, J. Zhu, and Y. J. Yan. Size dependence of young's modulus in zno nanowires. *Physical Review Letters*, 96(7):075505–1–075505–4, 2006.

A. Chremos, E. Glynos, V. Koutsos, and P. Camp. Adsorption and self-assembly of linear polymers on surfaces: A computer simulation study. *Soft Matter*, 5(3): 637–645, 2008.

H. K. Christenson. Adhesion and surface energy of mica in air and water. *The Journal of Physical Chemistry*, 97(46):12034–12041, 1993.

A. T. Clark and M. Lal. Effect of surface coverage on the configurational properties of adsorbed chains. *Journal of the Chemical Society, Faraday Transactions 2: Molecular and Chemical Physics*, 74:1857–1869, 1978.

A. T. Clark, M. Lal, M. A. Turpin, and K. A. Richardson. Configurational state of adsorbed chain molecules - behaviour of terminally anchored chains. *Faraday Discussions of the Chemical Society*, 59:189–195, 1975.

J. P. Cleveland, B. Anczykowsky, A. E. Schmid, and V. B. Elings. Energy dissipation in tapping-mode atomic force microscopy. *Applied Physics Letters*, 72(20): 2613–2615, 1998.

M. A. Cohen-Stuart and Hasashi Tamai. Dynamics of adsorbed polymers. 1. thickness relaxation of poly(vinylpyrro1idone) on glass. *Macromolecules*, 21(6):1863–1866, 1988.

R. H. Colby, L. J. Fetters, and W. W. Graessley. Melt viscocity-molecular weight relationship for linear polymers. *Macromolecules*, 20(9):2226–2237, 1987.

A. R. Conway, I. G. Enting, and A. J. Guttmann. Algebraic techniques for enumerating self-avoiding walks on the square lattice. *Journal of Physics A: Mathematical and General*, 26(7):1519–1534, 1992.

T. Cosgrove, C. A. Prestidge, and B. Vincent. Chemisorption of linear and cyclic polymethylsilocanes on alumina studied by fourier-transform infrared-spectroscopy. *Journal of the Chemical Society - Faraday Transactions*, 86(9): 1377–1382, 1990.

J. K. Cox, A. Eisenber, and R. B. Lennox. Patterned surfaces via self-assembly. *Current Opinion in Colloid & Interface Science*, 4(1):52–59, 1999.

S. Cuenot, S. Demoustier-Champagne, and B. Nysten. Surface tension effect on the mechanical properties of nanomaterials measured by atomic force microscopy. *Phys. Rev. Lett.*, 85(8):1690–1693, 2000.

S. Cuenot, S. Demoustier-Champagne, N. Fretigny, and B. Nysten. Size effect on the elastic modulus of nanomaterials as measured by resonant contact atomic force microscopy. *Nanotechnology*, 3:549–552, 2003.

M. Daoud and G. Jannink. Temperature-concentration diagram of polymer solutions. *Journal de physique*, 37(7–8):973–979, 1976.

M. Daoud, J. P. Cotton, G. Farnoux, B. Jannink, G. Sarma, H. Benoit, R. Duplessix, C. Picot, and P. G. de Gennes. Solutions of flexible polymers. neutron experiments and interpretation. *Macromolecules*, 8(6):804–818, 1975.

P. G. de Gennes. Scaling theory of polymer adsorption. *Journal de Physique*, 37 (12):1445–1452, 1976.

P. G. de Gennes. *Scaling Concepts in Polymer Physics*. Cornell University Press, 1979.

P. G. de Gennes. Polymer solutions near an interface. 1. Adsorption and depletion layers. *Macromolecules*, 14(6):1637–1644, 1981.

P. G. de Gennes. Polymers at an interface. 2. Interaction between two plates carrying adsorbed polymer layers. *Macromolecules*, 15(2):492–500, 1982.

P. G. de Gennes and P. Pincus. Scaling theory of polymer adsorption - proximal exponent. *journal de physique lettres*, 44(7):L241–L246, 1983.

R. Descas, J.-U. Sommer, and A. Blumen. Static and dynamic properties of tethered chains at adsorbing surfaces: A monte carlo study. *The Journal of Chemical Physics*, 120(18):8831–8840, 2004.

R. Descas, J.-U. Sommer, and A. Blumen. Grafted polymer chains interacting with substrates: computer simulations and scaling. *Macromolecular Theory and Simulations*, 17(9):8831–8840, 2008.

E. A. DiMarzio. Proper accounting of conformations of a polymer near a surface. *The Journal of Chemical Physics*, 42(6):2101–2106, 1965.

E. A. DiMarzio and F. L. McCrackin. One-dimensional model of polymer adsorption. *The Journal of Chemical Physics*, 43(2):539–547, 1965.

R. Dingreville, J. Qu, and M. Cherkaoui. Surface free energy and its effect on the elastic behavior of nano-sized particles, wires and films. *Journal of Mechanics and Physics of Solids*, 53(8):1827–1854, 2005.

J. Djikaev. Histogram analysis as a method for determining the line tension of a three-phase contact region by monte carlo simulations. *The Journal of Chemical Physics*, 123(18):184704–1–184704–12, 2005.

H. Dobbs. The modified young's equation for the contact angle of a small sessile drop from an interface displacement model. *International Journal of Modern Physics B*, 13(27):3255–3259, 1999.

M. Doi and S. F. Edwards. *The Theory of Polymer Dynamics*. Clarendon Press, Oxford, 1991.

A. K. Dolan and S. F. Edwards. Theory of stabilization of colloids by adsorbed polymer. *Proceedings of the Royal Society A - Mathematical, Physical and Engineering Sciences*, 337(1611), 1974.

D. J. Donahue and F. E. Bartell. The boundary tension at water organic liquid interfaces. *The Journal of Physical Chemistry*, 56(4):480–489, 1952.

L. M. Dossin and W. W. Graessley. Rubber elasticity of well-characterized polybutadiene networks. *Macromolecules*, 12(1):123–130, 1979.

J. F. Douglas, A. M. Nemirovsky, and K. F. Freed. Polymer-polymer and polymer-surface excluded volume effects in flexible polymers attached to an interface - comparison of renormalization group calculations with monte carlo and direct enumeration data. *Macromolecules*, 19(7):2041–2054, 1986.

J. M. Douillard, T. Zoungrana, and S. Partyka. Surface gibbs free energy of minerals: some values. *Journal of Petroleum Science and Engineering*, 14:51–57, 1995.

B. Du, O. K. C. Tsui, Q. Zhang, and T. He. Study of elastic modulus and yield strength of polymer thin films using atomic force microscopy. *Langmuir*, 17(11): 3286–3291, 2001.

A. Dupré. *Theorie Mechanique de la Chaleur*. Gauthier-Villar, Paris, 1869.

E. Eisenriegler. Dilute and semidilute polymer-solutions near an adsorbing wall. *The Journal of Chemical Physics*, 79(2):1052–1064, 1983.

E. Eisenriegler. *Polymers Near Surfaces*. Singapore, 1993.

E. Eisenriegler, K. Kremer, and K. Binder. Adsorption of polymer chains at surfaces: Scaling and monte carlo analyses. *The Journal of Chemical Physics*, 77 (12):6296–6320, 1982.

C. J. Ellison and J. M. Torkelson. The distribution of glass-transition temperatures in nanoscopically confined glass formers. *Nat. Mater.*, 2(10):695–700, 2003.

C. Engqvist, S. Forsberg, M. Norgren, H. Edlund, B. Andreassohn, and O. Karlssohn. Interactions between single latex particles and silica surfaces studies with afm. *Colloids and Surfaces A: Physicochem. Eng. Aspects*, 302:197–203, 2007.

A. E. A. S. Evangelopoulos, E. Glynos, F. Madani-Grasset, and V. Koutsos. Elastic modulus of a polymer nanodroplet: theory and experiment. *Langmuir*, 28(10): 4754–4767, 2012.

A. Falsafi, S. Mangipudi, and M. J. Owen. Surface and interfacial properties. In J. E. Mark, editor, *Physical Properties of Polymers Handbook*, pages 111–120. Springer, New York, USA, 2007.

J. D. Ferry. *Viscoelastic Properties of Polymers*. John Wiley & Sons, USA, 3rd edition, 1991.

L. J. Fetters, D. J. Lohse, D. Richter, T. A. Witten, and A. Zirkel. Connection between polymer molecular weight, density, chain dimensions, and melt viscoelastic properties. *Macromolecules*, 27(17):4639–4647, 1994.

G. J. Fleer, S. M. A. Cohen, J. M. H. M. Scheutjens, T. Cosgrove, and B. Vincent. *Polymers at Interfaces*. Chapman & Hall, 1993.

J. A. Forrest and K. Dalnoki-Veress. The glass transition in thin polymer films. *Advances in Colloid and Interface Science*, 94(1–3):167–196, 2001.

F. M. Fowkes. Determination of interfacial tensions, contact angles, and dispersion forces in surfaces by assuming additivity of intermolecular interactions in surfaces. *The Journal of Physical Chemistry*, 66(2):382, 1961.

F. M. Fowkes. Additivity of intermolecular forces at interfaces. i. determination of the contributions to surface and interfacial tensions of dispersion forces in various liquids. *The Journal of Physical Chemistry*, 67(12):2538–2541, 1963.

R. H. Fowler. A tentative statistical theory of macleod's equation for surface tension, and the parachor. *Proceedings of the Royal Society*, 159(A897):229–246, 1937.

R. H. Fowler and E. A. Guggenheim. *Statistical Thermodynamics*. Cambridge Press, 1939.

G. H. Fredrickson, V. Ganesan, and F. Drolet. Field-theoretic computer simulation methods for polymers and complex fluids. *Macromolecules*, 35(1):16–39, 2002.

K. F. Freed. Excluded volume effects in polymers attached to surfaces: Chain conformational renormalization-group. *The Journal of Chemical Physics*, 79(6): 3121–3132, 1983.

D. Frenkel and B. Smit. *Understanding Molecular Simulation*. Academic Press, 2002.

H. Freundlich. *Colloid and Capillary Chemistry*. Dutton & Co., 1922.

T. Furuta, A. Nakajima, M. Sakai, T. Isobe, Y. Kameshima, and K. Okada. Droplet size dependence of line tension for an ionic liquid on a smooth silane coating. *Chemistry Letters*, 38(6):580–581, 2009.

Galileo Galilei. *Bodies that Stay Atop Water, or Move in It*. 1612.

G. Galli and M. Pasquarello. *Computer Simulation in Chemical Physics*. Kluwer, Dordrecht, 1993.

J. Gaydos, L. Boruvka, and A. W. Neumann. A novel strategy for determining line tension from the shape of a liquid meniscus near a stripwise heterogeneous wall. *Colloids and Surfaces*, 43(2):307–326, 1990.

S. Ge, Y. Pu, W. Zhang, M. Rafailovich, and J. Sokolov. Shear modulation force microscopy study of near surface glass transition temperatures. *Physical Review Letters*, 85(11):2340–2343, 2000.

T. Getta and S. Dietrich. Line tension between fluid phases and a substrate. *Phys. Rev. E*, 57(1):655–671, 1998.

J. W. Gibbs. *The Scientific Papers*, volume I. Dover, New York, 1961.

L. A. Girifalco and R. J. Good. A theory for the estimation of surface and interfacial energies. i. derivation and application to interfacial tension. *The Journal of Chemical Physics*, 61:904–909, 1957.

E. Glynos. *Atomic Force Microscopy on Self-Assembled Polymer Structures*. PhD thesis, The University of Edinburgh, School of Engineering & Electronics, Centre for Materials Science and Engineering, Edinburgh, 2007.

E. Glynos, S. Pispas, and V. Koutsos. Unpublished.

E. Glynos, V. Koutsos, W. N. McDicken, C. M. Moran, S. D. Pye, J. A. Ross, and V. Sboros. Nanomechanics of biocompatible hollow thin-shell polymer microspheres. *Langmuir*, 25(13):7514–7522, 2009.

W. Gottstein, S. Kreitmer, M. Wittkop, D. Göritz, and F. Gotsis. Monte carlo simulations of the adsorption of a single polymer chain on rough surfaces. *Polymer*, 38(7):1607–1613, 1997.

V. Granier and A. Sartre. Ordering and adhesion of latex particles on model inorganic surfaces. *Langmuir*, 11:2179–2186, 1995.

V. Granier, A. Sartre, and M. Joanicot. An atomic force microscopy study of the wetting of an inorganic surface by latex particles. *The Journal of Adhesion*, 42 (4):255–263, 1993.

A. E. Green and J. E. Adkins. *Large Elastic Deformations*. Oxford University Press, Oxford, 1970.

M. X. Gu, C. Q. Sun, Z. Chen, T. C. A. Yeung, S. Li, and C. M. Tan. Size, temperature, and bond nature dependence of elasticity and its derivatives on extensibility, debye temperature, and heat capacity of nanostructures. *Phys. Rev. B*, 75(12):125403–1–125403–9, 2007.

L. Guzzardi, R. Rosso, and E. G. Virga. Residual stability of sessile droplets with negative line tension. *Phys. Rev. E*, 73:021602, 2006.

C. Haber, S. A. Ruiz, and D. Wirtz. Shape anisotropy of a single random-walk polymer. *Proceedings of the National Academy of Sciences*, 97(20):10792–10795, 2000.

J. M. Hammersley and S. G. Whittington. Self-avoiding walks in wedges. *Journal of Physics A: Mathematical and General*, 18(1):101–111, 1985.

J. M. Hammersley, G. M. Torrie, and S. G. Whittington. Self-avoiding walks interacting with a surface. *Journal of Physics A: Mathematical and General*, 15 (2):539–571, 1982.

R. Hegger and P. Grassberger. Irreversible adsorption of a concentrated polymer solution. *J. Phys. A*, 27(12):4069–4081, 1994.

D. R. Heine, G. S. Grest, and E. B. III Webb. Spreading dynamics of polymer nanodroplets. *Physical Review E*, 68(6):061603–1–061603–10, 2003.

C. A. J. Hoeve, E. A. DiMarzio, and P. Peyser. Adsorption of polymer molecules at low surface coverage. *The Journal of Chemical Physics*, 42(7):2558–2563, 1965.

J. Hu, X. d. Xiao, D. F. Ogletree, and M. Salmeron. The structure of molecularly thin films of water on mica in humid environments. *Surface Science*, 344(3): 221–236, 1995.

W. Humphrey, A. Dalke, and K. Schulten. VMD – Visual Molecular Dynamics. *Journal of Molecular Graphics*, 14:33–38, 1996.

S. Hvidt, O. Kramer, W. Batsberg, and J. D. Ferry. Contribution of entanglements to the equilibrium modulus of 1,2-polybutadiene networks at small strains and estimate of the front factor. *Macromolecules*, 13:933–939, 1980.

Y. Imanishi and I. Yoshihiro. Glucose-sensitive insulin-releasing molecular systems. *Pure and Applied Chemistry*, 67(12):2015–2021, 1995.

T. Ingebrigtsen and S. Toxvaerd. Contact angles of lennard-jones liquids and droplets on planar surfaces. *The Journal of Physical Chemistry C*, 111(24): 8518–8523, 2007.

A. Ishikawa, T. Tanji, and A. Kawai. Determination of young's modulus of polymer aggregate based on hertz theory. *Journal of Photopolymer Science and Technology*, 17(5):715–718, 2004.

V. A. Ivanov, M. R. Stukan, V. V. Vasilevskaya, W. Paul, and K. Binder. Structures of stiff macromolecules of finite chain length near the coil-globule transition: A monte carlo simulation. *Macromolecular Theory and Simulations*, 9(8):488–499, 2000.

V. A. Ivanov, J. A. Martemyanova, M. Müller, W. Paul, and K. Binder. Conformational changes of a single semiflexible macromolecule near an adsorbing surface: a monte carlo simulation. *The Journal of Physical Chemistry B*, 113 (12):3653–3668, 2009.

F. James. A review of pseudorandom number generators. *Computer Physics Communications*, 60(3):329–344, 1990.

C. A. Johnson and A. M. Lenhoff. Adsorption of charged latex particles on mica studied by atomic force microscopy. *Journal of Colloid and Interface Science*, 179(2):587–599, 1996.

K. L. Johnson. *Contact Mechanics*. CUP, 1985.

K. L. Johnson, K. Kendall, and A. D. Roberts. Surface energy and the contact of elastic solids. *Proceedings of the Royal Society A - Mathematical, Physical and Engineering Sciences*, 324(1558):301–313, 1971.

I. S. Jones and P. Richmond. Effects of excluded volume on conformation of adsorbed polymers. *Journal of the Chemical Society, Faraday Transactions 2: Molecular and Chemical Physics*, 73:1062–1070, 1977.

R. A. L. Jones and R. W. Richards. *Polymers at Surfaces and Interfaces*. CUP, Cambridge, 1999.

C. S. Kan and J. H. Blackson. Effect of ionomeric behavior on the viscoelastic properties and morphology of carboxylated latex films. *Macromolecules*, 29(21): 6853–6864, 1996.

E. Karaiskos, I. A. Bitsanis, and S. H. Anastasiadis. Monte carlo studies of tethered chains. *Journal of Polymer Science Part B - Polymer Physics*, 47(24):2449–2461, 2009.

M. Kawaguchi and A. Takahashi. Polymer adsorption at solid-liquid interfaces. *Advances in Colloid and Interface Science*, 37(3–4):219–317, 1992.

E. Killmann, H. Maier, and J. A. Baker. Hydrodynamic layer thicknesses of various adsorbed polymers on precipitated silica and polystyrene latex. *Colloids and Surfaces*, 31:51–71, 1988.

J. G. Kirkwood and F. P. Buff. The statistical mechanical theory of surface tension. *The Journal of Chemical Physics*, 17(3):338–343, 1949.

S. Kirsch, A. Pfau, E. Hädicke, and J. Leuninger. Interface and bulk properties in films of phase separated dispersion particles. *Progress in Organic Coatings*, 45 (2–3):193–204, 2005.

M. Kopycinska-Muller, R. H. Geiss, J. Muller, and D. C. Hurley. Elastic-property measurements of ultrathin films using atomic force acoustic microscopy. *Nanotechnology*, 16(6):703–709, 2005.

M. K. Kosmas. On the adsorption of a theta-polymer. *Die Makromolekulare Chemie - Rapid communications*, 2(9–10):563–567, 1981.

E. Y. Kramarenko, R. G. Winkler, P. G. Khalatur, A. R. Kokhlov, and P. Reineker. Molecular dynamics simulation study of adsorption of polymer chains with variable degree of rigidity. 1. static properties. *J. Chem. Phys.*, 104(12):4086–4813, 1995.

K. Kremer. Adsorption of a self-avoiding walk, a real space renormalisation group study for $d = 2, 3$. *Journal of Physics A: Mathematical and General*, 16(18): 4333–4342, 1983.

C. Kugge, V. S. J. Craig, and J. Daicic. A scanning electron microscope study of the surface structure of mineral pigments, latices and thickeners used for paper coating on non-absorbent substrates. *Colloids and Surfaces A - Physicochemical and Engineering Aspects*, 238(1–3):1–11, 2004.

W. Kuhn. Concerning the shape of thread shapes molecules in solution. *Kolloid-Zeitschrift*, 68(1):2–15, 1934.

S. Kumar and Y. Singh. Surface adsorption and the collapse transition of a linear polymer chain: Some exact results on fractal lattices. *Physical Review E*, 48(2): 734–742, 1993.

M.-O. Lafon and M. Trannoy. Influence of drying temperature on the morphology of latex at the surface of pigments - consequences on the paper properties. In *Advanced Coating Fundamentals Symposium*, Turku, Finland, February 2006.

P.-Y. Lai. Statics and dynamics of a polymer chain adsorbed on a surface: Monte carlo simulation using the bond-fluctuation model. *Physical Review E*, 49(6): 5420–5430, 1994.

L. D. Landau and E. M. Lifshitz. *Statistical Physics*. Elsevier Butterworth-Heinemann, 1980.

A. W. C. Lau, M. Portigliatti, E. Raphaël, and L. Léger. Spreading of latex particles on a substrate. *Europhysics Letters*, 60(5):717–723, 2002.

M. Lax. Configuration of an adsorbed polymer molecule: Solvent effect. *The Journal of Chemical Physics*, 60(5):1931–1936, 1974a.

M. Lax. Numerical results on the radius of gyration of surface interacting self-avoiding walks. *The Journal of Chemical Physics*, 60(7):2627–2629, 1974b.

M. Lax and S. Windwer. Properties of self-avoiding walks not constrained to lattices. *The Journal of Chemical Physics*, 55(9):4167–4173, 1971.

L.-H. Lee. *Adhesion and adsorption of polymers*. Plenum Press, New York, USA, 1980.

L.-H. Lee. Correlation between lewis acid-base surface interaction components and linear solvation energy relationship solvatochromic α and β parameters. *Langmuir*, 12(6):1681–1687, 1996.

L.-H. Lee. The unified lewis acid-base approach to adhesion and solvation at the liquid-polymer interface. *The Journal of Adhesion*, 76(2):163–183, 2001.

Y. Lépine and A. Caillé. Configuration of a polymer-chain interacting with a plane interface. *Canadian Journal of Physics*, 56(4):403–408, 1978.

G. R. Lester. Contact angles of liquids at deformable solid surfaces. *Journal of Colloid Science*, 16(4):315–326, 1961.

S. Levine, M. M. Thomlinson, and K. Robinson. Models of polymer adsorption with excluded volume on parallel colloidal plates and their interaction. *Faraday Discussions of the Chemical Society*, 65:202–214, 1978.

D. Li. Drop size dependence of contact angles and line tensions of solid-liquid systems. *Colloids and Surfaces A*, 116:1–23, 1996.

G. Liu, C. Zhang, J. Zhao, and Y. Zhu. Molecular dynamics study of adsorption and spreading of a polymer chain onto a flat surface. *Polymer*, 40(26):7285–7293, 1999.

H. Liu and A. Chakrabarti. Molecular dynamics study of adsorption and spreading of a polymer chain onto a flat surface. *Polymer*, 40(26):7285–7239, 2009.

S. Livne and H. Meirovitch. Computer-simulation of long polymers adsorbed on a surface. 1. corrections to scaling in an ideal chain. *The Journal of Chemical Physics*, 88(7):4498–4506, 1988.

F. Madani. *Polydimethylsiloxane (PDMS) monolayers: morphology, nanostructure, adhesive and frictional properties.* PhD thesis, School of Engineering & Electronics *and* Centre for Materials Science & Engineering, 2005.

S. N. Magonov, V. Elings, and M.-H. Whangbo. Phase imaging and stiffness in tapping-mode atomic force microscopy. *Surface Science*, 375:L385–L391, 1997.

H. Malandrini, R. Sarraf, B. Faucompré, S. Partyka, and J.M. Douillard. Characterization of quartz partcle surfaces by immersion calorimetry. *Langmuir*, 13: 1337–1341, 1997.

M. W. Matsen. The standard gaussian model for block copolymer melts. *Journal of Physics: Condensed Matter*, 14(2):R21–R47, 2002.

D. Maugis. *Contact, Adhesion and Rupture of Elastic Solids.* Springer-Verlag, 2000.

F. L. McCrackin. Configuration of isolated polymer molecules adsorbed on solid surfaces studied by montecarlo computer simulation. *The Journal of Chemical Physics*, 47(6):1980–1986, 1967.

V. Médout-Marère, H. Malandrini, T. Zoungrana, J. M. Douillard, and S. Partyka. Thermodynamic investigation of surface of minerals. *Journal of Petroleum Science an Engineering*, 20(12):223–231, 1998.

N. Metropolis. The beginning of the monte carlo method. *Los Alamos Science*, 15: 125–130, 1987.

N. Metropolis, A. W. Rosenbluth, M. N. Rosenbluth, A. H. Teller, and E. Teller. Equation of state calculations by fast computing machines. *The Journal of Chemical Physics*, 21(6):1087–1092, 1953.

S. Metzger, M. Müller, K. Binder, and J. Baschnagel. Adsorption transition of a polymer chain at a weakly attractive surface: Monte carlo simulation of off-lattice models. *Macromolecular Theory and Simulations*, 11(9):985–995, 2002.

A. Michel and S. Kreitmeier. Adsorption of a single polymer chain on a surface: A molecular dynamics simulation study. *Journal of Polymer Science Part B - Polymer Physics*, 39(20):2333–2339, 2001.

A. Michel, D. Goritz, and S. Kreitmeier. Molecular dynamics simulation study - localization and multi-flip effects in a single polymer chain on a surface. *Kautschuk Gummi Kunststoffe*, 55(9):447–453, 2002.

K. M. Middlemiss and S. G. Whittington. Exact enumeration of self-avoiding walks on cubic lattice terminally attached to an interface. *The Journal of Chemical Physics*, 64(11):4684–4688, 1976.

A. Milchev and K. Binder. Static and dynamic properties of adsorbed chains at surfaces: Monte Carlo simulation of a bead-spring model. *Macromolecules*, 29 (1):343–354, 1996.

A. Milchev and K. Binder. Polymer melt droplets adsorbed on a solid wall: A monte carlo simulation. *The Journal of Chemical Physics*, 114(19):8610–8618, 2001.

A. Milchev, A. Milchev, and K. Binder. Nanodroplets on a solid plane: wetting and spreading in a Monte Carlo simulation. *Computer Physics Communications*, 146(1):38–53, 2002.

A. I. Milchev and A. A. Milchev. Wetting behaviour of nanodroplets: The limits of young's rule validity. *Europhysics Letters*, 56(5):695–701, 2001.

R. E. Miller and V. B. Shenoy. Size-dependent elastic properties of nanosized structural elements. *Nanotechnology*, 11(13):139–147, 2000.

S. T. Milner and T. C. B. McLeish. Parameter-free theory for stress relaxation in star polymer melts. *Macromolecules*, 30(7):2159–2166, 1997.

P. K. Mishra, D. Giri, S. Kumar, and Y. Singh. Does a surface attached globule phase exist. *Physica A*, 318(1–2):171–178, 2003.

K. Miyake, N. Satomi, and S. Sasaki. Elastic modulus of polystyrene film from near surface to bulk measured by nanoindentation using atomic force microscopy. *Appl. Phys. Lett.*, 89(3):031925–1–031925–3, 2006.

D. Mukherji, G. Bartels, and H. Müser. Scaling laws of single polymer dynamics near attractive surfaces. *Physical Review Letters*, 100(6):068301–1–068301–4, 2008.

A. M. Nemirovsky and K. F. Freed. Excluded volume effects for polymers in presence of interacting surfaces: Chain conformation renormalization group. *The Journal of Chemical Physics*, 83:4166–4182, 1985.

S. G. Nilsson, X. Borrisé, and L. Montelius. Size effect on young's modulus of thin chromium cantilevers. *Appl. Phys. Lett.*, 85:3555–3557, 2004.

P. A. O'Connell and G. B. McKenna. Rheological measurements of the thermoviscoelastic response of ultrathin polymer films. *Science*, 307:1760–1763, 2005.

P. A. O'Connell and G. B. McKenna. Dramatic stiffening of ultrathin polymer films in the rubbery regime. *E. Phys. J. E*, 20:143–150, 2006.

A. Patrykiejew, S. Sokolowski, and K. Binder. Phase transitions in adsorbed layers formed on crystals of square and rectangular surface lattice. *Surface Science Reports*, 37(6–8):209–344, 2000.

G. M. Pharr and W. C. Oliver. Measurement of thin-film mechanical properties using nanoindentation. *MRS Bull.*, 17(7):28–33, 1992.

T. Pompe and S. Herminghaus. Three-phase contact line energetics from nanoscale liquid surface topographies. *Phys. Rev. Lett.*, 85(9):1930–1933, 2000.

M. Portigliatti, V. Koutsos, H. Hervet, and L. Léger. Adhesion and deformation of a single latex particle. *Langmuir*, 16:6374–6376, 2000.

R. D. Priestley, C. J. Ellison, L. J. Broadbelt, and J. M. Torkelson. Structural relaxation of polymer glasses at surfaces, interfaces, and in between. *Science*, 309(5733):456–459, 2005.

R. Rajesh, D. Dhar, D. Giri, S. Kumar, and Y. Singh. Adsorption and collapse transitions in a linear polymer chain near an attractive wall. *Physical Review E*, 65(5):056124–1–056124–7, 2002.

A. R. Rennie, R. J. Crawford, E. M. Lee, R. K. Thomas, T. L. Crowley, S. Roberts, M. S. Qureshi, and R. W. Richards. Adsorption of poly(ethylene oxide) at the air solution interface studied by neutron reflection. *Physical Review E*, 22(8): 3466–3475, 1989.

E. Riande, R. Diaz-Calleja, M. G. Prolongo, R. M. Masegosa, and C. Salom. *Polymer Viscoelasticity*. Marcel Deker, Inc., 2000.

A. N. Rissanou, S. H. Anastasiadis, and I. A. Bitsanis. Monte carlo study of the coil-to-globule transition of a model polymeric system. *Journal of Polymer Science: Part B: Polymer Physics*, 44(24):3651–3666, 2006.

A. N. Rissanou, S. H. Anastasiadis, and I. A. Bitsanis. A monte carlo study of the coil-to-globule transition of model polymer chains near an attractive surface. *Journal Polymer Science: Part B: Polymer Physics*, 47(24):2462–2467, 2009.

R.-J. Roe. Conformation of an isolated polymer molecule at an interface. ii. dependence on molecular weight. *The Journal of Chemical Physics*, 43(5):1591–1598, 1965.

S. Ross and P. Becher. The history of the spreading coefficient. *Journal of Colloid and Interface Science*, 149(2):575–579, 1992.

R. Rosso. Modelling line tension in wetting. *Modeling of Soft Matter*, 141:133–168, 2005.

R. Rosso and E. G. Virga. *J. Phys. A*, 37:3989, 2004a.

R. Rosso and E. G. Virga. Sign of line tension in liquid bridge stability. *Phys. Rev. E*, 70:031603, 2004b.

J. S. Rowlinson and B. Widom. *Molecular Theory of Capillarity*. International Series of Monographs on Chemistry. OUP, 1982.

R. J. Rubin. A random walk model of chain polumer adsorption at a surface. ii. effect of correlation between neighboring steps. *Journal of research of the National Bureau of Standards. B - Mathematical sciences*, B69(4):301–312, 1965a.

R. J. Rubin. Random-walk model of chain-polymer adsorption at a surface. *The Journal of Chemical Physics*, 43(7):2392–2407, 1965b.

R. J. Rubin. A random walk model of chain polymer adsorption at a surface. iii. mean square end-to-end distance. *Journal of research of the National Bureau of Standards. B - Mathematical sciences*, B70(4):237–247, 1966a.

R. J. Rubin. Random-walk model of adsorption of a chain-polymer molecule on a long rigid-rod molecule. *The Journal of Chemical Physics*, 44(5):2130–2138, 1966b.

M. Rubinstein and R. H. Colby. *Polymer Physics*. Oxford University Press, 2003.

E. Ruckenstein and D.B. Chung. Surface modification by a two-liquid process deposition of ab block copolymers. *Journal of Colloid and Interface Science*, 123 (1):170–185, 1988.

G. Rychlewski and S. G. Whittington. Self-avoidingwalks and polymer adsorption: Low temperature behaviour. *Journal of Statistical Physics*, 145(3):661–668, 2011.

Brown I.G. Vaz A.R. Salvadori, M. C., L. L. Melo, and M. Cattani. Measurement of the elastic modulus of nanostructured gold and platinum thin films. 2003.

V. M. Samsonov and A. S. Ratnikov. Comparative molecular dynamics study of simple and polymer nanodroplet spreading. 2006.

L. Schimmele and S. Dietrich. Line tension and the shape of nanodroplets. *European Physical Journal E*, 30(4):427–430, 2009.

L. Schimmele, M. Napiórkowski, and S. Dietrich. Conceptual aspects of line tensions. *J. Chem. Phys.*, 127:164715–1–164715–28, 2007.

F. Schmid. Self-consistent-field theories for complex fluids. *Journal of Physics: Condensed Matter*, 10(37):8105–8138, 1998.

J. Schultz, K. Tsutsumi, and J.-B. Donnet. Surface properties of high-energy solids i. determination of the dispersive component of the surface free energy of mica and its energy of adhesion to water and n-alkanes. *Journal of Colloid and Interface Science*, 59(2):272–276, 1977a.

J. Schultz, K. Tsutsumi, and J.-B. Donnet. Surface properties of high-energy solids ii. determination of the nondispersive component of the surface free energy of

mica and its energy of adhesion to polar liquids. *Journal of Colloid and Interface Science*, 59(2):277–282, 1977b.

R. Seemann, K. Jacobs, and R. Blossey. Polystyrene nanodroplets. *Journal of Physics: Condensed Matter*, 13:4915–4923, 2001.

P. Seppecher. Line tension effect upon static wetting. *Oil and Gas Science and Technology - Rev. IFP*, 56(1):77–81, 2001.

M. E. R. Shanahan. Contact angle equilibrium on thin elastic solids. *The Journal of Adhesion*, 18(4):247–267, 1985.

M. E. R. Shanahan. The spreading dynamics of a liquid drop on a viscoelastic solid. *J. Phys. D: Appl. Phys.*, 21:981–985, 1988.

M. E. R. Shanahan. Is a sessile drop in an atmosphere saturated with its vapour really at equilibrium? *Langmuir*, 18(21):7763–7765, 2002.

M. E. R. Shanahan and A. Carré. Anomalous spreading of liquid drops on an elastomeric surface. *Langmuir*, 10:1647–1649, 1994.

M. E. R. Shanahan and P. G. de Gennes. Equilibrium of the triple line solid/liquid/fluid of a sessile drop. *Adhesion*, 11:71–81, 1987.

P. Sharma, S. Ganti, and N. Bhate. Effect of surfaces of the size-dependent elastic state of nano-inhomogeneities. *Appl. Phys. Lett.*, 82(4):535–537, 2002.

V. B. Shenoy. Atomistic calculations of elastic properties of metallic fcc crystal surfaces. *Phys. Rev. B*, 71(9):094104–1–094104–11, 2005.

M. K. Shin, S.I. Kim, S.J. Kim, S. K. Kim, H. Lee, and G.M. Spinks. Size-dependent elastic modulus of single electroactive polymer nanofibers. *Applied Physics Letters*, 89(23):231929–1–231929–3, 2006.

R. Shuttleworth. The surface tension of solids. *Proceedings of the Physical Society*, 63(5):444–457, 1949.

A. Sikorski. Computer simulation of adsorbed polymer chains with a different molecular architecture. *Macromolecular Theory and Simulations*, 10(1):38–45, 2001.

A. Sikorski. Structure of adsorbed polymer chains: A monte carlo study. *Macromolecular Theory and Simulations*, 11(3):359–364, 2002.

A. Sikorski and P. Romiszowski. Computer simulations of adsorbed polymer chains. *Acta Physica Polonica B*, 36(5):1779–1789, 2005.

R. Simha, H. L. Frisch, and F. R. Eirich. The adsorption of flexible macromolecules. *The Journal of Physical Chemistry*, 57(6):584–589, 1953.

Y. Singh, S. Kumar, and D. Giri. Surface adsorption and collapse transition of a linear polymer chain in three dimensions. *Journal of Physics A: Mathematical and General*, 32(36):L407–L411, 1999.

Y. Singh, D. Giri, and S. Kumar. Crossover of a polyme chain from bulk to surface states. *Journal of Physics A: Mathematical and General*, 34(8):L67–L74, 2001.

F. Sommer, T. M. Duc, R. Pirri, G. Meunier, and C. Quet. Surface morphology of poly(butyl acrylate)/poly(methyl methacrylate) core shell latex by atomic force microscopy. *Langmuir*, 11:440–448, 1995.

D. J. Steigmann and D. Li. Energy-minimizing states of capillary systems with bulk, surface, and line phases. *IMA J. Appl. Math.*, 55(1):1–17, 1995.

F. H. Streitz, R. C. Cammarata, and K. Sieradzki. Surface-stress effects on elastic properties .1. thin metal-films. *Phys. Rev. B*, 49(15):10699–10706, 1994.

F. Svec and J. M. J. Frechet. Continuous rods of macroporous polymer as high-performance liquid chromatography separation media. *Analytical Chemistry*, 64 (7):820–822, 1992.

A. Takahashi and M. Kawaguchi. The structure of macromolecules adsorbed on surfaces. *Advances in Polymer Science*, 46:1–65, 1982.

A. Takahashi, M. Kawaguchi, K. Hayashi, and T. Kato. Ellipsometric study of adsorption of poly-electrolyte onto a metal surface. *ACS Symposium Series*, 240: 39–52, 1984.

J. Tamayo and R. García. Deformation, contact time, and phase contrast in tapping mode scanning force microscopy. *Langmuir*, 12:4430–4435, 1996.

E. P. S. Tan, Y. Zhu, T. Yu, L. Dai, C. H. Sow, V. B. C. Tan, and C. T. Lim. Crystallinity and surface effects on young's modulus of cuo nanowires. *Applied Physics Letters*, 90(16):163112–1–163112–3, 2007.

S. Tan, R. L. Jr. Sherman, D. Qin, and W. T. Ford. Surface heterogeneity of polystyrene latex particles determined by dynamic force microscopy. *Langmuir*, 21:43–49, 2005.

R. C. Tolman. The effect of droplet size on surface tension. *The Journal of Chemical Physics*, 17(3):333–337, 1948.

J. M. Torres, C. M. Stafford, and B. D. Vogt. Elastic modulus of amorphous polymer thin films: Relationship to the glass transition temperature. *ACSnano*, 3(9):2677–2685, 2009.

G. Torrie and S. G. Whittington. Exact enumeration of neighbor-avoiding walks on tetrahedral and body-centered cubic lattices. *Journal of Physics A: Mathematical and General*, 8(7):1178–1184, 1975.

G. Torrie, K. M. Middlemiss, S. H. P. Bly, and S. G. Whittington. Self-avoiding walks interacting with an interface. *The Journal of Chemical Physics*, 65(5): 1867–1871, 1976.

B. V. Toshev and M. Z. Avramov. On the thermodynamic stbility of small droplets at positive line tension. *Colloids and Surfaces A*, 75:33–37, 1993.

B. V. Toshev, D. Platikanov, and A. Scheludko. Line tension in three-phase equilibrium systems. *Langmuir*, 4(3):489–499, 1988.

T. Y. Tsui and G. M. Pharr. Substrate effects on nanoindentation mechanical property measurement of soft films on hard substrates. *J. Mater. Res.*, 14(1): 292–301, 1999.

C. A. Tweedie, G. Constantinides, K. E. Lehman, D. J. Brill, G. S. Blackman, and K. J. Van Vliet. Enhanced stiffness of amorphous polymer surfaces under confinement of localized contact loads. *Adv. Mater.*, 19(8):2540–2546, 2007.

W. N. Unertl. Wetting and spreading of styrene-butadiene latexes on calcite. *Langmuir*, 14:2001–2207, 1998.

Z. Usatenko. Adsorption of long flexible polymer chains at planar surfaces: scaling analysis and critical exponents. *Journal of Statistical Mechanics: Theory and Experiment*, P03009:2001–2207, 2006.

D. W. van Krevelen and P. J. Hoftyzer. *Properties of Polymers*. Elsevier, 1976.

C. J. van Oss, M. K. Chaudhury, and R. J. Good. Monopolar surfaces. *Advanced Colloid and Interface Science*, 28(1):35–64, 1987.

C. J. van Oss, M. K. Chaudhury, and R. J. Good. Interfacial lifshitz-van der waals and polar interactions in macroscopic systems. *Chemical Reviews*, 88(6):927–941, 1988a.

C. J. van Oss, R. J. Good, and M. K. Chaudhury. Additive and nonadditive surface tension components and the interpretation of contact angles. *Langmuir*, 4(4):884–891, 1988b.

Y. Vandecan and J. O. Indekeu. Theoretical study of the three-phase contact line and its tension in adsorbed colloid-polymer mixtures. *J. Chem. Phys.*, 128(10): 104902–1–104902–5, 2008.

M. R. VanLandingham, J. S. Villarrubia, W. E. Guthrie, and G. F. Meyers. Nanoindentation of polymers: An overview. *Macromol. Symp.*, 167(1):15–43, 2001.

F. Varnik and K. Binder. Multiscale modeling of polymers and interfaces. *International Journal of Materials Research*, 100(11):1494–1502, 2009.

V. K. Vendra, L. Wu, and S. Krishnan. Polymer thin films for biomedical applications. In C. S. S. R. Kumar, editor, *Nanomaterials for the Life Sciences*, volume 5. Wiley, 2011.

P. Villain, P. Goudeau, P. O. Renault, and K. F. Badawi. Size effect on intragranular elastic constants in thin tungsten films. *Appl. Phys. Lett.*, 81(23):4365–4367, 2002.

P. Villain, P. Beauchamp, K. F. Badawi, P. Goudeau, and P. O. Renault. Atomistic calculation of size effects on elastic coefficients in nanometre-sized tungsten layers and wires. *Scripta Materialia*, 50(9):1247–1251, 2004.

J. P. R. B. Walton and K. E. Gubbins. The pressure tensor in an inhomogeneous fluid of non-spherical molecules. *Molecular Physics*, 55(3):679–688, 1985.

J. Y. Wang, S. Betelu, and B. M. Law. Line tension approaching a first-order wetting transition: Experimental results from contact angle measurements. *Phys. Rev. E*, 2001.

C. A. Ward and J. Wu. Effect of contact line curvature on solid-fluid surface tensions without line tension. *Physical Review Letters*, 100(25):256103–1–256103–4, 2008.

T. Werder, J. H. Walther, R. L. Jaffe, T. Halicioglu, and P. Koumoutsakos. On the water-carbon interaction for use in molecular dynamics simulations of graphite and carbon nanotubes. *The Journal of Physical Chemistry B*, 107(6):1345–1352, 2003.

C. Werner, M. F. Maitz, and C. Sperling. Current strategies towards hemocompatible coatings. *Journal of Materials Chemistry*, 17(32):3376–3384, 2007.

M. D. Whitmore and J. D. Vavasour. Self-consistent mean field-theory of the microphase diagram of block copolymer neutral solvent blends. *Macromolecules*, 25(7):2041–2045, 1992.

S. G. Whittington. Self-avoiding walks terminally attached to an interface. *The Journal of Chemical Physics*, 63(2):779–785, 1975.

B. Widom. Surface-stress-induced structure and elastic behaviour of thin-films. *Applied Physics Letters*, 58(19):2081–2083, 1991.

B. Widom. Line tension and the shape of a sessile drop. *The Journal of Physical Chemistry*, 99:2803–2806, 1995.

Q. H. Xiong, N. Duarte, S. Tadigadapa, and P. C. Eklund. Force-deflection spectroscopy: A new method to determine the young's modulus of nanofilaments. *Nano Letters*, 6(9):1904–1909, 2006.

Y.-Q. Xue, X.-C. Yang, Z.-X. Cui, and W.-P. Lai. The the effect of microdroplet size on the surface tension and tolman length. *The Journal of Physical Chemistry*, 115(1):109–112, 2011.

T. Yamamoto, T. Fukushima, Y. Kanda, and K. Higashitani. Molecular scale observation of the surface of polystyrene particles by afm. *Journal of Colloid and Interface Science*, 292:392–396, 2005.

Z. Yang, Y. Fujii, F. K. Lee, C.-H. Lam, and O. K. C. Tsui. Glass transition dynamics and surface layer mobility in unentangled polystyrene films. *Science*, 328(5986):1676–1679, 2010.

Z. Y. Yang and Y. P. Zhao. Size-dependent elastic properties of ni nanofilms by molecular dynamics simulation. *Surface review and letters*, 14(4):661–665, 2007.

T. Young. An essay on the cohesion of fluids. *Philosophical Transactions of the Royal Society of London*, 95:65–85, 1805.

L. G. Zhou and H. C. Huang. Are surfaces elastically softer or stiffer? *Applied Physics Letters*, 84(11):1940–1942, 2004.